2007

Seismic Reflection and Gravity Constraints on the Bedrock Configuration in the Greater East Missoula Area

Frank Janiszewski
The University of Montana

SEISMIC REFLECTION AND GRAVITY CONSTRAINTS ON THE BEDROCK CONFIGURATION IN THE GREATER EAST MISSOULA AREA

By

Frank David Janiszewski

B.S., Michigan Technological University
Houghton, Michigan, 2004

Thesis

presented in partial fulfillment of the requirements
for the degree of

Master of Science
in Geophysics

The University of Montana
Missoula, MT

Spring 2007

Approved by:

Dr. David A. Strobel, Dean
Graduate School

Dr. Steven Sheriff
Geosciences

Dr. James Sears
Geosciences

Dr. Jesse Johnson
Computer Sciences

Janiszewski, Frank, M.S., May 2007 Geophysics

Seismic Reflection and Gravity Constraints on the Bedrock Configuration in the Greater East Missoula Area

Chairperson: Steven Sheriff

The greater East Missoula, MT area is the site of numerous studies to track possible groundwater contamination from the EPA Superfund Site at the Milltown Dam. The accuracy of these groundwater models depends on many factors, one of which is the accuracy to which the bedrock topography is mapped. Currently, a map based heavily on a gravity survey provides the most detailed map of the bedrock. The accuracy of this map may be improved through the use of seismic reflection techniques, better estimates of the density contrast used in the gravity modeling, and by extending the gravity survey to include more data and a broader area.

The seismic reflection technique used to supplement the gravity data is the optimum offset technique. This method simplifies field collection of the data and processing of the data. The final result of this method is a seismic section showing the depth to different reflectors in the subsurface, one of which is the bedrock. In order to improve the estimate of the density contrast used in the gravity modeling, the homogeneity of the valley fill was tested. This was done by comparing the results from two different modeling programs, one of which let the density contrast vary, to see if there was an improvement in the final result. The gravity survey was also extended to incorporate a larger area and more data.

The results show that seismic reflection can be used to improve the depth estimate in the valley where the depth is shallow and that the density contrast is most likely homogeneous. The extended gravity survey provided more data to work with and the final result is a map of the bedrock topography for the greater East Missoula Area that incorporates all currently known data and provides a sufficiently accurate estimate of the depth to be used in groundwater models.

To my Parents
for all they have given me

TABLE OF CONTENTS

Page

LIST OF FIGURES

LIST OF TABLES

LIST OF APPENDICIES

Appendix **Page**

INTRODUCTION

In west-central Montana, Milltown Valley (Figure 1), located at the confluence of the Clark Fork River and the Blackfoot River, has been the subject of intense scrutiny since the discovery of heavy metal groundwater contamination in 1981. The area is currently an Environmental Protection Agency Superfund site. The cleanup effort will involve removal of Milltown dam and some of the contaminated sediments behind it (Milltown Reservoir Sediments EPA Superfund Site). A chief concern of the citizens in the area is how the contamination will move downstream after the removal of the dam. The aquifer below Milltown Valley is directly connected to the Missoula Valley Aquifer, which serves as the main drinking water supply for the city of Missoula, Montana. Several studies have been completed to address the question of where the contamination may go [Associates, 1987; Camp, 1989; Woessner, 1993; Woessner, 1984; Woessner, 1982].

A key component of these studies was the determination of the configuration of bedrock surface beneath the valley. The three-dimensional configuration of bedrock surface plays an important role in local groundwater flow. A bedrock map (Gestring, 1994) was used as an input for the groundwater models (Figure 2). Gestring's (1994) map of the bedrock was based on bedrock exposures, drill core data and some limited seismic data. The limited amount of bedrock exposures in the valley and sporadic spacing of the wells left large areas in the study with little or no data. The lack of data and control points led to the mapping of some suspect features. The accuracy of this map was not great enough to support the grid size of 91.4 meters used in the groundwater

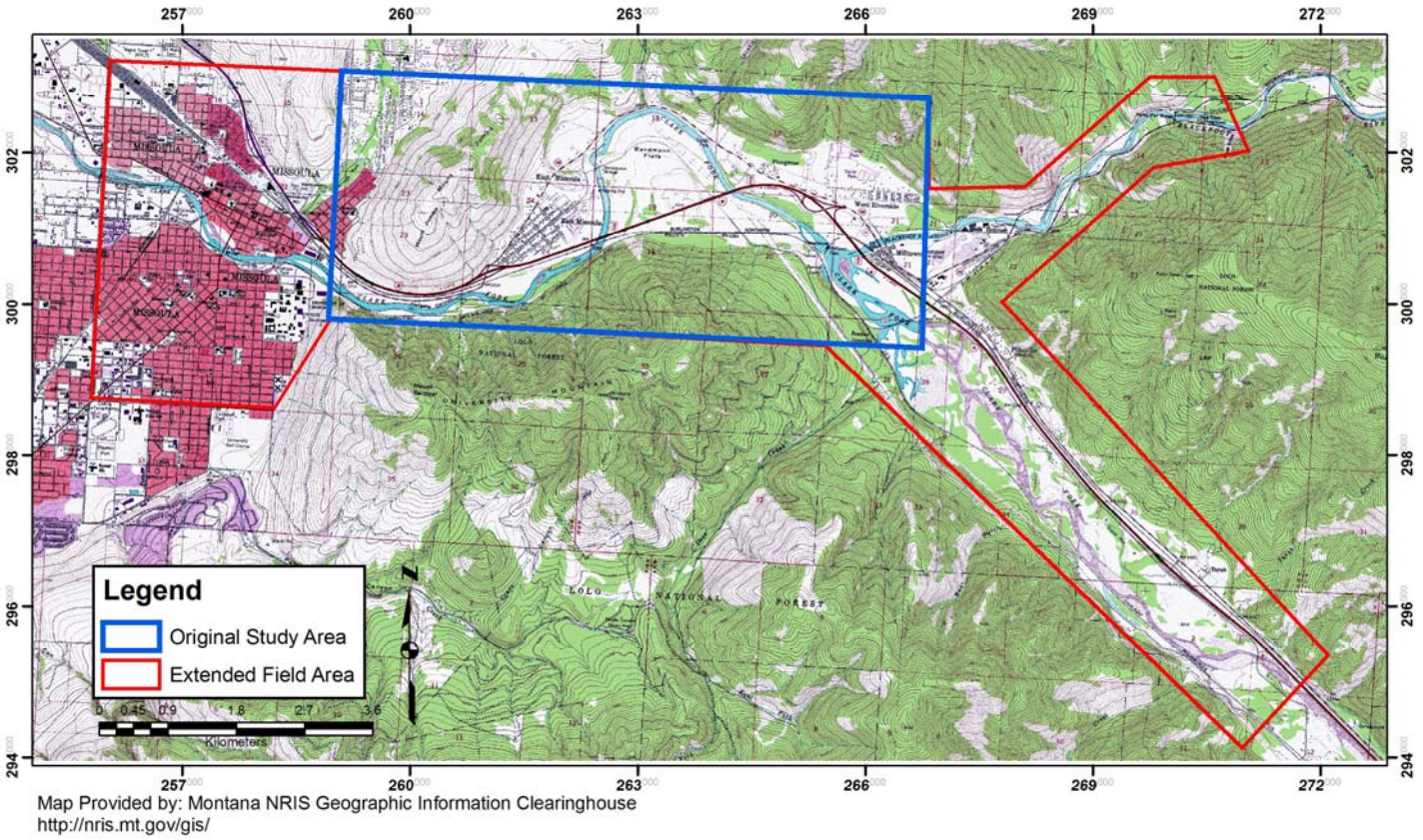

Figure 1: Topographic map of the study area. The area outlined in blue is the original study area. The area outlined in red is the extended study area. Coordinate system is Montana State Plane NAD83.

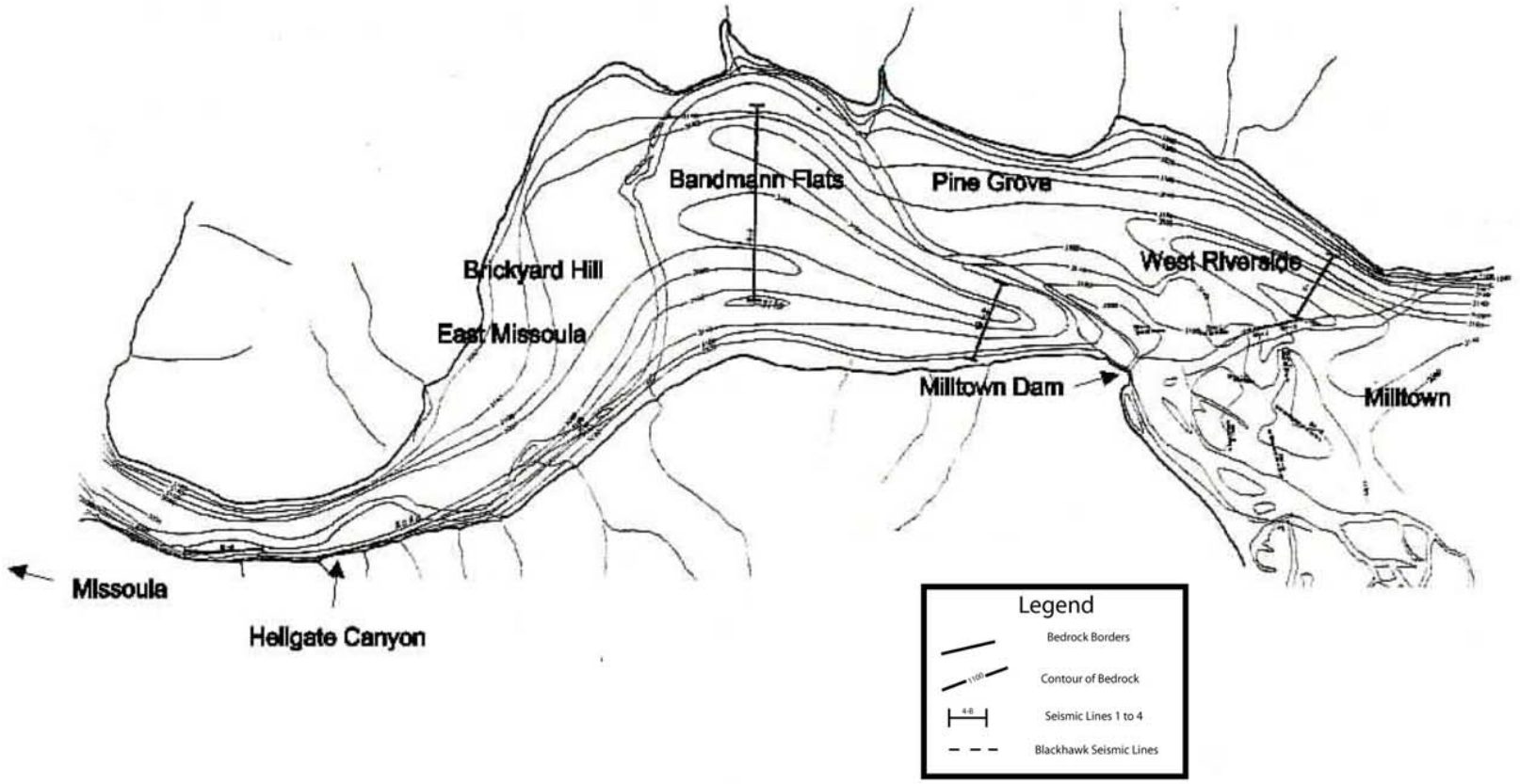

Figure 2. Bedrock model of Gestring (1994), based on bedrock outcrops, well information and seismic lines. This part of the valley outlined in blue on Figure 1.

model constructed by Gestring. The resulting groundwater model proved difficult to calibrate [*Nyquest*, 2001].

To improve on this map, Nyquest (2001) supplemented Gestring's map with a gravity survey of the area. By collecting data at 394 gravity stations and combining those data points with gravity data from the National Geophysical Data Center and the U.S. Defense Mapping Agency, Nyquest (2001) created a regional gravity profile of the study area. The gravity data were then used to create a depth-to-bedrock model and an improved map of the bedrock surface (Figure 3). Nyquest's (2001) map contained considerably more detail than Gestring's and differed in many places. In addition to the gravity measurements collected by Nyquest (2001), Anthony Bertholote collected 204 new gravity stations in 2006. The new gravity stations extend the survey area to the east along the Clark Fork River and to the northeast along the Blackfoot River. In this thesis, I use these new gravity measurements and my own seismic experiments to further improve and extend the bedrock model.

My objective is to test previous results and possibly improve the bedrock surface map in the Milltown Valley area through collection and analysis of seismic data, along with reinterpretation of previously collected gravity data. Nyquest's (2001) bedrock surface map improved upon Gestring's (1994) map. However, Nyquest's (2001) interpretation of the gravity data did not take into account the possible heterogeneity of the valley fill. Nyquest (2001) used a density contrast of -725 kg/m^3 for the valley fill in his model. The density contrast was found by modeling the gravity data with a range of density contrasts. The density contrast that minimized the error between known depths (from wells and drill cores) and the modeled depth was assumed to be correct for the

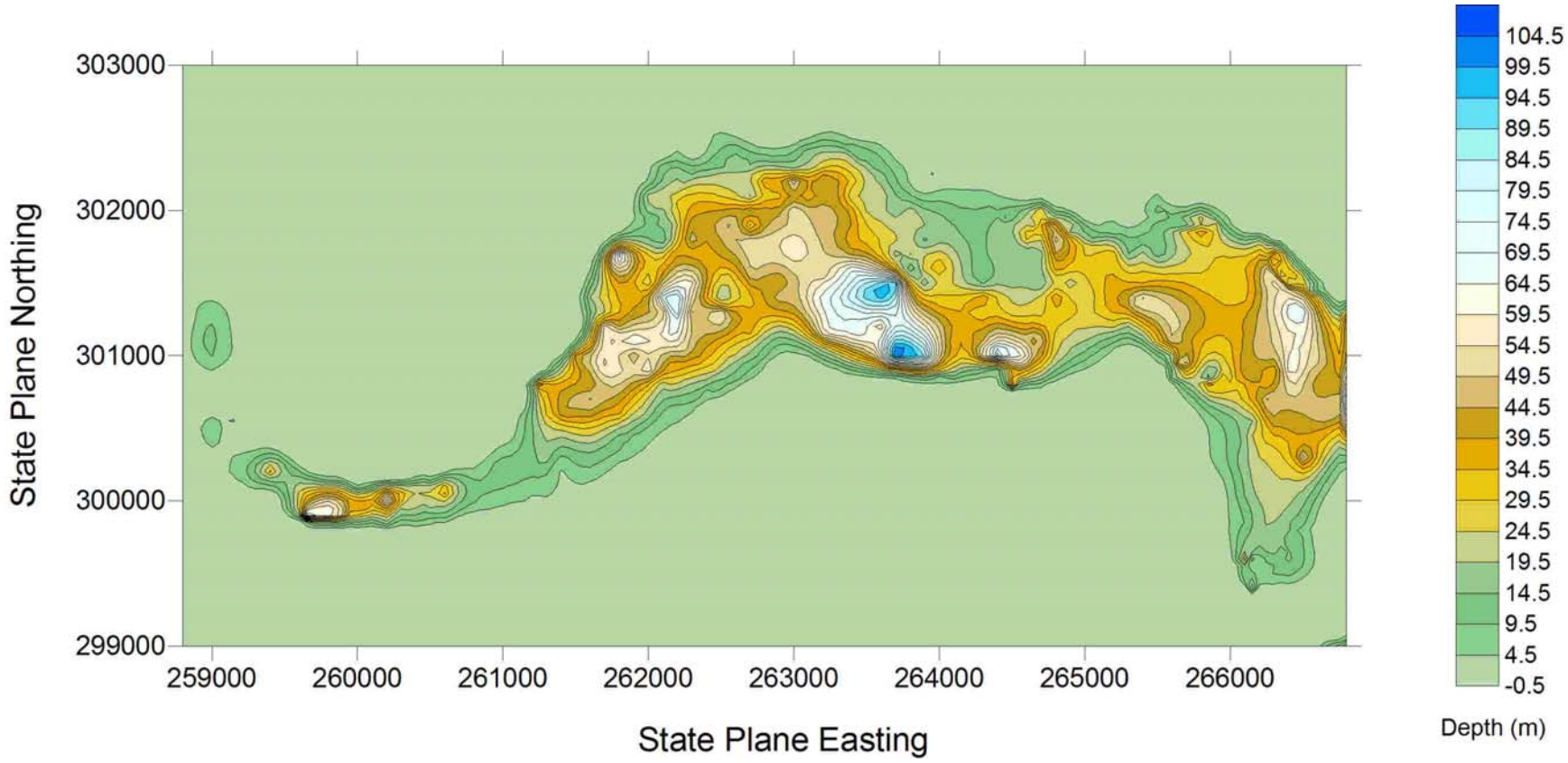

Figure 3: Nyquest's (2001) depth to bedrock model. This model was created by inverting approximately 400 gravity measurements collected throughout the valley. This map shows many features that were not previously mapped in Gestrings (1994) depth to bedrock model. This map is in the same location as the map presented in figure 2.

entire valley. In order to test if the density contrast varies with depth, the reinterpretation of the gravity data I performed involved allowing the density of the valley fill to increase with depth. The seismic reflection data collected throughout the area provide an additional control on the interpreted gravity data. By comparing the interpreted seismic data to the gravity model the accuracy of the gravity model can be validated. Also, there are many known depth-to-bedrock data throughout the valley from previous seismic data, drill core data and groundwater wells completed to bedrock (Appendix A) which can be used to validate the final bedrock map. The final product is a map of bedrock elevations that is constrained with all available data, which includes: depth to bedrock from drill core data from cores and wells completed to bedrock, bedrock outcrops, gravity data, and seismic refraction and reflection data.

SEISMIC DATA COLLECTION AND INTERPRETATION

Introduction

Nyquest (2001) presents a depth to bedrock model based mainly on gravity measurements. Parts of this map are not well constrained due to lack of depth control (i.e. drill core and well data) and sparse gravity measurements. Some of these areas appear to be sufficiently shallow to conduct an engineering-scale seismic reflection survey to test Nyquest's (2001) interpretations. I conducted three surveys at locations throughout the valley based on access and proximity to wells. Nyquest (2001) referenced the seismic refraction data used by Gestring (1994) to construct his bedrock model. The data from these seismic surveys is contained in Appendix A, which consists of all known depth to bedrock points.

Seismic reflection techniques were chosen over seismic refraction techniques for two main reasons. First, seismic refraction surveys had already been successfully completed in the survey area. I wanted to test seismic reflection methods to see if I could produce similar results. Second, the increase computing technology since the 1970's and 1980's has drastically reduced the time it takes to manipulate and process seismic reflection data. With the computing power available the processing of seismic reflection data takes much less time than it did 30 years ago and results can be found relatively quickly.

I collected seismic data along ten lines located throughout the study area as seen in Figure 4. The lines collected near Bonner Elementary school tested the utility of seismic reflection techniques for determining depth to bedrock. The lines collected in the Bandmann flats were used to directly compare results from the gravity interpretation and

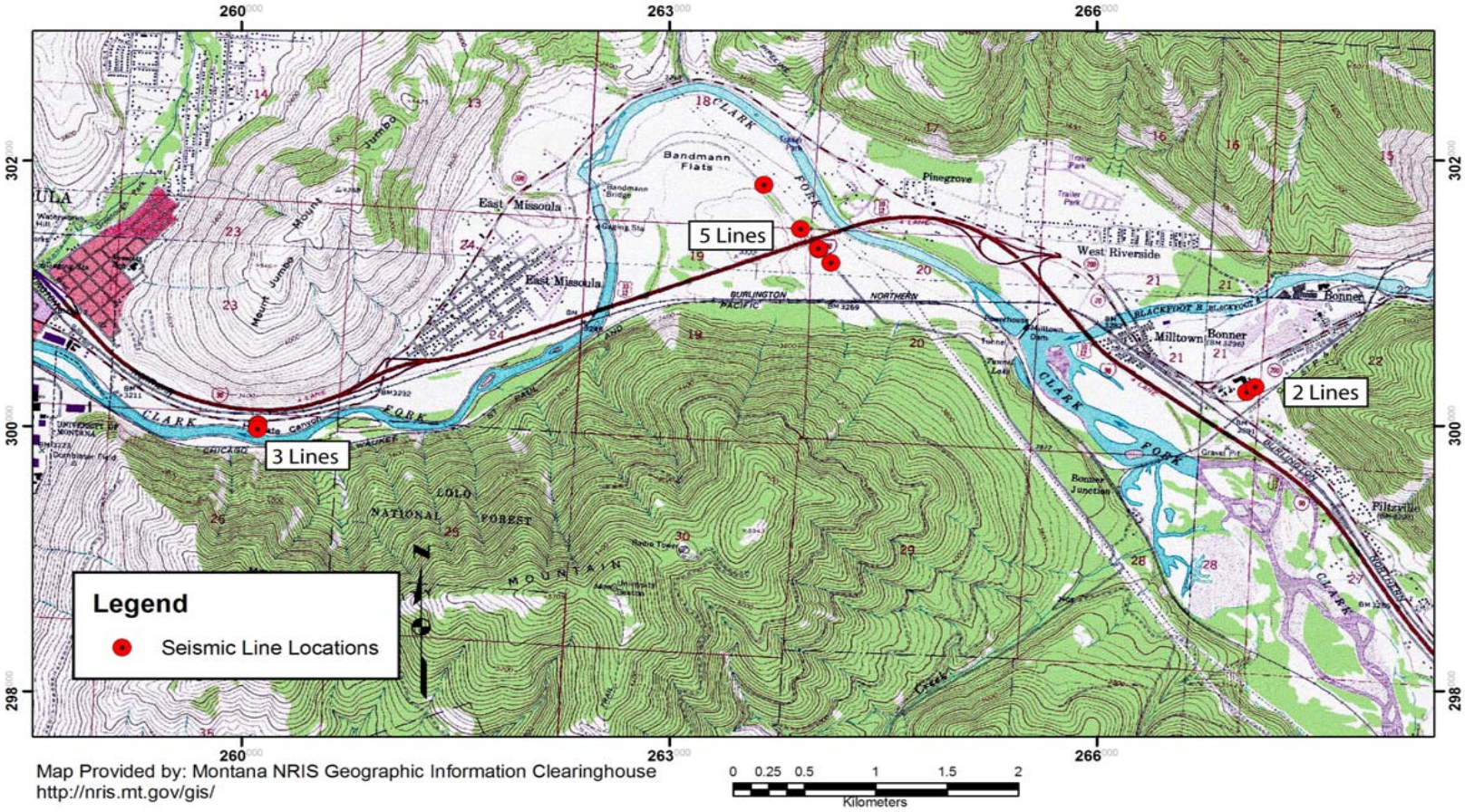

Figure 4: Location of the seismic lines collected in 2005. Three seismic lines were collected in the Hellgate Canyon in Hellgate Park. Five seismic lines were collected in the central part of the study area along Deer Creek Road. Two seismic lines were collected at the east end of the study area behind Bonner Elementary School.

the seismic interpretation. The lines collected in Hellgate Park were a test of the maximum depth possible using engineering scale seismic reflection techniques with the available equipment; the seismic source used is the main limitation.

Seismic reflection surveys measure the time taken for an elastic wave to travel from a source through the subsurface to an interface between rock types where it is reflected and returns to the surface, where it is recorded by a receiver. The receiver measures the ground deformation caused by the returning elastic wave and the travel time of the wave from the source to the receiver. An array of receivers is used to collect these data over the length of the survey line. For this survey I used a Bison Instruments accelerated weight drop as the energy source (Figure 5). To record the arrivals of the refraction and reflection waves I used a Geometrics Smartseis 24 Channel seismograph and twenty-four 40 hertz geophones.

I collected the seismic data with the optimum offset-technique [*Pullan and Hunter*, 1991; *Steeples and Miller*, 1991], the offset being the distance between the source and a geophone. For each source location there are at least three types of waves that return to the receivers on the surface: the refracted wave or direct wave, the reflected wave and ground roll, all arriving at different times. The optimum offset distance is the offset from the source to a geophone at which the reflected wave arrives between the direct wave and the ground roll (Figure 6). The optimum offset technique constructs a seismic section one seismic trace at a time, one from each location of the Bison Instrument signal source.

The optimum offset technique streamlines the field collection process, allowing the geophone array to remain stationary and only requiring the shot point to move. The

Figure 5: Bison Industries elastic wave generator. This accelerated weight drop system works by dropping a steel beam (yellow arrow) into the ground. The beam is lifted using a hydraulic ram (blue arrow) and is accelerated into the ground using a large elastic band (red arrow). This source is capable of generating a large amount of seismic energy.

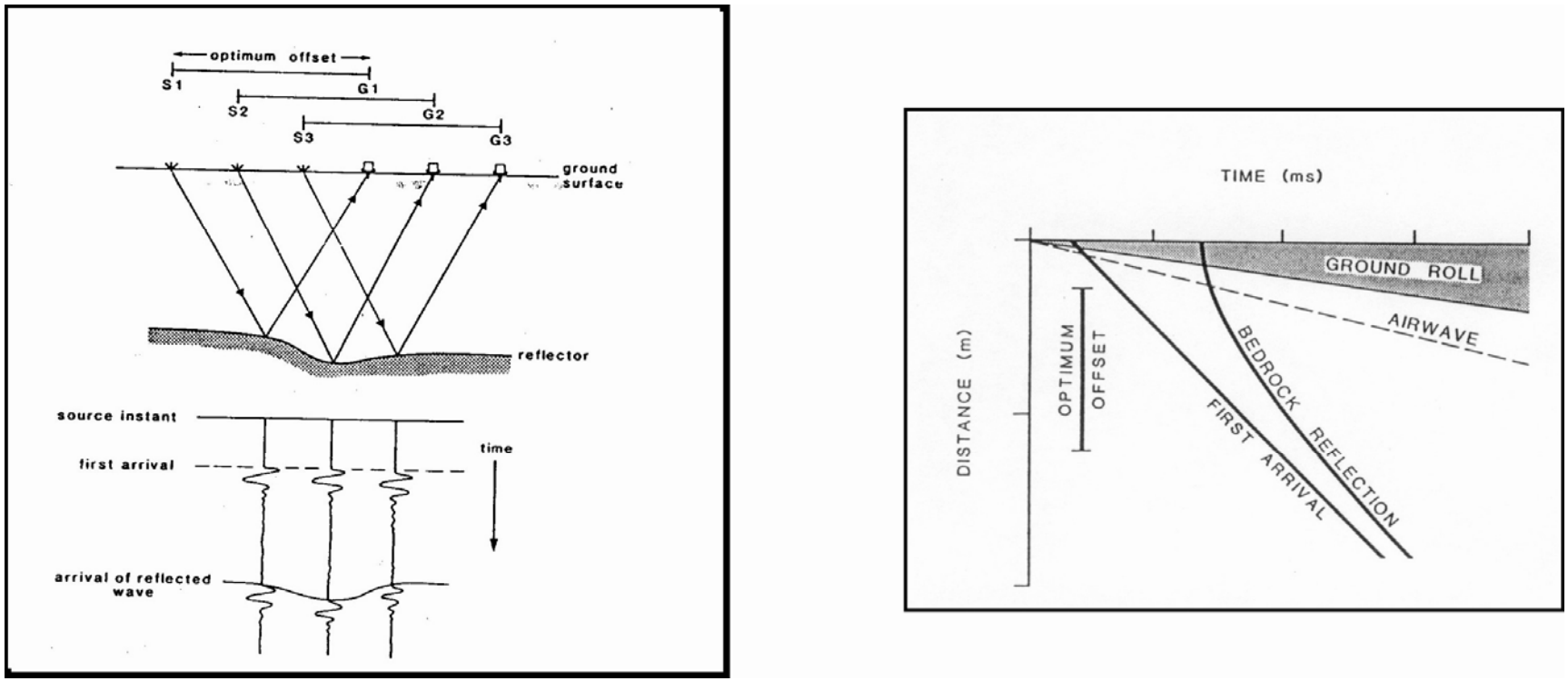

Figure 6: The optimum offset technique for seismic reflection surveys. The panel on the left shows the basic principle of the optimum offset technique. A single geophone is used to record the arrival of the different waves. The geophone and the source are separated by the optimum offset. Each geophone (labeled G) and source (labeled S) pair represent one trace of the final seismic section. The panel on the right shows why optimum offset works. The reflected wave from bedrock arrives after the first arrival but before the ground roll and airwave. This simplifies the collection and processing of the seismic data. Figure taken from Pullan and Hunter (1991).

optimum offset is specific to each location and set of subsurface conditions and can be determined after the data have been collected. The primary benefit of the optimum offset technique over other seismic reflection techniques (common midpoint gathers and common shot point gathers) is that it simplifies the processing. In both common midpoint gathers and common shot point gathers the processing required to generate a final section requires more steps and more user inputs. A common midpoint survey processed by two different processors may produce different results, based on each processor's choice of inputs [Reynolds, 1997]. An optimum offset survey requires fewer steps and less user inputs to process, reducing the likelihood of a processing mistake and increasing the repeatability of the experiment.

Seismic Data Collection

For each seismic reflection line, the geophones were arranged in a straight line with a spacing of two meters. The Bison elastic wave generator was initially positioned 12 to 30 meters in line from the first geophone depending on estimates of the depth to bedrock from Nyquest's (2001) map or water wells located nearby. The source was triggered three times, and the data from each triggering were added together in phase to cancel random events and thereby improve the signal to noise ratio. The source was then moved closer to the first geophone by two meters, and the process repeated. This entire procedure was repeated between 17 and 30 times depending on site constraints. The location of the first geophone was recorded using a handheld GPS unit and the direction of the line was recorded using a Brunton Compass (Appendix B).

Seismic Data Interpretation

Following acquisition in the field, I used Seismic Unix NT to do the initial processing of the seismic data. Seismic Unix NT was also used to calculate the offset and midpoint of each shot from each of the 24 geophones. The offset is the distance between any geophone and the source, and the midpoint is the location halfway between each geophone and the source. All remaining processing steps were completed using Seismic Unix, a freely distributed Unix-based processing package available from the Colorado School of Mines.

During processing, one starts with raw data (Figure 7), determines and collates the traces at optimal offset for each source location, and proceeds until an interpretable seismic section is created. The ultimate goal is to come up with a result from which one can determine the depth to the velocity contrast between the valley fill and underlying bedrock. For each survey location the data from the first shot at each location was analyzed to determine what the optimum offset should be. By analyzing the seismic signal traces in the section, I determined which trace had the reflected data arriving between the direct wave and the ground roll (Figure 8). Table 1 shows the optimum offset value used for each seismic line. After the optimum offset was determined, the traces that had an offset equal to the optimum offset were extracted from the raw data and placed into a new file. For each source location in a survey there was only one trace that corresponded to the optimum offset, meaning if the survey contained 15 source locations then the new file would contain 15 traces. The result being a seismic profile of 15 traces, each separated by 2 meters, all collected at the optimum offset.

Location	Line	Optimum Offset Value (m)
Bonner School	1	12
Bonner School	2	12
Deer Creek Rd.	1	28
Deer Creek Rd.	2	36
Deer Creek Rd.	3	36
Deer Creek Rd.	4	32
Deer Creek Rd.	5	36
Hellgate Park	1	30
Hellgate Park	2	30
Hellgate Park	3	30

Location	Layer	Velocity (m/s)
Bonner School	1	600
	2	1300
	3	2800
Deer Creek Rd	1	600
	2	1100
	3	2500
Hellgate Park	1	600
	2	1500
	3	**

Table 1. Velocity of the three layers for each location along with the optimum offset used at each location. The third layer velocity for Hellgate Park is not listed because the seismic energy did not penetrate to the third layer.

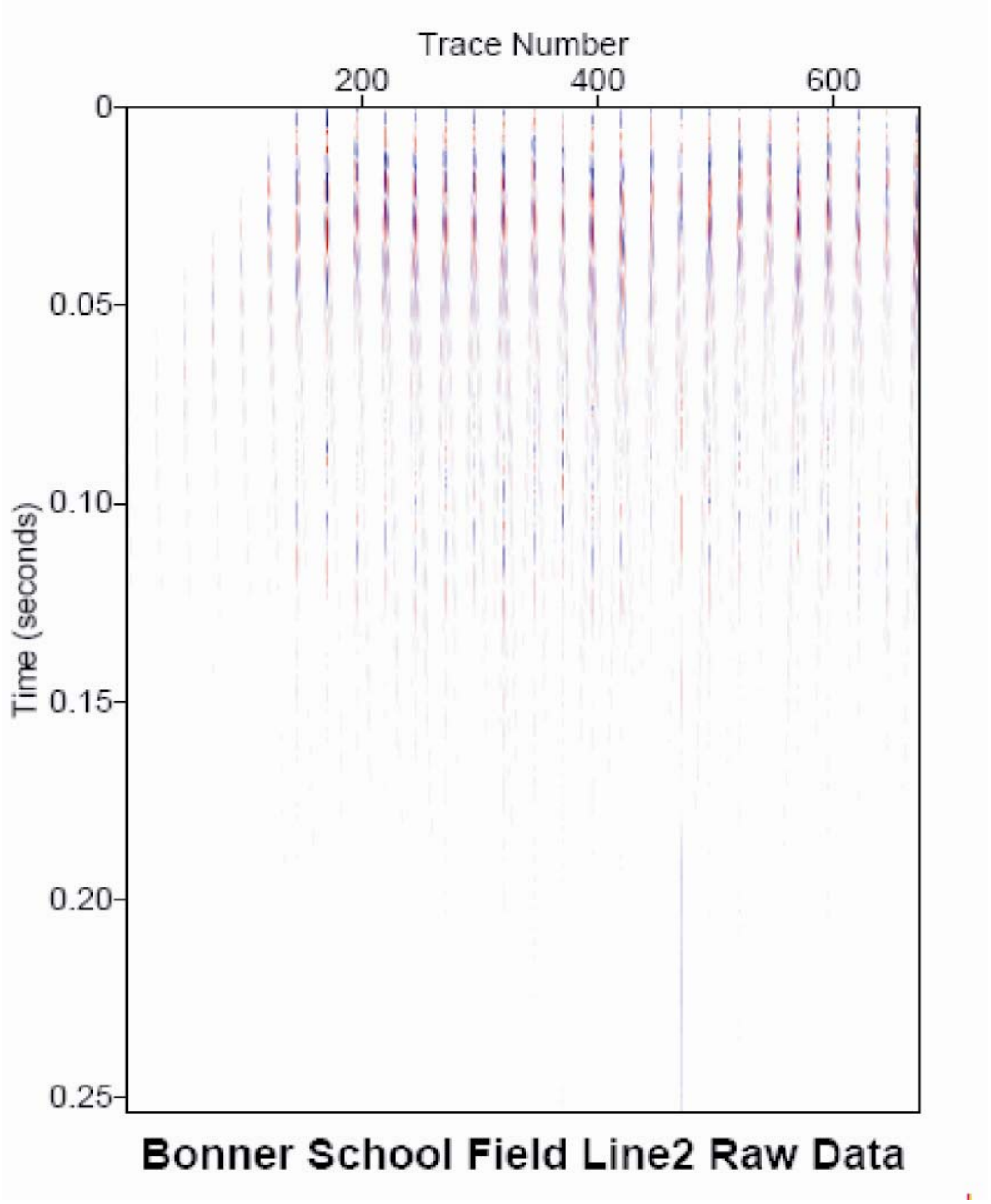

Figure 7: An example of the raw seismic field data collected. The raw field data contains all of the traces from each source location. The next step in processing is extracting the traces that correspond to the optimum offset distance.

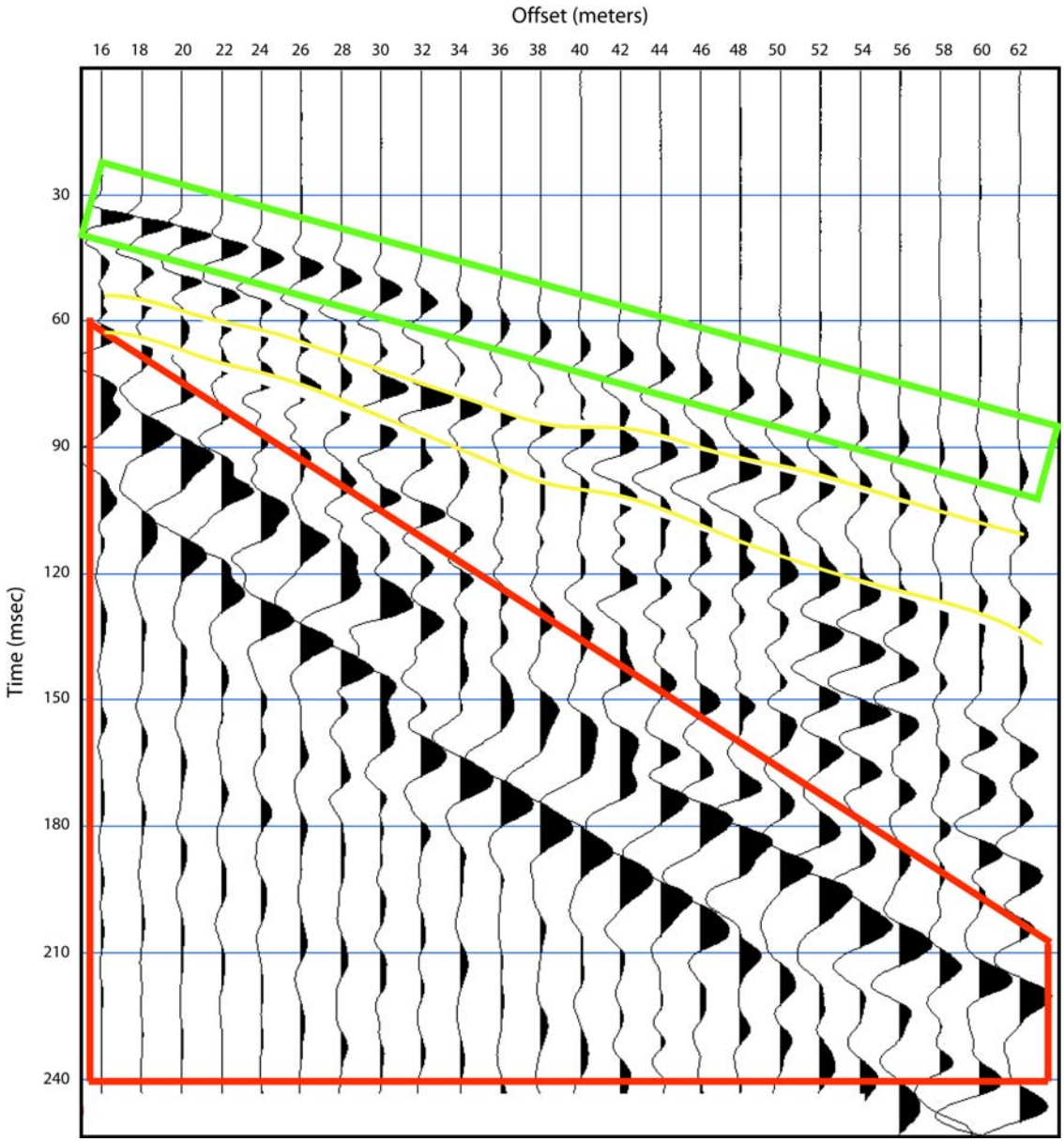

Figure 8: Time distance plot showing the three types of waves present and how the optimum offset is chosen. The waves highlighted by the green box are the arrivals of the direct waves. The waves highlighted by the red box are ground roll and air shock waves arriving. In between the two are the reflected waves of interest, highlighted by yellow. The optimum offset is chosen so that the reflected waves arrive after the direct wave but before the ground roll. The offset chosen for this section is 28 meters.

After collating the optimum offset traces, the traces were filtered to remove unwanted noise and enhance the signal and then were gained using an automatic gain control. Filtering of seismic data involves removing certain frequencies that contain noise (i.e. highway vibrations, wind, power line interference, etc). This is typically done using a bandpass filter which truncates low and high frequencies, leaving only the seismic waves generated by the source. I employed 40 Hz geophones, and the signal source has most of its power between the frequencies of 5 and 70 Hz [*Thompson*, 1997], so filtering out frequencies above and below this range should leave coherent reflection data. Seismic Unix allows one to adjust the upper and lower cutoff frequencies until a satisfactory seismic section results. The bandpass filter tapered from 30 Hz up to 45 Hz and down from 120 Hz to 175 Hz. Looking at a representative section of raw data after collation but before filtering (Figure 9) shows how noise can obscure reflectors. There is low frequency noise present in the section that overpowers what could be reflectors. Looking at the same data after the bandpass filter was applied (Figure 10) shows the unwanted frequencies removed. What are left in the section are now coherent reflectors without unwanted noise to obscure them (Figure 11). Looking at the frequency spectrum of the data before and after the filtering (Figure 12), it is apparent that the low frequency noise was removed, leaving the data between 30 and 120 Hz.

Gaining the data amplifies the seismic signals with increasing time, which simplifies interpretation by making the reflectors more pronounced (Figure 13). Seismic Unix uses automatic gain control which uses the average signal amplitude over a window of time to adjust the gain over the whole seismic trace. The time window size can be adjusted to increase or decrease the level of gain. The automatic gain control window

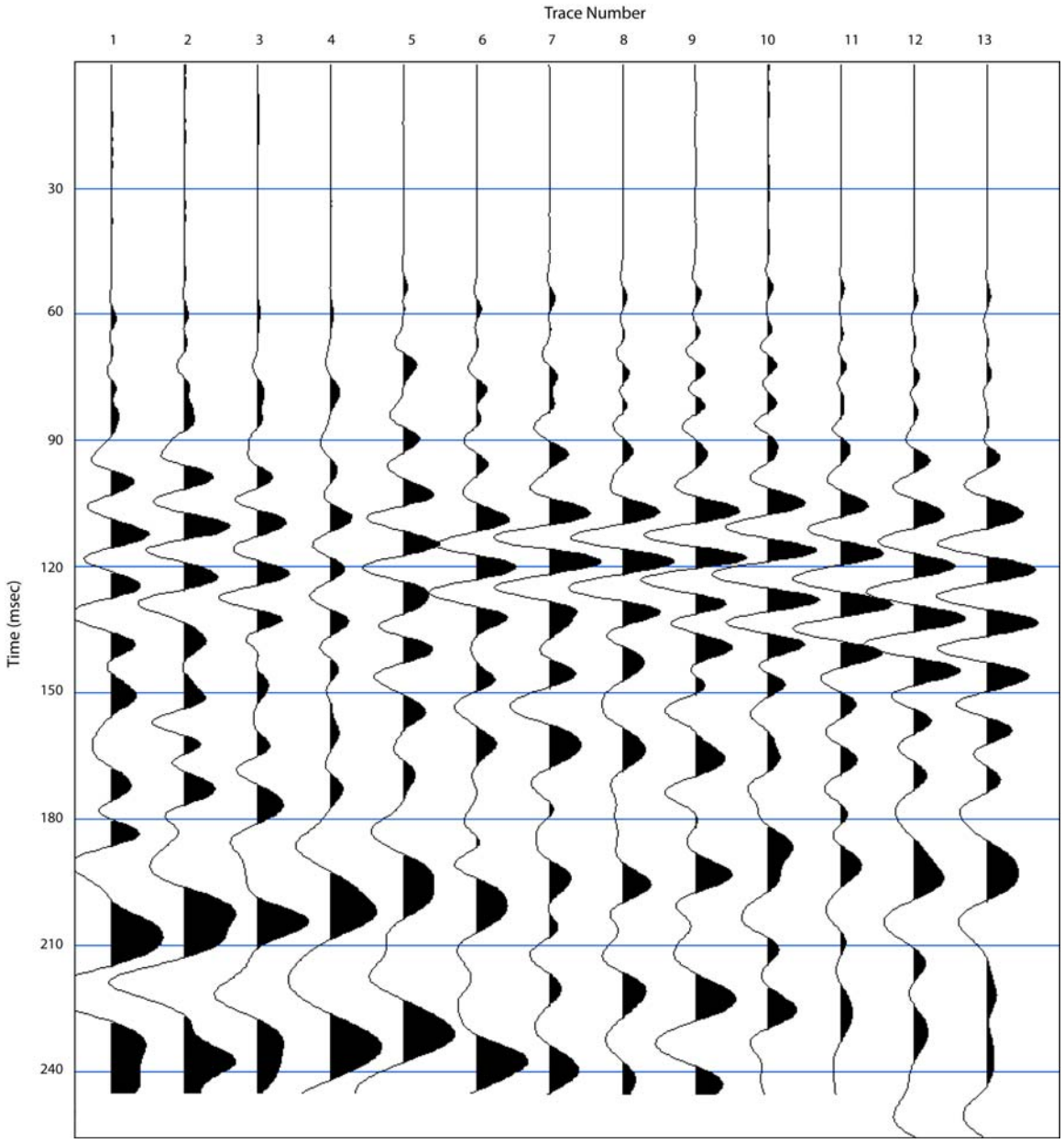

Figure 9: Deer Creek Road Line 2 raw data. Notice the low frequency noise present in the bottom half of the section.

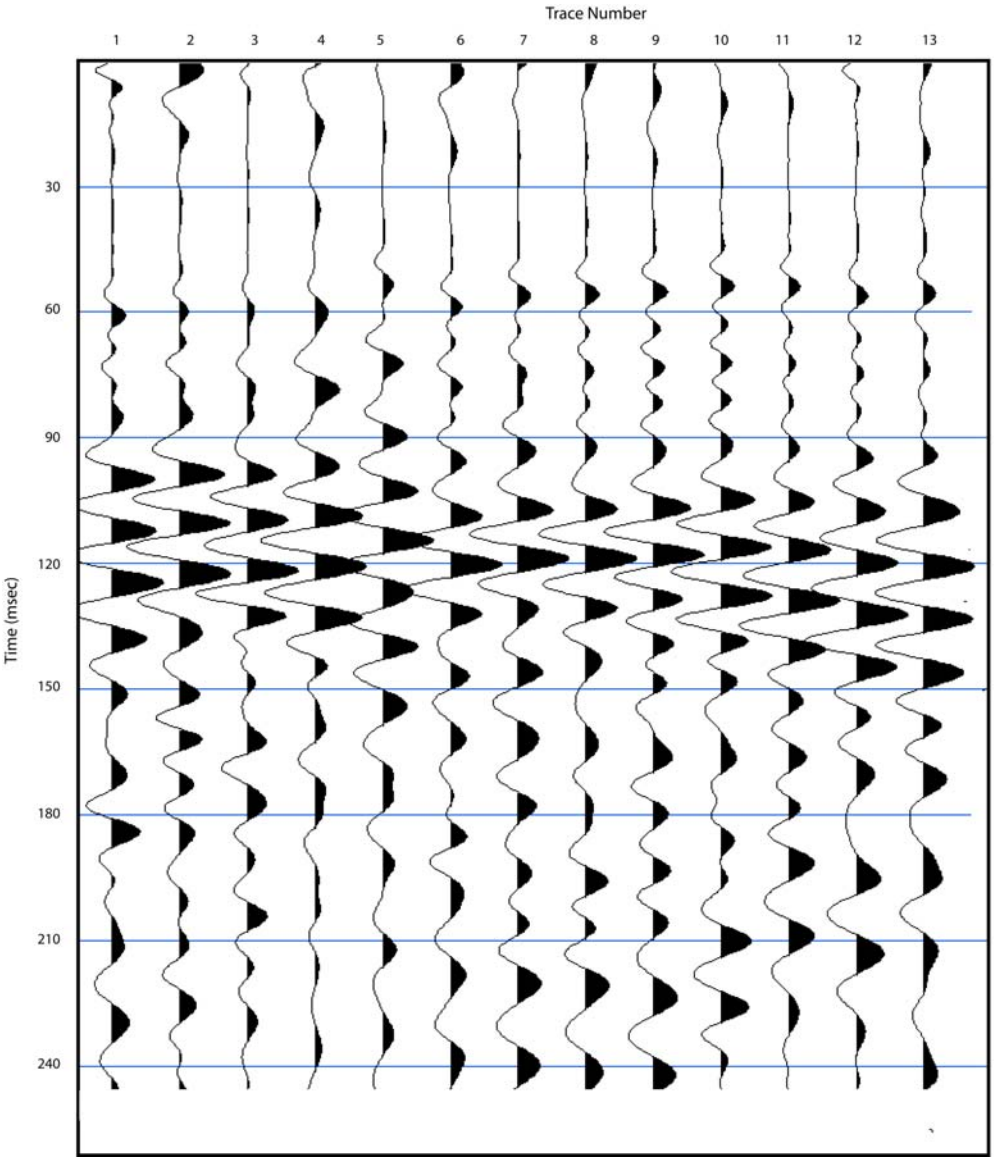

Figure 10: The same data as seen in the previous figure from Deer Creek Road after the bandpass filter was applied. Notice that the low frequency noise that was present in the section has been removed. This leaves the features in the center of the section as the most prominent feature.

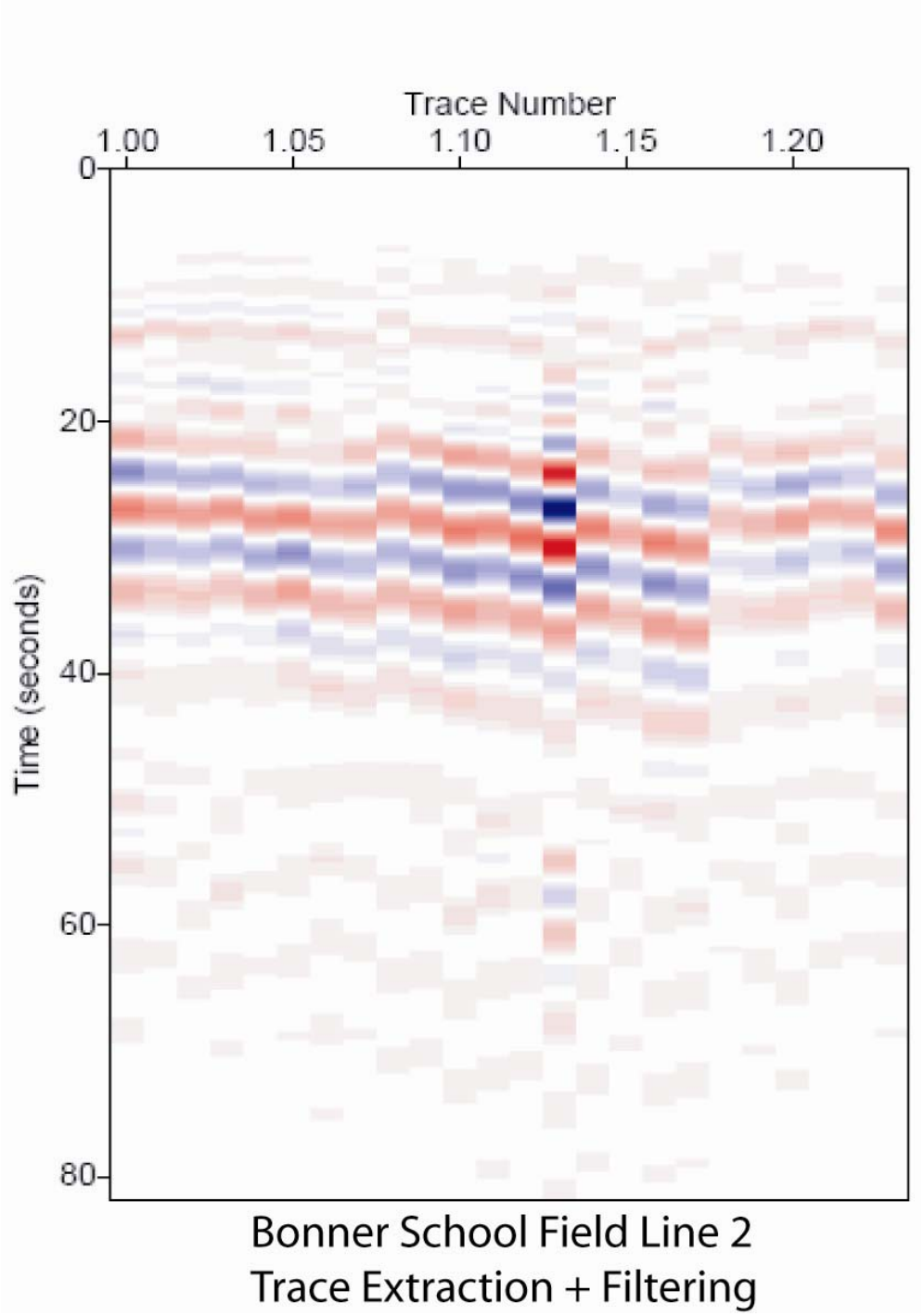

Figure 11: An example of the seismic data after trace extraction. The data went from containing over 600 traces to just 24 traces. The raw field data contained traces with offsets ranging from 2 meters to 60 meters. The extracted traces all have the same offset which corresponds to the optimum offset. The data was also filtered using a band pass filter to remove both high and low frequency noise.

Frequency Spectrum Pre Filter

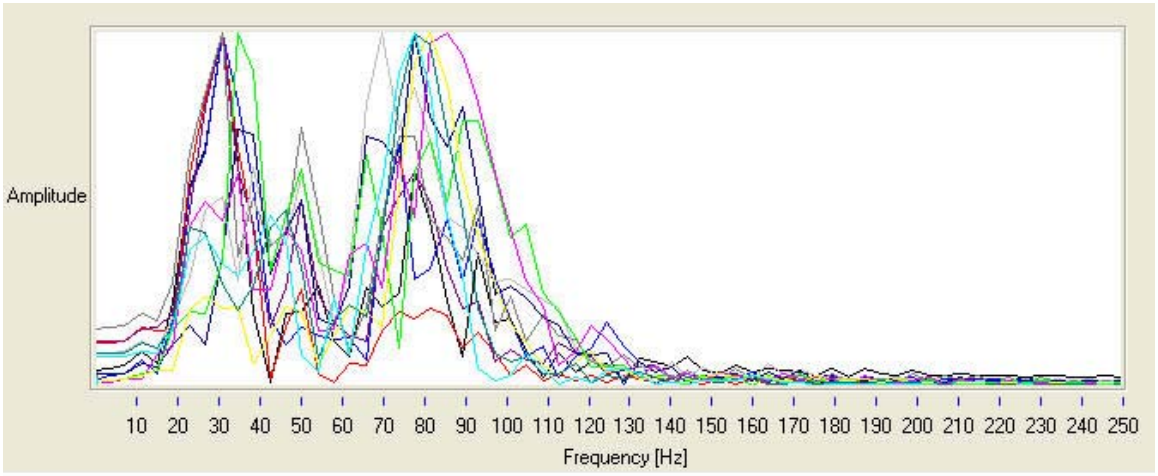

Frequency Spectrum Post Filter

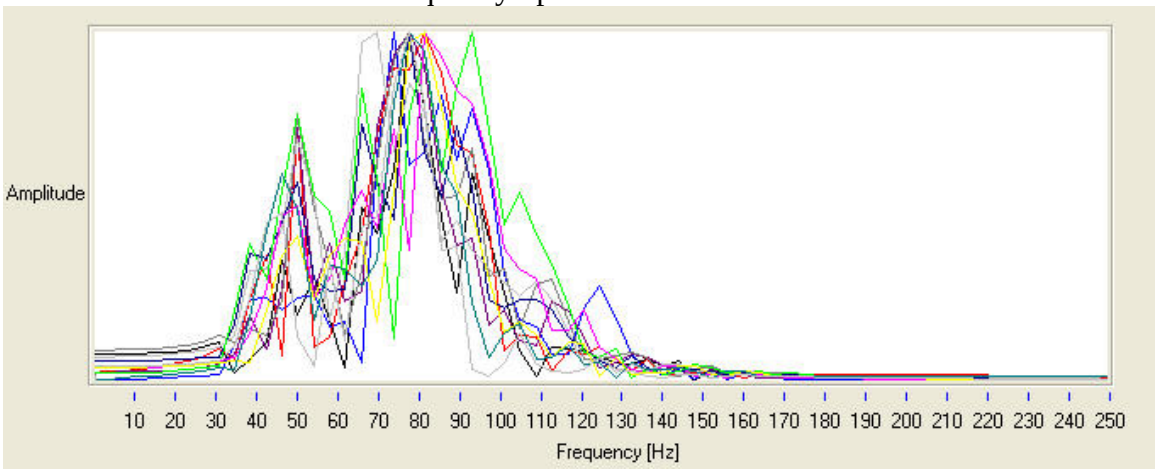

Figure 12: Frequency spectrum of the data shown in the previous two figures. The top panel shows the frequency spectrum of the unfiltered data and the bottom panel shows the frequency spectrum of the filtered data. In the unfiltered data there is a large amount of amplitude present in the low frequencies (below 35 Hz). Filtering the data removes the low frequencies while leaving frequencies that contain reflection data (40 to 130 Hz).

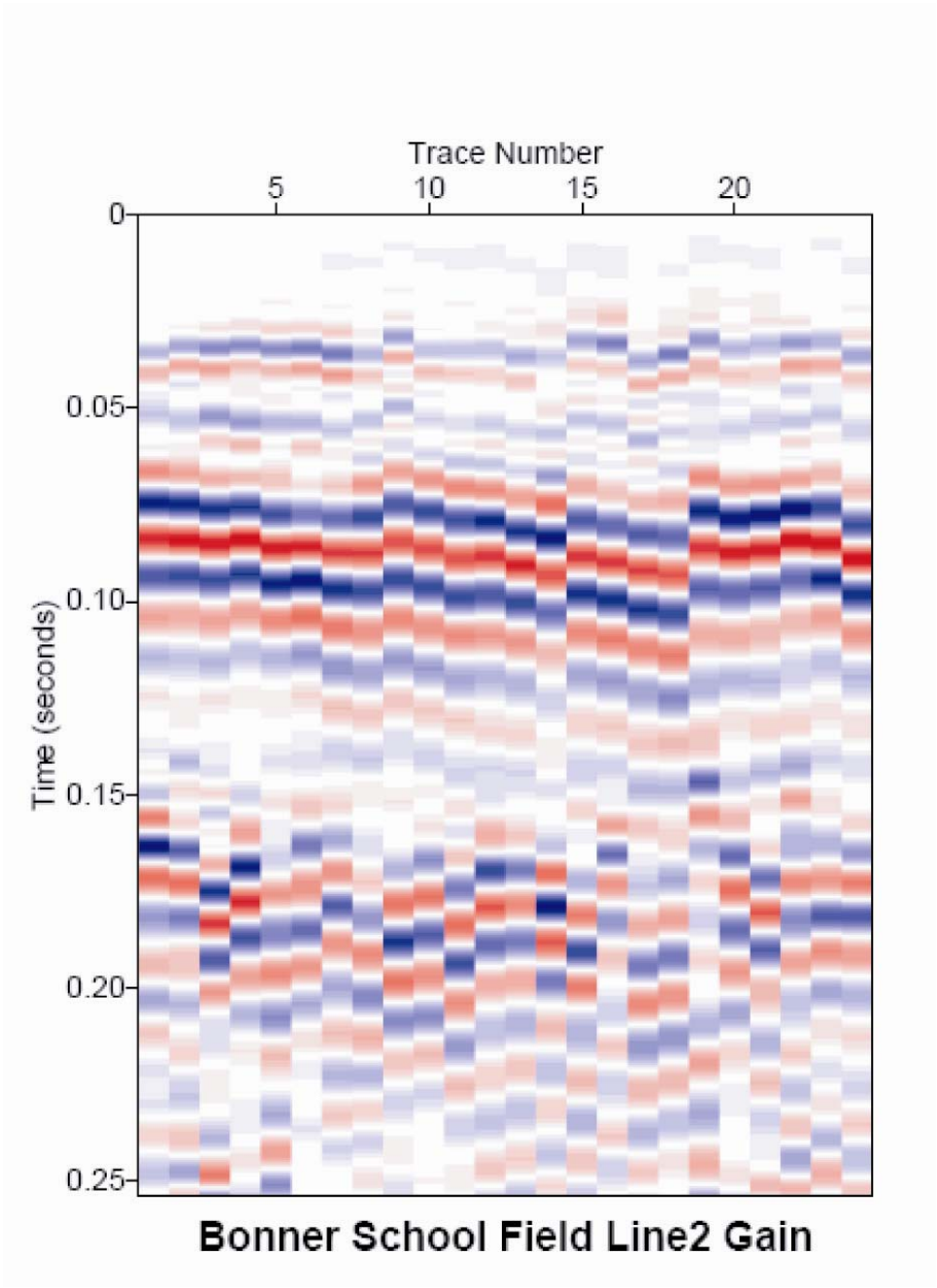

Figure 13: An example of seismic data that has been filtered and gained. The data is amplified using automatic gain control. This increases and normalizes the signal making it easier to see and interpret what is happening. At this point the seismic data is ready for interpretation.

was set to 0.09 seconds. All data collected were processed in a similar manner using the same filtering and gain parameters.

To interpret each line the velocity of the first layer needed to be determined. The velocities of the layers are related to the first arrival times in the seismic record (Figure 14). The first arrivals are the direct wave traveling through the uppermost layer or critically refracted waves from subsequently deeper layers [Reynolds, 1997]. To find the velocity, the first arrival times are plotted on the y-axis and the distance between the receivers are plotted on the x-axis (Figure 15). The points should all fall on a straight line (time = distance / speed) and the inverse slope of the line yields the velocity of the layer. Breaks in the slope of the line represent the next deepest layer, with the number of breaks in slope representing the number of layers visible in the seismic section. An assumption made in interpreting the data is that the velocity of each layer is consistent for the entire depth extent of the layer, and the only changes in velocity occur at the interface of two layers. For this assumption to hold the first arrival times for each layer have to lie along a straight line. If the velocity changed gradually with depth then the plot of the first arrivals would lie along a curve. Looking at a representative time-distance plot (Figure 15), the first arrivals plot along straight lines with an R^2 value of 0.98 or higher, meaning the assumption of a constant velocity within each layer holds true.

Table 1 shows the velocity of the different layers for each location, and Figure 16 represents the data graphically. The velocity of the first layer is consistent at each location, approximately 600 m/s. This falls within the ranges of dry sand (200 to 1000 m/s) and near surface (less than 2 km) sand and gravel (400 to 2300 m/s) [Reynolds, 1997]. The velocity of the second layer varies slightly from location to location, ranging

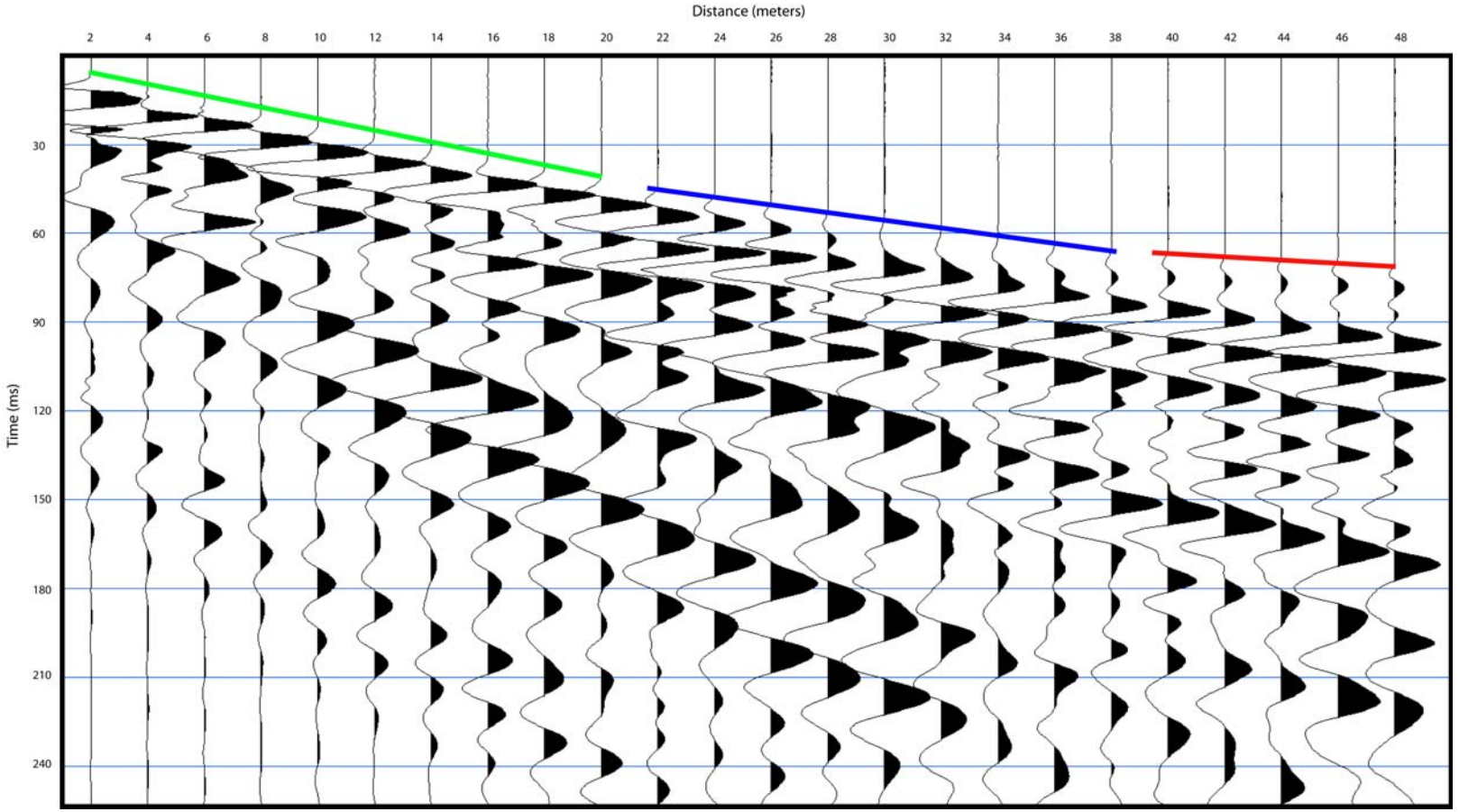

Figure 14: First arrival picks from a time distance plot. The first arrivals are the direct wave arriving at the geophone and can be seen as a deflection of the trace to the left. Plotting a straight line through the first arrivals determines the velocity of each layer. In this plot there are three distinct changes in the slope of the first arrivals, corresponding to three different layers.

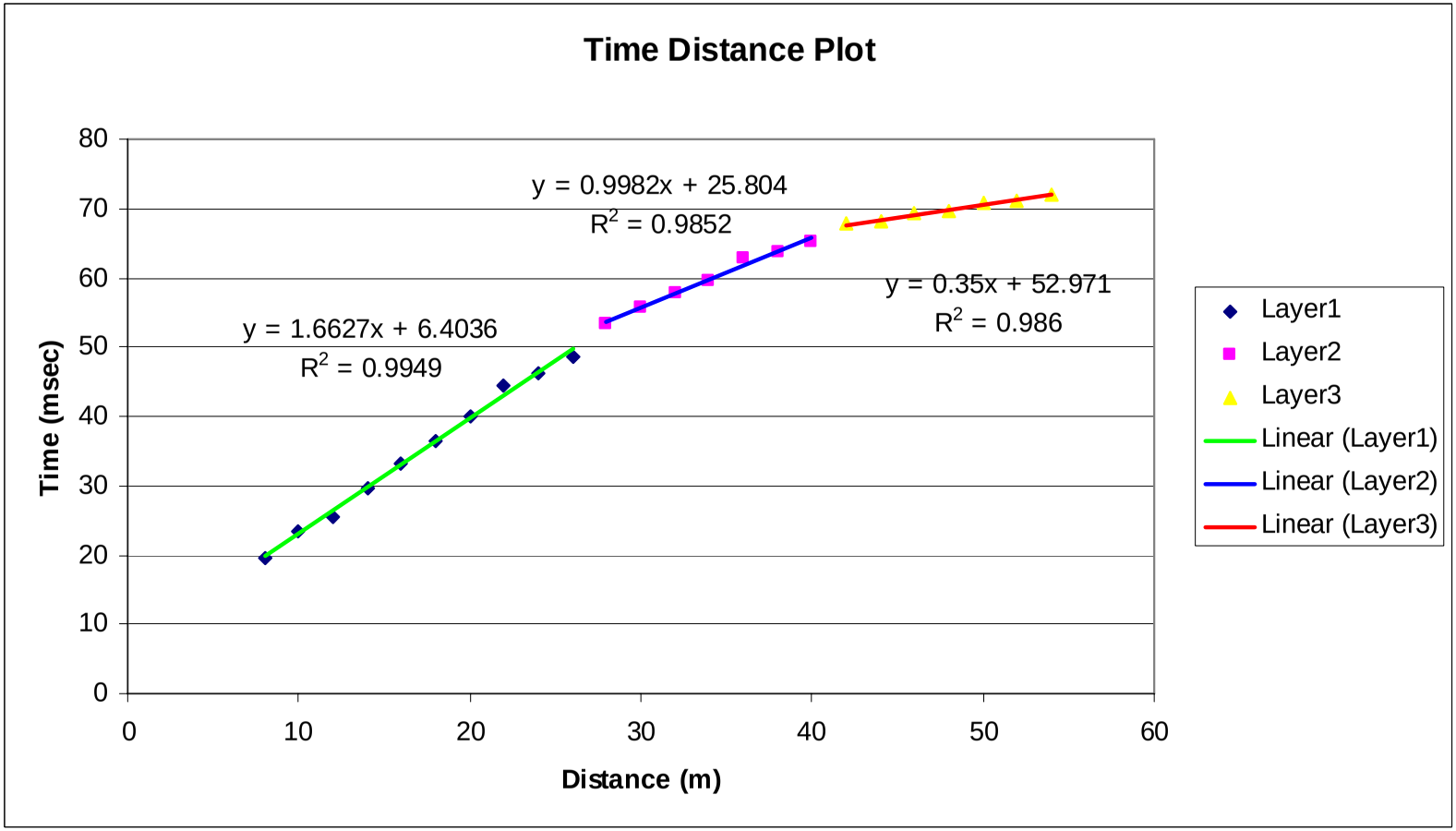

Figure 15: Linear velocity analysis plot. The x axis shows the distance of the geophone from the source location and the y-axis shows the arrival time in milliseconds of the first arrival of seismic energy. There are three groups of points, each group falling along a straight line with a specific slope. The slope of the line is the inverse of the velocity of each layer. The R^2 value for each line is close to 1, meaning statistically the points fall along a straight line. The colors of the lines correspond to the lines through the first arrivals on the previous figure.

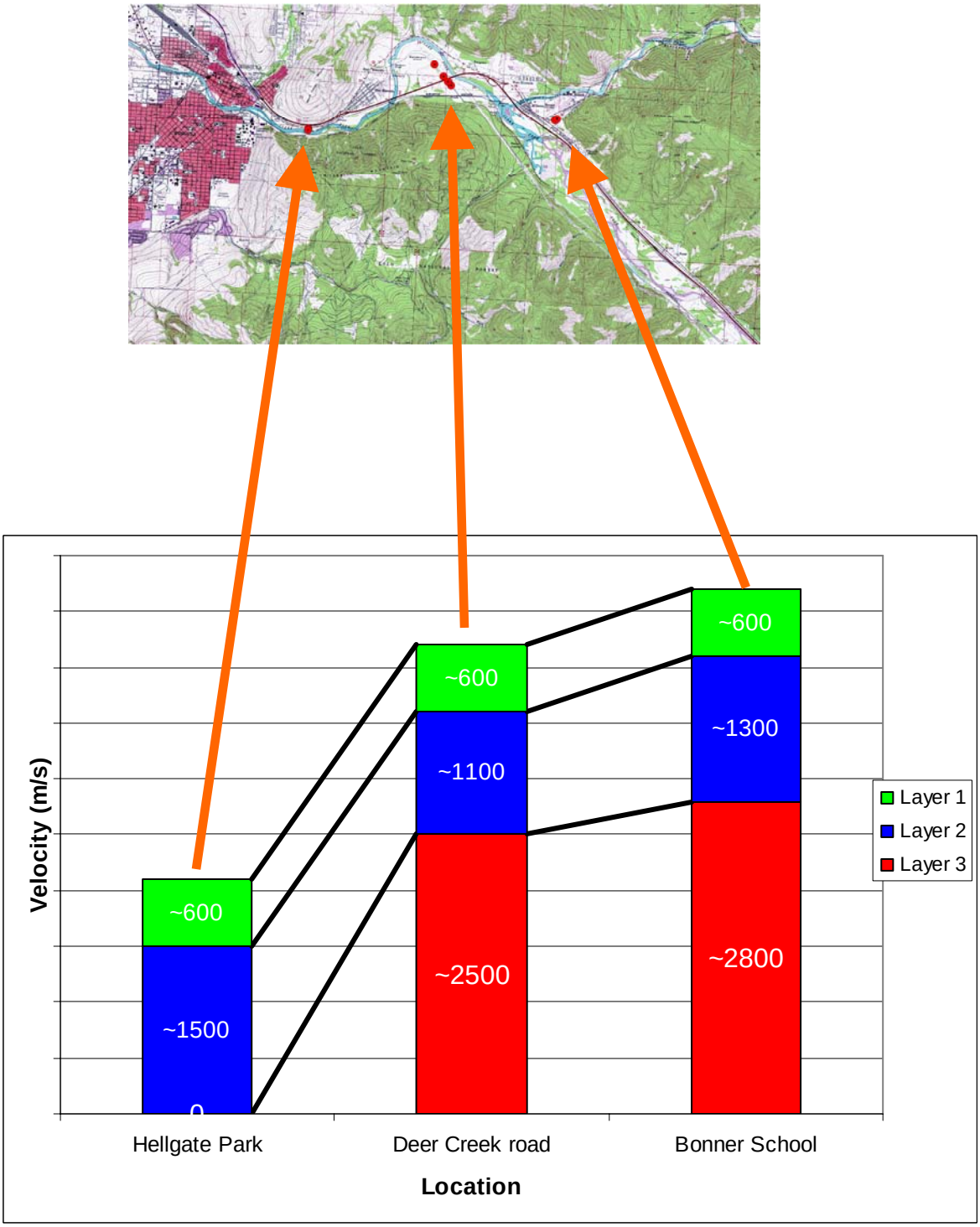

Figure 16: Results from the velocity analysis of the seismic data at three different locations across the valley. The velocity of each layer is the result of averaging the velocity data from a number of source locations on each line collected. The velocity of each layer is consistent across the valley. Hellgate park does not have a layer 3 velocity because the third layer is to deep to see. Velocities are listed as m/s.

from 1100 m/s along Deer Creek Road to 1900 m/s in Hellgate Park. The velocity increase between layer 1 and layer 2 is due to the valley-fill being saturated with water [Reynolds, 1997]. The seismic lines collected behind Bonner Elementary school and along Deer Creek Road show a third layer in the direct wave arrivals. This layer has a velocity of approximately 2800 m/s which matches the velocity of the underlying bedrock (2500 to 3000 m/s) [*Blackhawk Geosciences*, 1990]. The velocities listed were found by averaging the velocity of each layer found using each source location. Appendix C contains details on the processing steps used.

The final step in interpreting the seismic data consists of picking the reflectors on each of the processed seismic sections. In some of the sections the reflectors are fairly apparent, while, for others, choosing reflectors requires more finesse. Once the reflectors are chosen, the two-way travel time for each reflector can be determined. Multiplying one half of the two-way travel time by the velocity of the first layer yields the depth of the reflector. These reflectors can then be translated into depth to bedrock [*Bradford*, 2002; *Goforth and Hayward*, 1992; *Steeples and Miller*, 1998].

Seismic Results and Discussion

Two seismic lines were collected in the field north of Bonner Elementary School at the east end of the study area (Figure 4). The first line consisted of 768 traces collected from 24 geophones and 32 positions of the Bison signal source, resulting in 32 optimum offset traces. The second line contained 864 traces that resulted in 36 optimum offset traces. Figures 17 and 18 show the final processed seismic sections from Bonner Elementary. In both sections there are two prominent reflectors located above 0.1

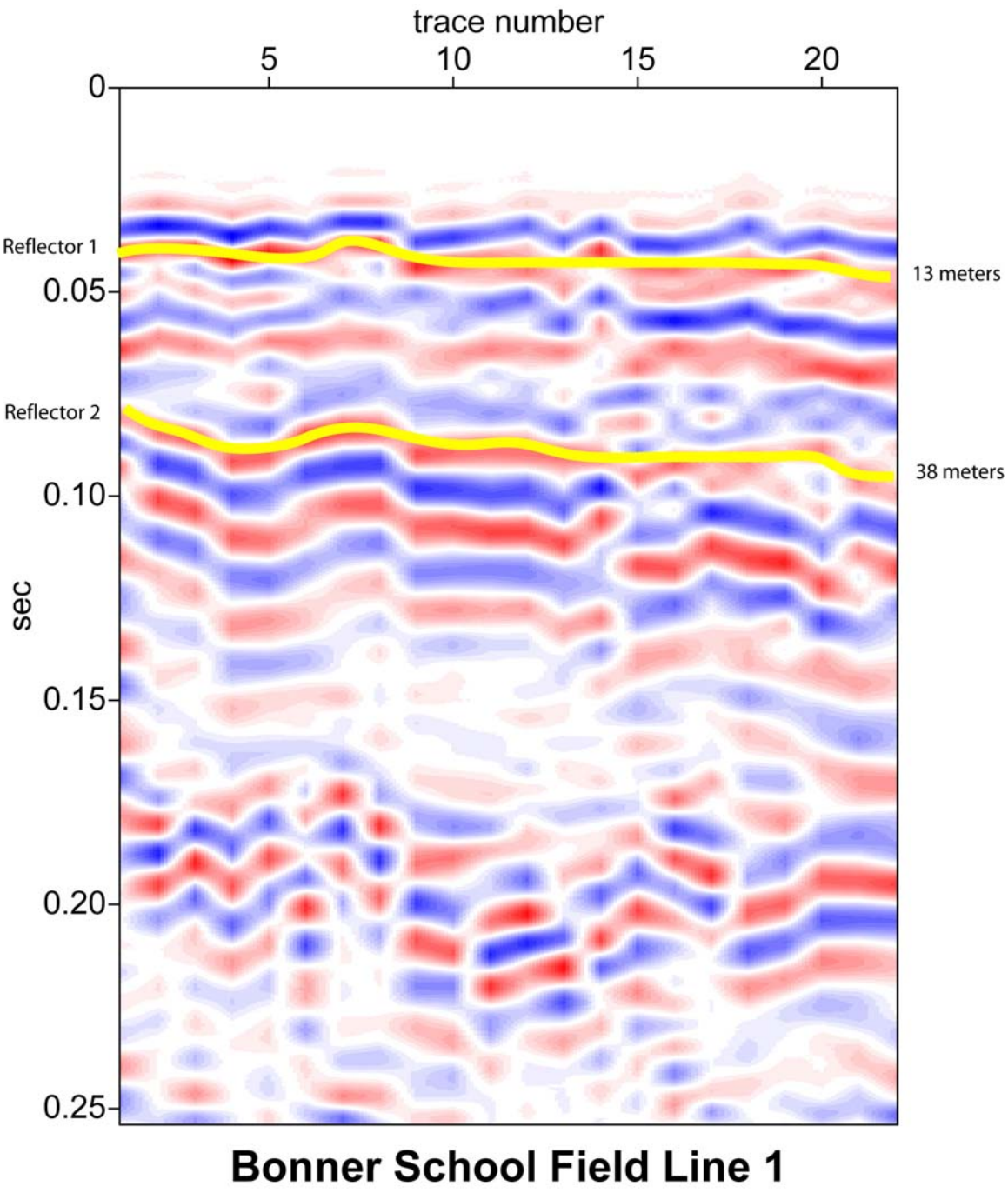

Figure 17: Final interpreted seismic section from Bonner Elementary School Line 1. There are two possible reflectors interpreted on this section; one at approximately 13 meters and one at approximately 38meters. The trace separation is 2 meters.

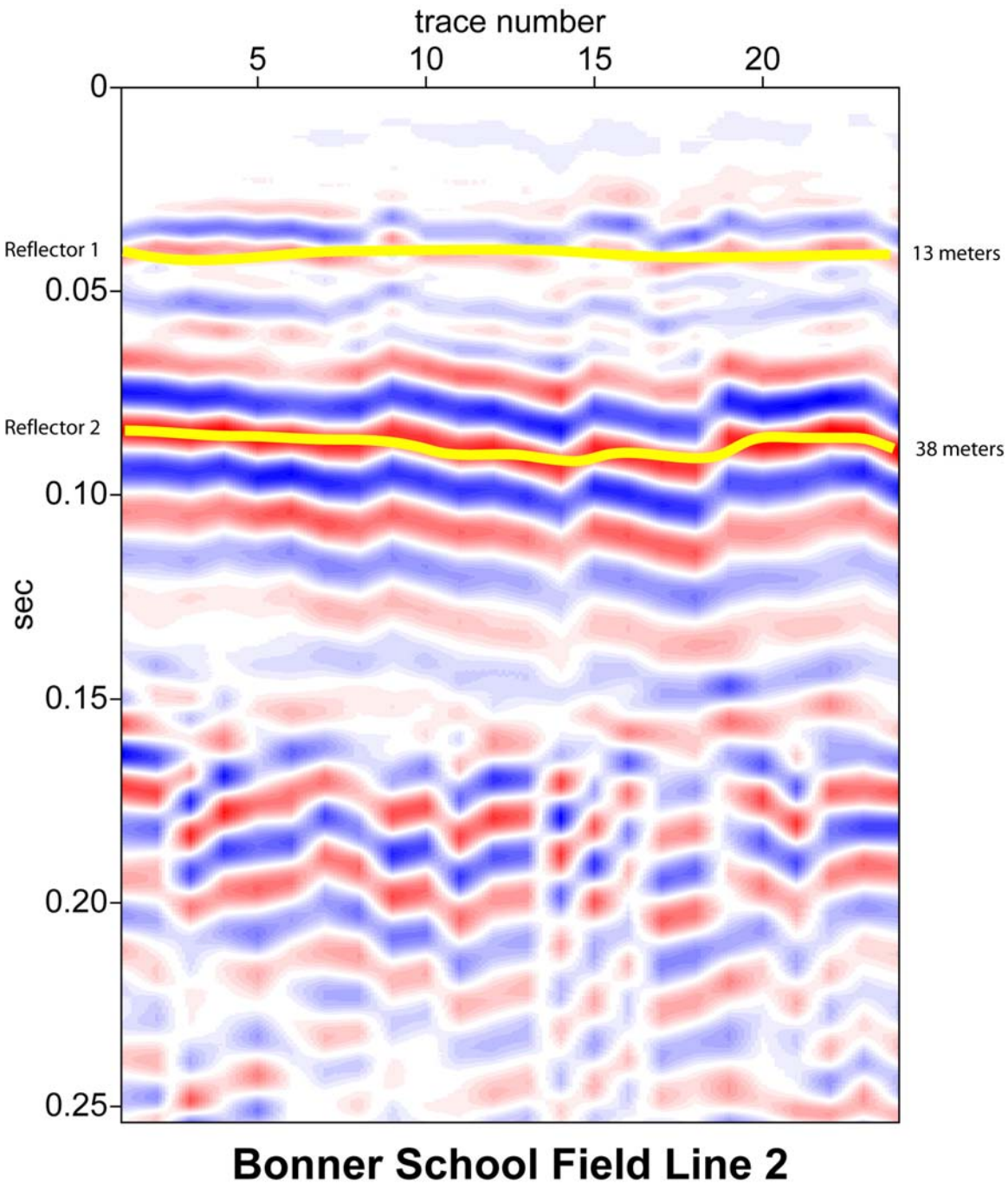

Figure 18: Final interpreted section from Bonner Elementary School Line 2. There are two reflectors interpreted on this section; one at approximately 13 meters and a second at approximately 38 meters. The trace separation is 2 meters.

seconds, one at approximately 0.04 seconds and one at approximately 0.08 seconds. Using the first arrivals to determine the velocity yields a velocity for the first layer of approximately 600 m/s and a velocity of the second layer of approximately 1300 m/s. Using this velocity and the two way travel times the depth of the first reflector is approximately 13 meters deep, and the second reflector is 38 meters deep. The depths of the first reflectors, at approximately 13 meters, are much shallower than the known depth to bedrock of 38 meters from a well drilled approximately 50 meters to the north east. I interpret this reflector to be the water table in the area. The velocity above and below the reflector is approximately 600 m/s and 1300 m/s respectively, which is typical for a change from dry sand to saturated sand. The second reflector in both sections occurs at approximately 38 meters in depth, which matches the bedrock depth from the well. This reflector is the strongest reflector in both sections and occurs at the same depth in both sections. The velocity below the reflector is 2800 m/s , which is a typical velocity for Belt Supergroup rocks [*Blackhawk Geosciences*, 1990]. Table 2 summarizes the data from Bonner School Field.

Five seismic lines comprise the Deer Creek data set. These lines cross Bandmann Flats in the central part of the study area (Figure 4), each containing contains 336 traces, and resulted in 14 optimum offset traces per line. Figures 19 through 23 show the final processed sections. These sections were collected along the road where there was less control over environmental factors like road traffic and urban noise. Despite using various gain functions and a multitude of different frequency filters, I was not able to produce sections with signal-to-noise ratio as high as in the Bonner area. Consequently the sections are more difficult to interpret than the sections from Bonner School Field.

Bonner School Field				
Line	Reflector	2-way Travel Time (ms)	Velocity	Depth (m)
1	1	0.04	600	13
1	2	0.08	1300	38
2	1	0.04	600	13
2	2	0.08	1300	38

Table 2. Summary of the results from the seismic lines collected behind Bonner Elementary School. Bedrock reflectors are highlighted in yellow

Deer Creek Road				
Line	Reflector	2-way Travel Time (ms)		Depth (m)
1	1	0.09	600	27
1	2	0.135	1100	52
2	1	0.105	600	31
2	2	0.13	1100	45
3	1	0.11	600	33
3	2	0.16	1100	60
4	1	0.099	600	30
4	2	0.14	1100	52
5	1	0.1	600	30
5	2	0.14	1100	52

Table 3. Summary of the results from the seismic lines collected along Deer Creek Road. Bedrock reflectors are highlighted in yellow.

Hellgate Canyon Park				
Line	Reflector	2-way Travel Time (ms)		Depth (m)
1	1	0.055	600	17
2	1	0.06	600	18
3	1	0.075	600	22

Table 4. Summary of the results from the seismic lines collected in Hellgate Canyon Park.

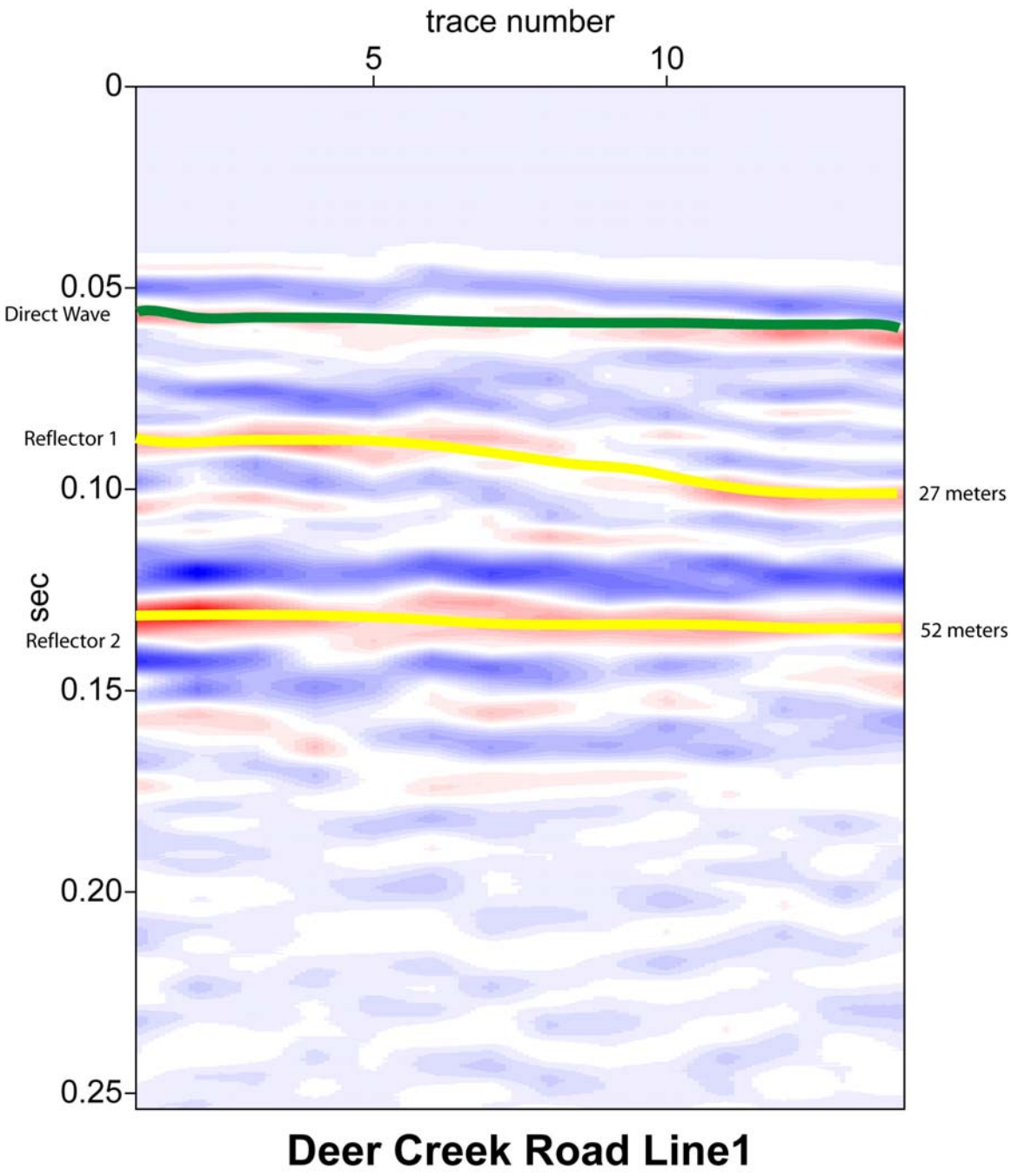

Figure 19: Final interpreted section from Deer Creek Road line 1. This section shows the arrival of the direct wave (green line) and two reflectors (yellow lines). The reflectors occur at 27 meters and 52 meters. The trace separation is 2 meters.

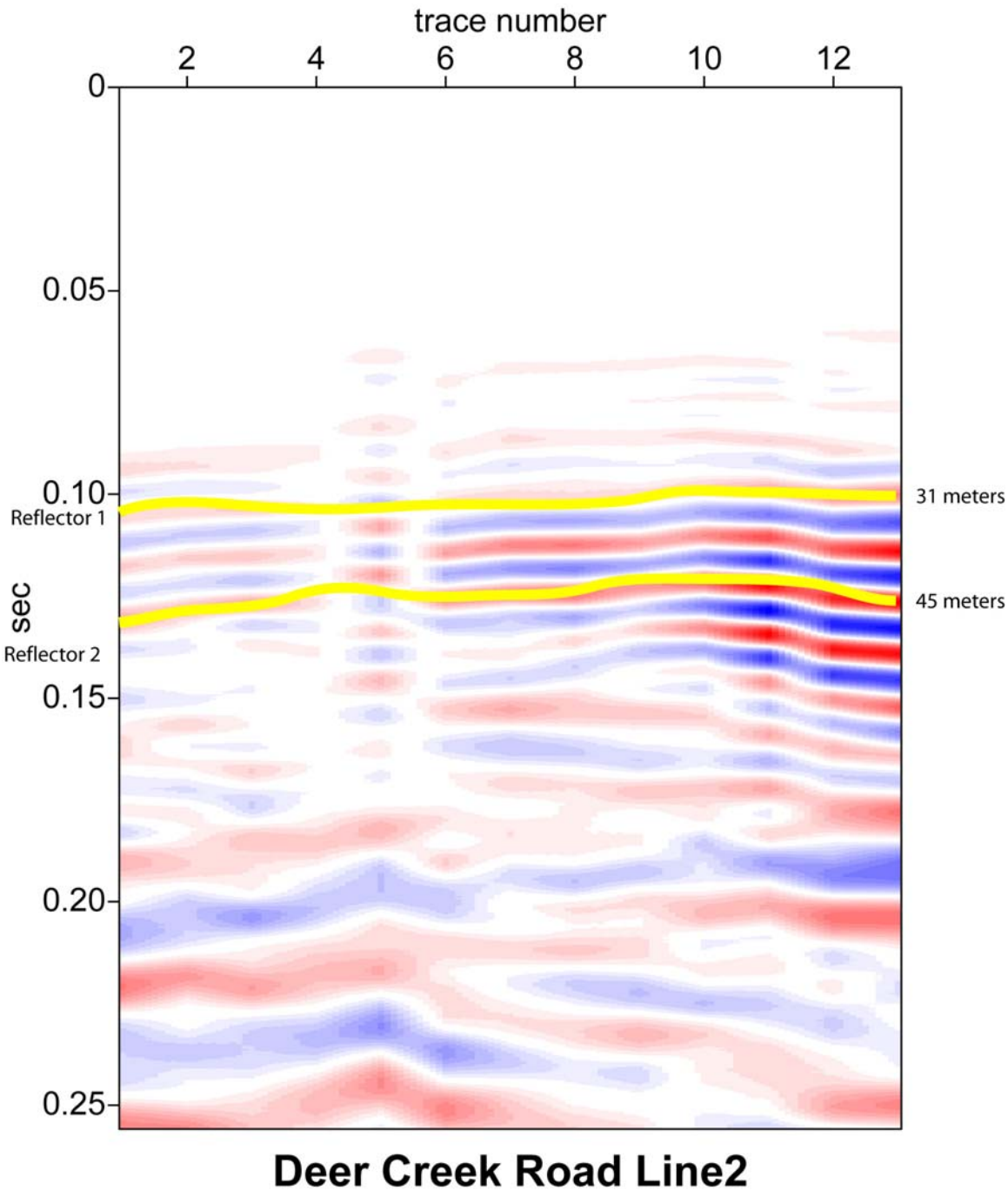

Figure 20: Final interpreted section from Deer Creek Road Line 2. This section shows two possible reflectors, one at 31 meters and one at 45 meters. The trace separation is 2 meters.

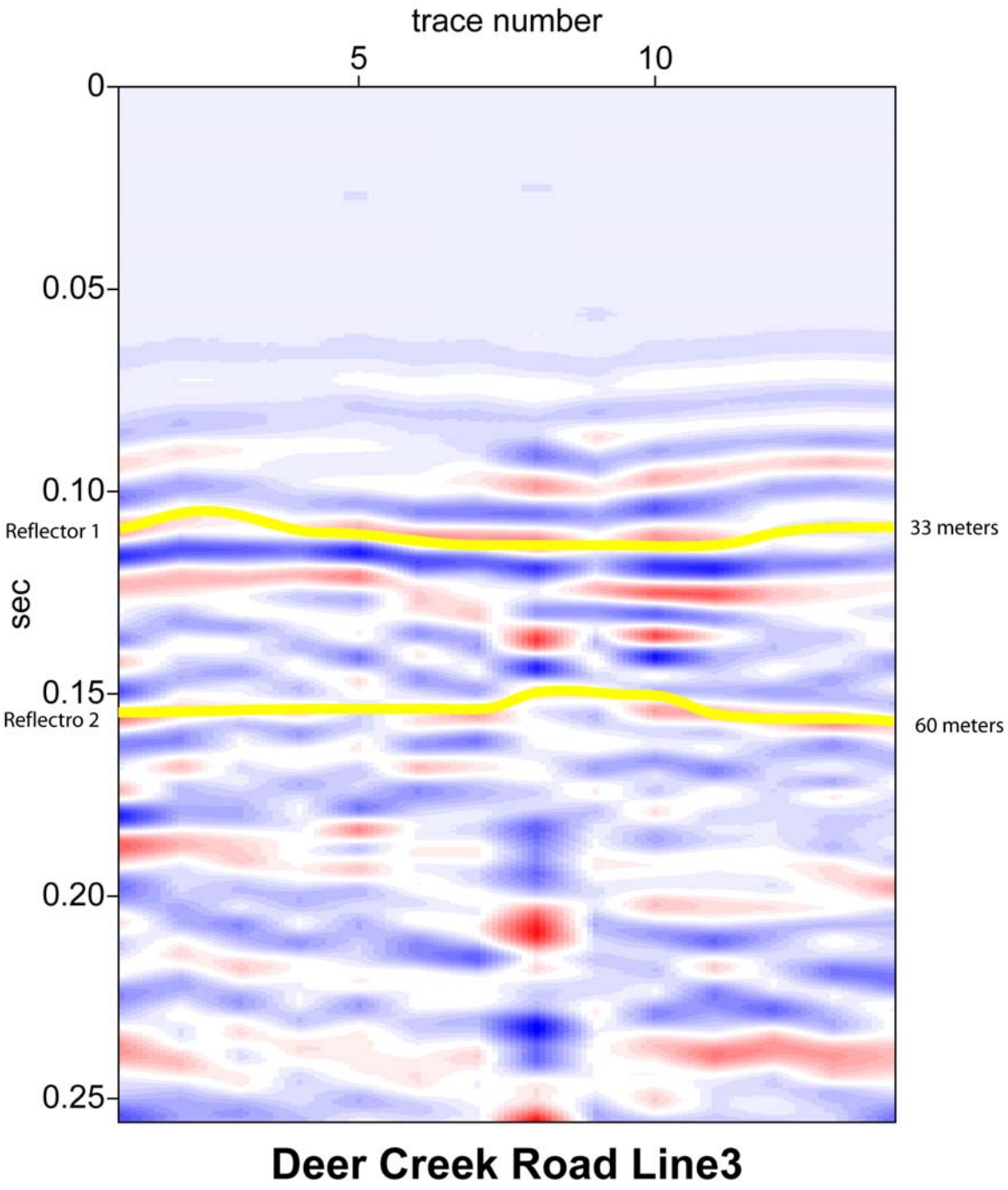

Figure 21: Final section from Deer Creek Road Line 3. This section shows two possible reflectors, one at 33 meters and one at 60 meters. The trace separation is 2 meters.

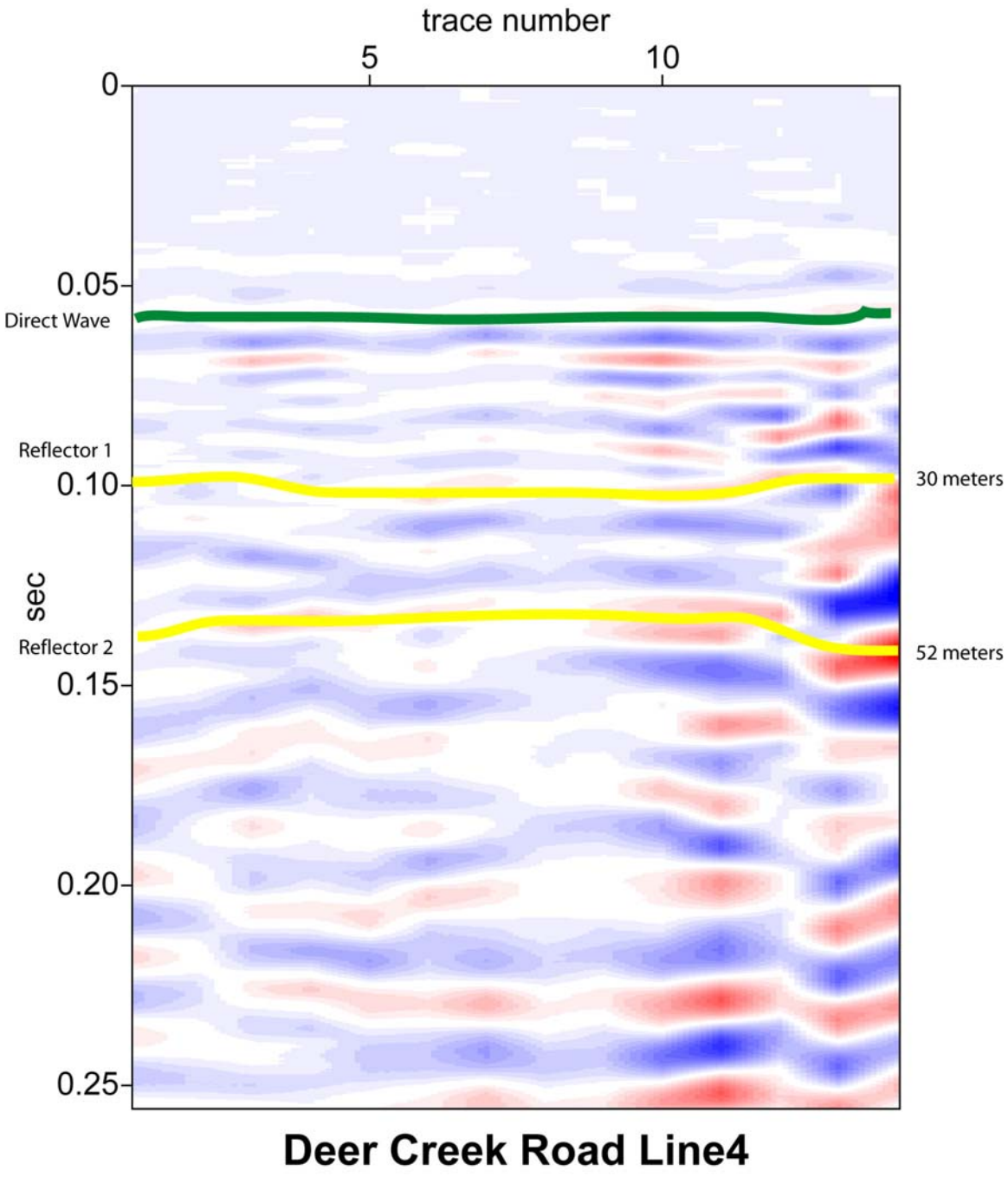

Figure 22: Final section from Deer Creek Road Line 4. This section shows the arrival of the direct wave and two possible reflectors. The first reflector is at 30 meters and the second reflector is at 52 meters. The trace separation is 2 meters.

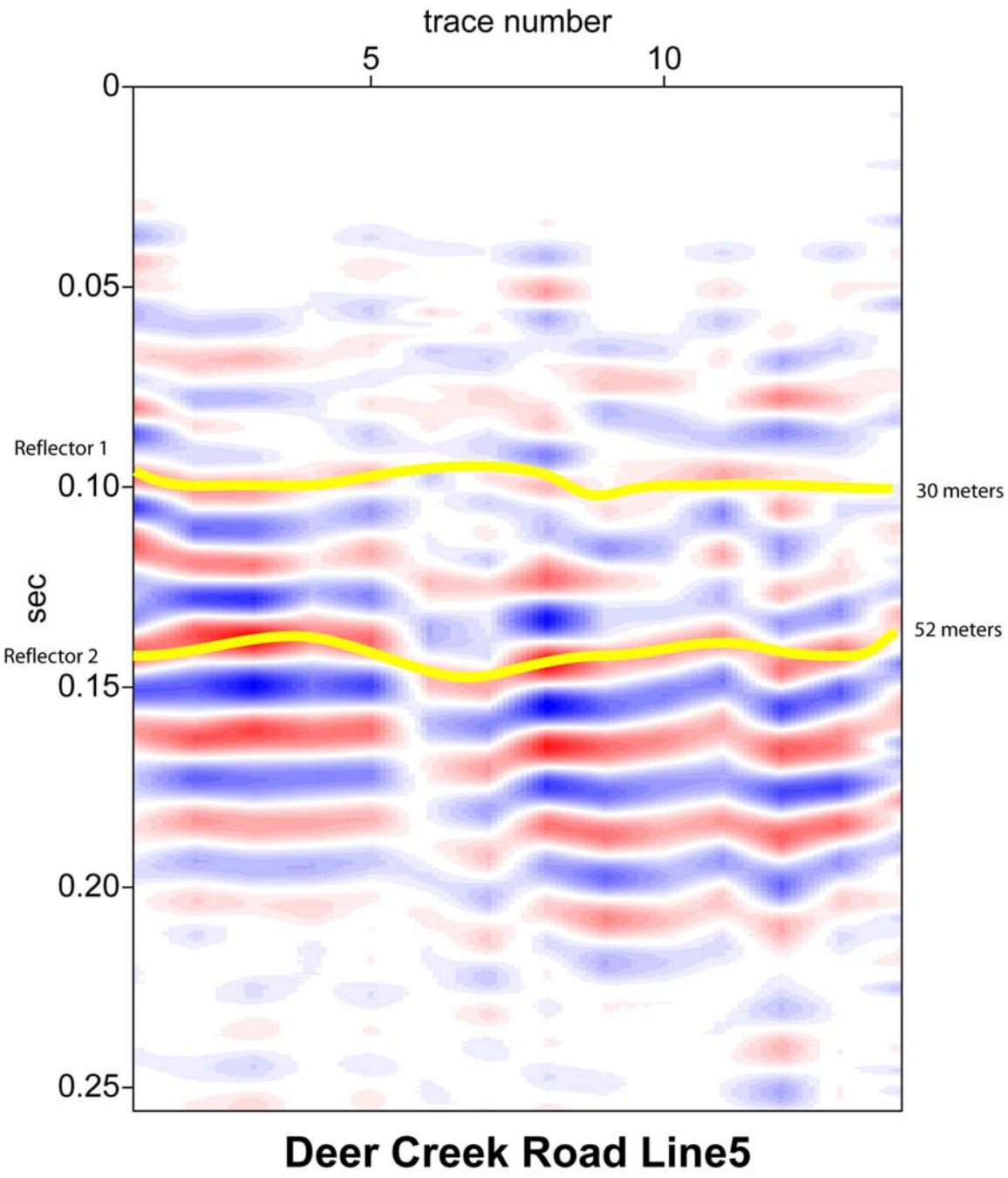

Figure 23: Final interpreted section from Deer Creek Road Line 5. This section shows 2 possible reflectors, one at 30 meters and one at 52 meters. The trace separation is 2 meters.

DCR Line 1 (Figure 19) shows 2 prominent reflectors. The first reflector is located at 0.09 seconds and the second reflector is located at 0.135 seconds. Also visible in this reflector is the direct wave, which can be seen at 0.055 seconds. DCR Line 2 (Figure 20) shows much less detail than Deer Creek Road line 1 but it is still possible to pick out 2 reflectors. The first reflector occurs at 0.105 seconds and the second at 0.13 seconds. DCR line 3 (Figure 21) also shows 2 possible reflectors. The first reflector occurs at 0.11 seconds and the second reflector at 0.16 seconds. DCR line 4 (Figure 22) also lacks in detail, but there are two reflectors at 0.099 seconds and 0.14 seconds. The direct wave is also visible in this section at 0.075 second. The final seismic line collected along Deer Creek Road, line 5 (Figure 23), shows two reflectors, one at 0.10 seconds and one at 0.14 seconds. Using the first arrivals of the refracted waves from a number of different source locations along Deer Creek Road yields an average first layer velocity of approximately 600 m/s and an average second layer velocity of 1100 m/s, which are used to calculate the depth of the reflectors in each section.

Line 1 (Figure 19) along the road showed the clearest reflections and was the easiest to interpret. Line 1 showed two reflections and the arrival of the direct wave. The reflector that occurs at 0.055 seconds is the direct wave arriving. By dividing the offset for this line (28 meters) by the velocity of the first layer (600 m/s) the approximate time of the arrival of the direct wave can be calculated (0.05 seconds), which matches the time of the first reflector. The second reflector occurs at a depth of 27 meters which is close to the depth of the water table (25 meters) reported at a nearby irrigation well (Canyon River Irrigation Well). The velocity change at this reflector matches the velocity change seen going from dry sand to wet sand. The final reflector in this section occurs at 52

meters in depth. This is the bedrock reflection, which is confirmed by the velocity change (1100 m/s above, 2500 m/s below).

Deer Creek Road line 2 (Figure 20) is difficult to interpret. The data were collected near a highway overpass, which introduced noise of a similar frequency to the reflections (between 45 and 120 Hz). The two reflectors seen in this section occur at 32 meters and 45 meters. The velocity change at each reflector confirms that the reflections are the water table and the bedrock respectively.

The third line (Figure 21) collected along Deer Creek Road was also collected near the highway overpass so much of its data was also masked by noise from the highway. The two reflectors visible in this section occur at 33 meters and 60 meters. The velocity change at each reflector again indicates that they are the water table and bedrock.

Line 4 (Figure 22) from Deer Creek Road was collected in an area of damp soil. Because of this, the signal was highly attenuated and the seismic section shows only weak reflections. There are two possible reflections in this section, the first occurs at 29 meters and the second occurs at 52 meters. The velocity change at each reflector suggests that they are the water table and bedrock respectively.

The final section (Figure 23) along Deer Creek Road was collected in similar conditions to line 4 but shows a slightly better signal to noise ratio. There are two reflectors visible in this section, the first at 30 meters and the second at 52 meters. Again these are water table and bedrock.

Three seismic lines were collected in Hellgate Canyon Park at the west end of the study area, each containing 360 traces, and resulted in 15 optimum offset traces. Hellgate

Canyon Park Line 1 (Figure 24) shows one prominent reflector that occurs at 0.055 seconds. Hellgate Canyon Park Line 2 (Figure 25) also shows one prominent reflector that occurs at 0.06 seconds. The final seismic line (Figure 26) collected in Hellgate Canyon Park also shows one prominent reflector occurring at 0.075 seconds. Below the first reflector in each section are what appear to be additional reflectors having the same general shape as the first reflector in each section. These are multiples of the first reflectors. Multiples occur when seismic energy is "bouncing" around through the subsurface. Multiples of dipping beds generally have a steeper gradient than the original reflector that produces them. In the sections from Hellgate Canyon Park it appears that the reflections seem to increase in steepness as they get deeper.

Using the first arrival times of the refracted waves yields a velocity of the first layer approximately 600 m/s. In this area the bedrock was too deep to return seismic reflection or refraction data. The only reflection visible in the sections occurs at approximately 18 – 20 meters. The velocity changes from 600 m/s above the reflector to 1500 m/s below the reflector, meaning that the reflection is most likely the water table. Below the water table reflection the sections contain multiples of the water table and noise. Table 4 summarizes the data from Hellgate Canyon Park

Conclusion

The seismic results from Bonner school and Deer Creek road confirm the results from Nyquest (2001), matching closely both his results modeled from gravity and known depth to bedrock from wells near the seismic lines. The seismic lines along Deer Creek Road correspond to a line of gravity measurements taken by Nyquest (2001). There are

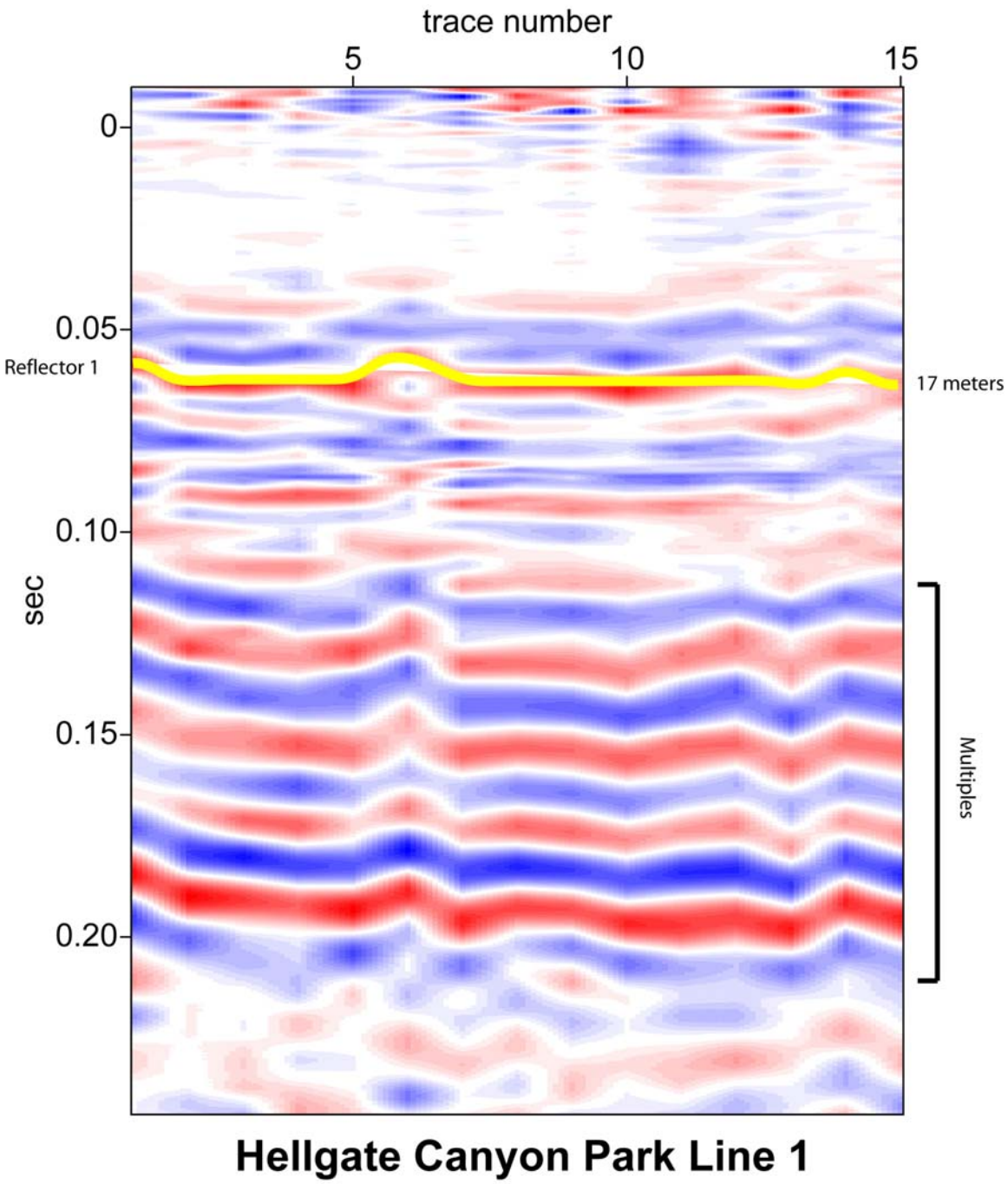

Figure 24: Final interpreted section from Hellgate Canyon Park Line 1. This section only shows 1 reflector at 17 meters. Below the reflector are multiples of the reflector.

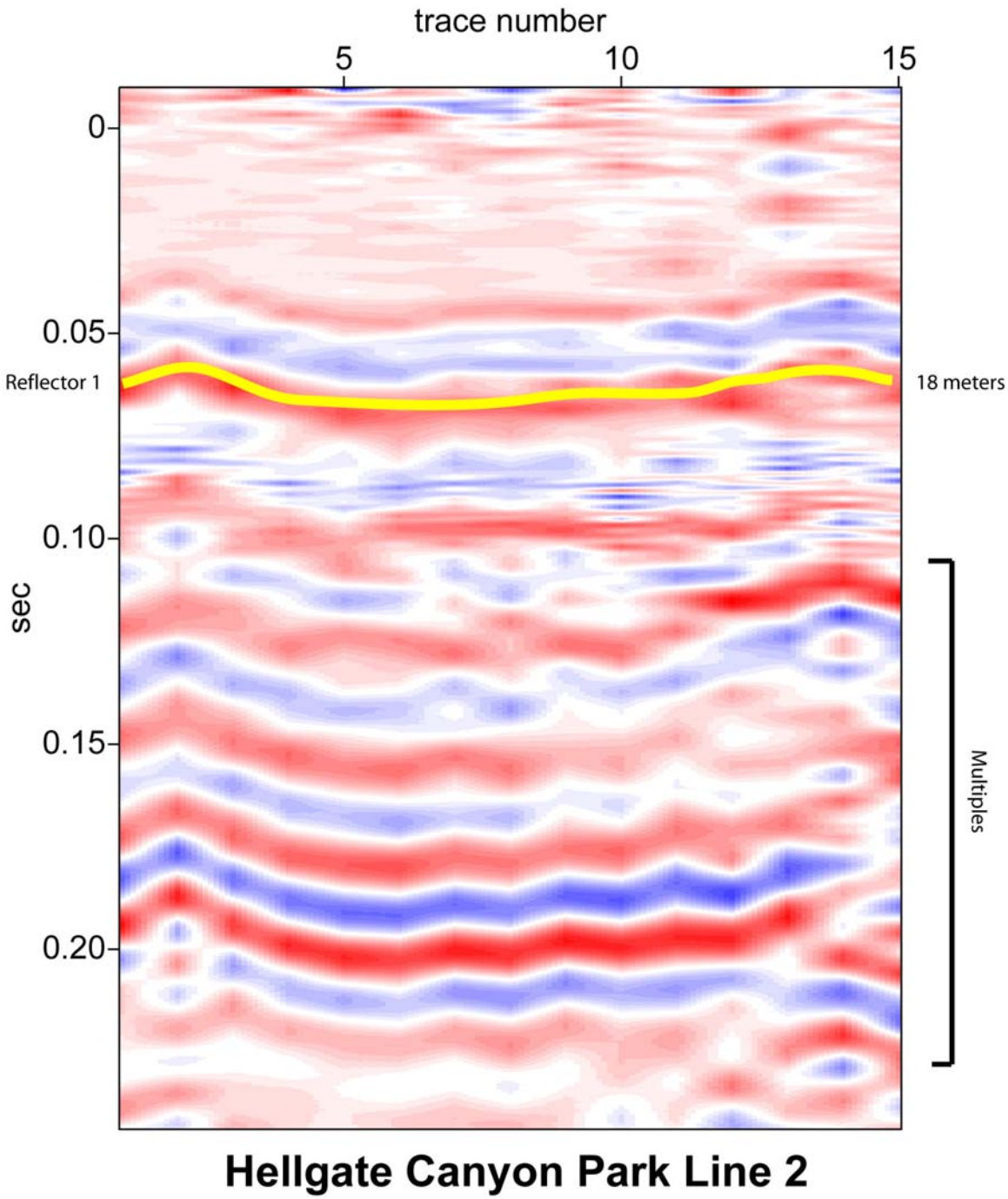

Figure 25: Final interpreted section from Hellgate Canyon Park Line 2. This section only shows one reflector at 18 meters. Below the reflector are multiples of the reflector.

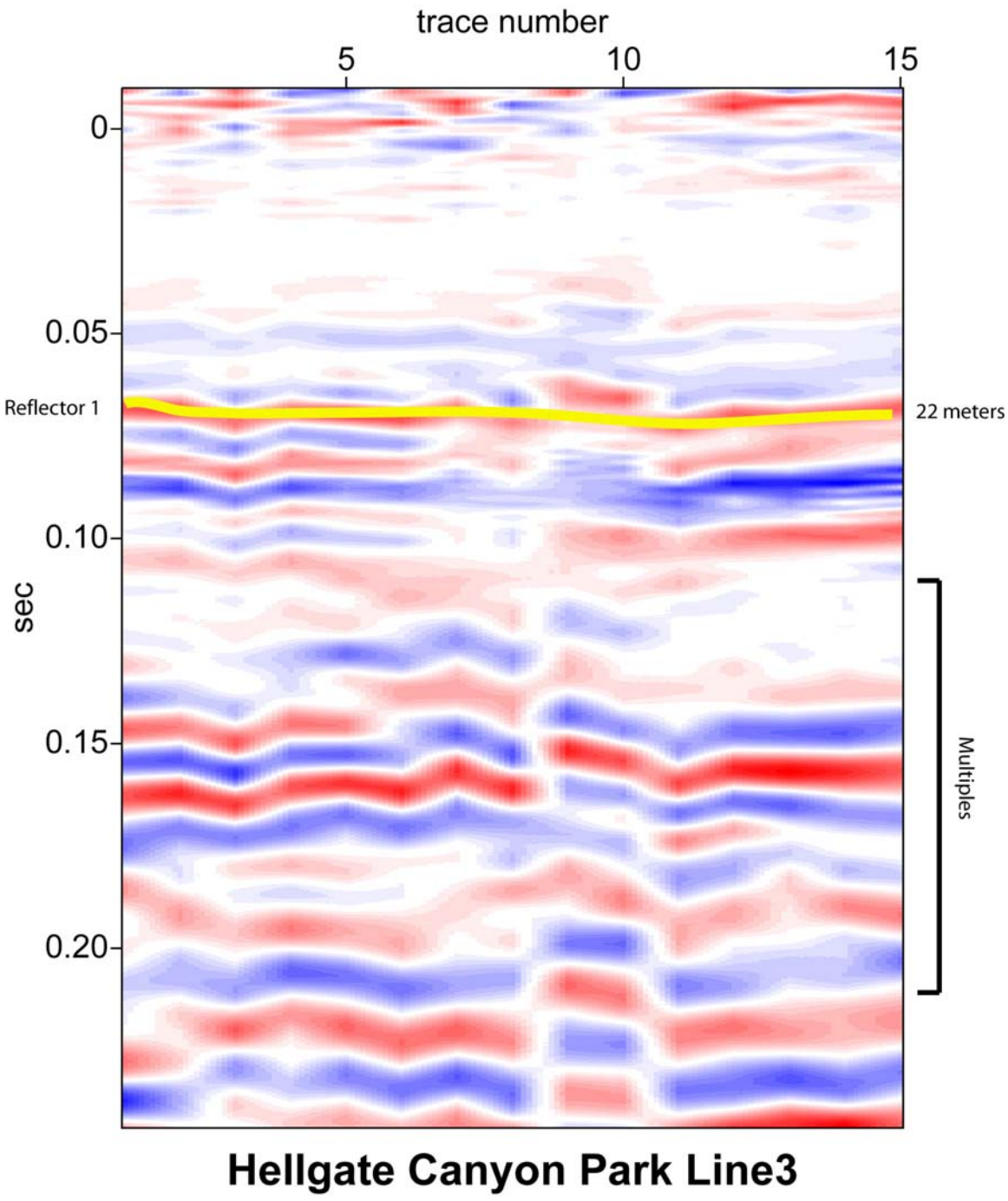

Figure 26: Final interpreted section from Hellgate Canyon Park line 3. This section only shows 1 reflector at 22 meters in depth. Below the reflector are multiples of the reflector.

approximately 15 gravity measurements in the area which he estimated the bedrock depth to be between 40 and 60 meters. A well in the area (gwic ID 217492) drilled to bedrock at approximately 50 meters. The seismic results along Deer Creek Road fell between 15 meters and 60 meters. The seismic lines from Bonner School were not near any gravity measurements taken by Nyquest (2001) but a well drilled near there (gwic id 68155) possibly hit bedrock at 38 meters. The seismic results also showed a bedrock depth of 38 meters. The seismic method did not perform well in Hellgate Canyon Park. No bedrock reflectors were seen in these sections. The bedrock in this area is deeper than the effective depth of the seismic source used.

The error associated with this method comes from two different sources, the accuracy of the velocities used to calculate depths from two way travel times and the interpreter's ability to accurately pick two way travel times. The velocities used were found by picking first arrivals off of each seismic section and fitting a line to the data on a time-distance plot. Using Seismic Unix NT the first arrivals were able to be picked to the hundredth of a second, and the lines fit to the points had an R^2 value of 0.98 or greater. The two way travel times were found in Seismic Unix and are accurate to 0.005 seconds, and assuming an average velocity of 1000 m/s across the entire seismic section would result in an error of ± 5 meters in the final results.

The normal move out of the reflectors was not taken into account. The normal moveout of a seismic reflection occurs when you increase the offset distance between the source and the receiver. As the offset increases the distance the reflected seismic wave has to travel increases. Reflections of a flat reflector will arrive at the surface increasingly later as the offset distance increases. The flat reflector will have concave

downward parabolic shape when viewed with increasing offset on the x-axis and increasing time on the y-axis. The normal moveout can be corrected so that the reflector appears flat in the seismic section. The correction needed to flatten the reflector can be estimated by the following equation:

$$\Delta T = x^2 / 2V^2 t_0$$

Where:

ΔT = normal move out correction

x^2 = offset squared

V^2 = velocity of the layer squared

t_0 = the time the reflector at the smallest offset

By substituting an offset equal to 36 meters and an average velocity of 1000 m/s for a reflector with an initial arrival of 0.1 seconds into the equation, the resultant in ΔT is 0.006 seconds. 0.006 seconds is very close to the accuracy I can pick reflectors so I chose to ignore the normal moveout corrections. The case presented above is for the maximum offset used to create the optimum offset sections. Where the offset is less, the normal moveout correction will be even smaller.

The seismic method used was successful in accurately determining the depth to bedrock in the Milltown Valley in limited areas. This method can be employed in other areas throughout the valley as long as the depth to bedrock is less than 50 meters and for optimum results, less than 40 meters. The seismic method requires more time, personnel, and equipment than the gravity measurements. Also it was more difficult to obtain land access for this technique due to the more invasive nature of the survey (i.e. noise, driving vehicles on land and equipment set up). This technique could be improved by using a

more powerful seismic source with less surface noise (i.e a Betsey Gun or explosives). Despite the limitation faced in the Milltown Valley this technique could be successfully implemented in other valleys of similar geometry, especially with the addition of a more powerful seismic source.

GRAVITY DATA INTERPRETATION

Introduction

Unlike seismic techniques, gravity data is simple and relatively quick to collect in the field, and therefore a gravity survey is well suited for a large-scale depth-to-bedrock model. Unfortunately, the interpretation of gravity data is more complex and requires extensive processing of the data collected. This is particularly so with respect to separating the regional and residual anomalies. The final model from the gravity measurements is based heavily upon the processor's interpretation of the regional gravity field. Also different bedrock configurations can result in similar gravity anomalies, therefore gravity modeling is a more subjective and non-unique determination of depth to bedrock than seismic techniques. Regardless, with reasonable geologic knowledge of the subsurface, gravity methods are well suited for depth to bedrock investigations.

The goal of this portion of the thesis was to take into account the possibility that the density contrast used to calculate the depth to bedrock may vary with depth, an idea that was previously not taken into account in the Milltown Valley (Nyquest 2001). To test this hypothesis, I used the same data used by Nyquest (2001) and simply reinterpreted his result using a different modeling program that allowed the density contrast to decrease with depth. If the density contrast did truly vary with depth, my model results would provide a better match to known depth to bedrock data throughout the valley.

Previous Work

Nyquest (2001) collected 397 gravity readings throughout the study area (Figure 27) and then combined his results with findings from the National Geophysics Data Center and the U.S. Defense Mapping Agency (NGS/DMA) to build a regional map of the gravity. He then reduced the gravity measurements to the Complete Bouguer Anomaly (Figure 28) using a series of corrections which take into account the Earth's imperfect shape and rotation, the location on the spheroid, elevation above sea-level, the gravitational attraction of the rocks between the observation point and sea-level, and the surrounding topography. Before the data can be modeled the regional gravity effects must be removed from the data. Nyquest (2001) removed the regional gravity (Figure 29) effect from the Complete Bouguer Anomaly data he collected to find the residual gravity anomaly (Figure 30), which is the gravity effect due only to the density contrast between the valley fill and the bedrock.

For this thesis I used Nyquest's (2001) residual anomaly to find the bedrock topography of the basin using two different gravity modeling programs, GI3 [*Cordell and Henderson*, 1968] and GRAVMOD3D [*Chakravarthi and Sundararajan*, 2004]. Both of these programs use inverse modeling to calculate the depth to bedrock. Inverse gravity modeling (inversion) involves calculating the statistically best-fit basin geometry to produce the observed gravity anomaly. In both GI3 and GRAVMOD3D the best fit is determined by regression.

In order to compare how well the output of each program fits the actual bedrock topography and provide a means to compare the outputs of each program to each other

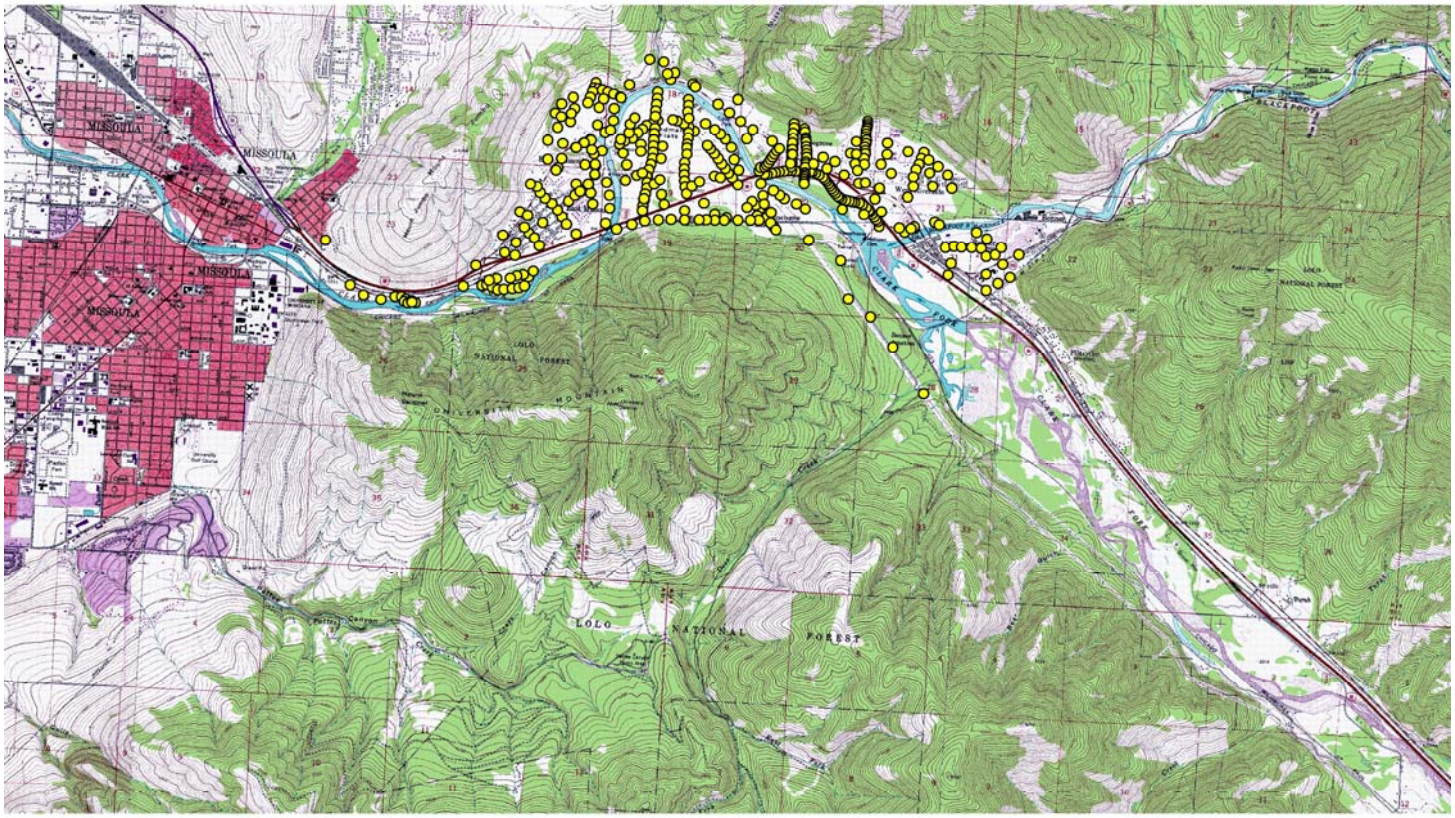

Figure 27: Location of gravity observations collected and used by Nyquest (2001) to create his depth to bedrock model.

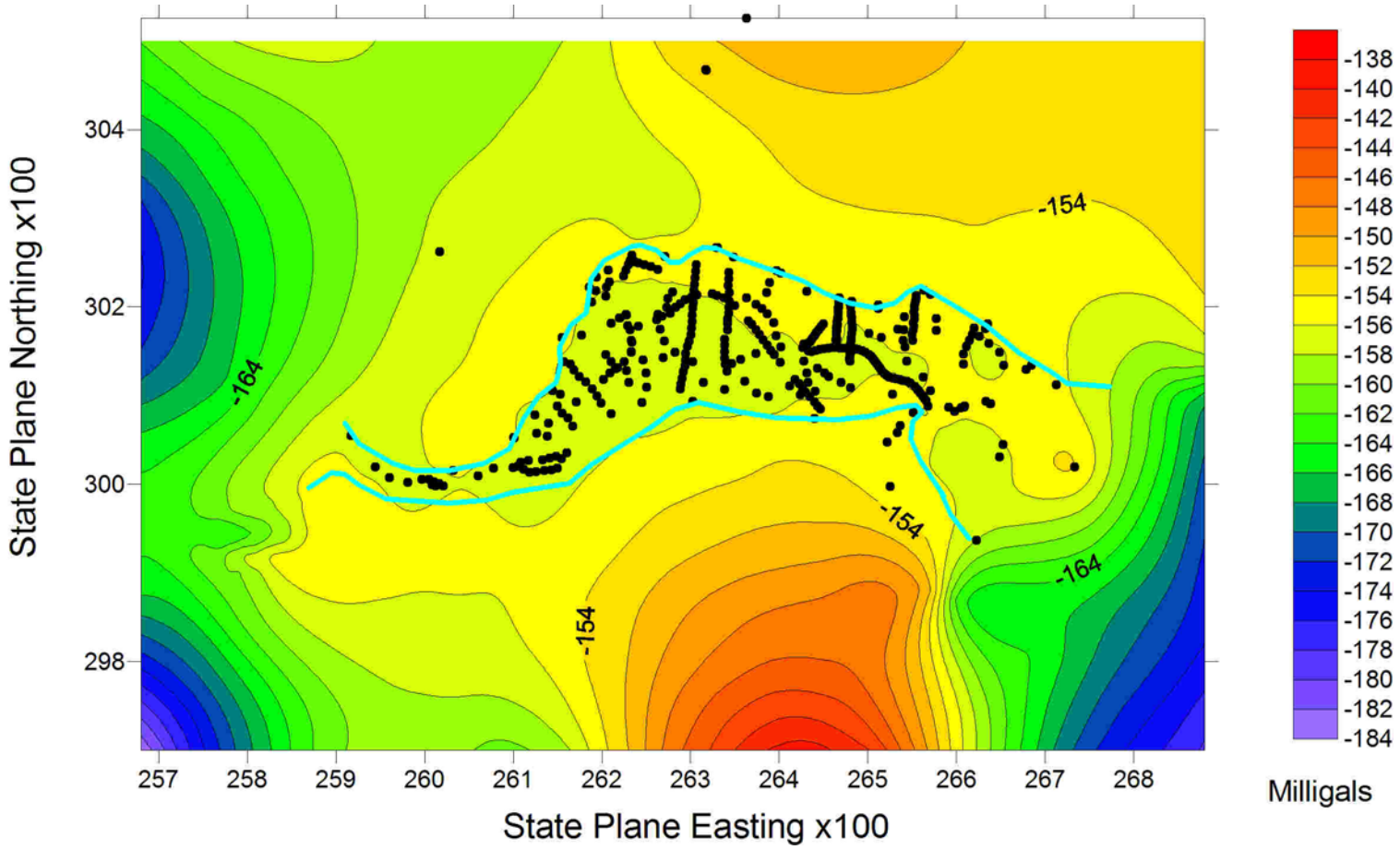

Figure 28. The Complete Bouguer Anomaly used by Nyquest (2001). This was generated by gridding the CBA gravity data. The outline of the valley is shown as blue lines and the data used to create the grid is represented by black dots.

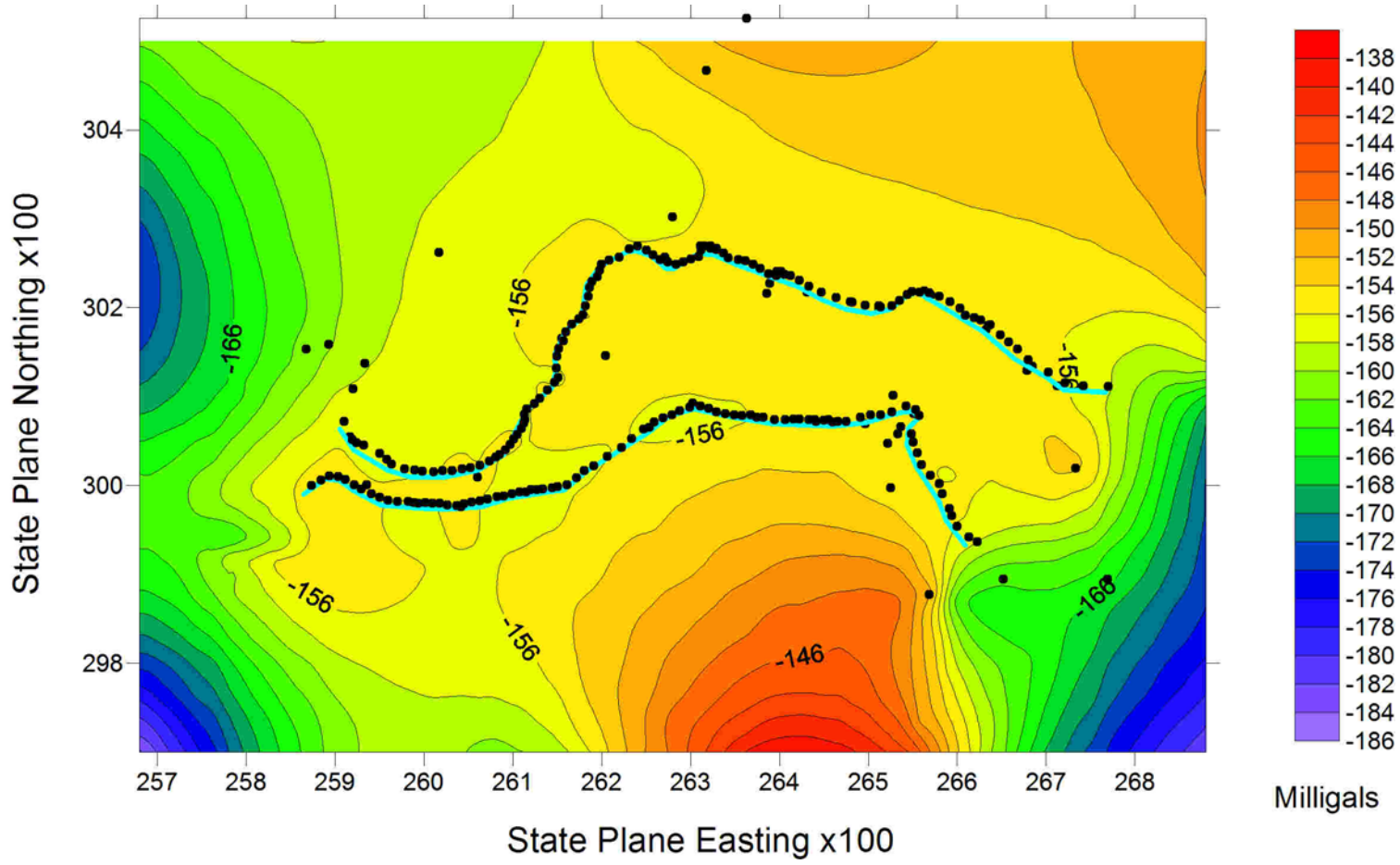

Figure 29: The regional gravity field developed by Nyquest (2001). This along with the total CBA were used to construct the residual anomaly that Nyquest inverted to find the depth to bedrock. The valley outline is shown as light blue lines and the points used to construct the grid are shown as black dots.

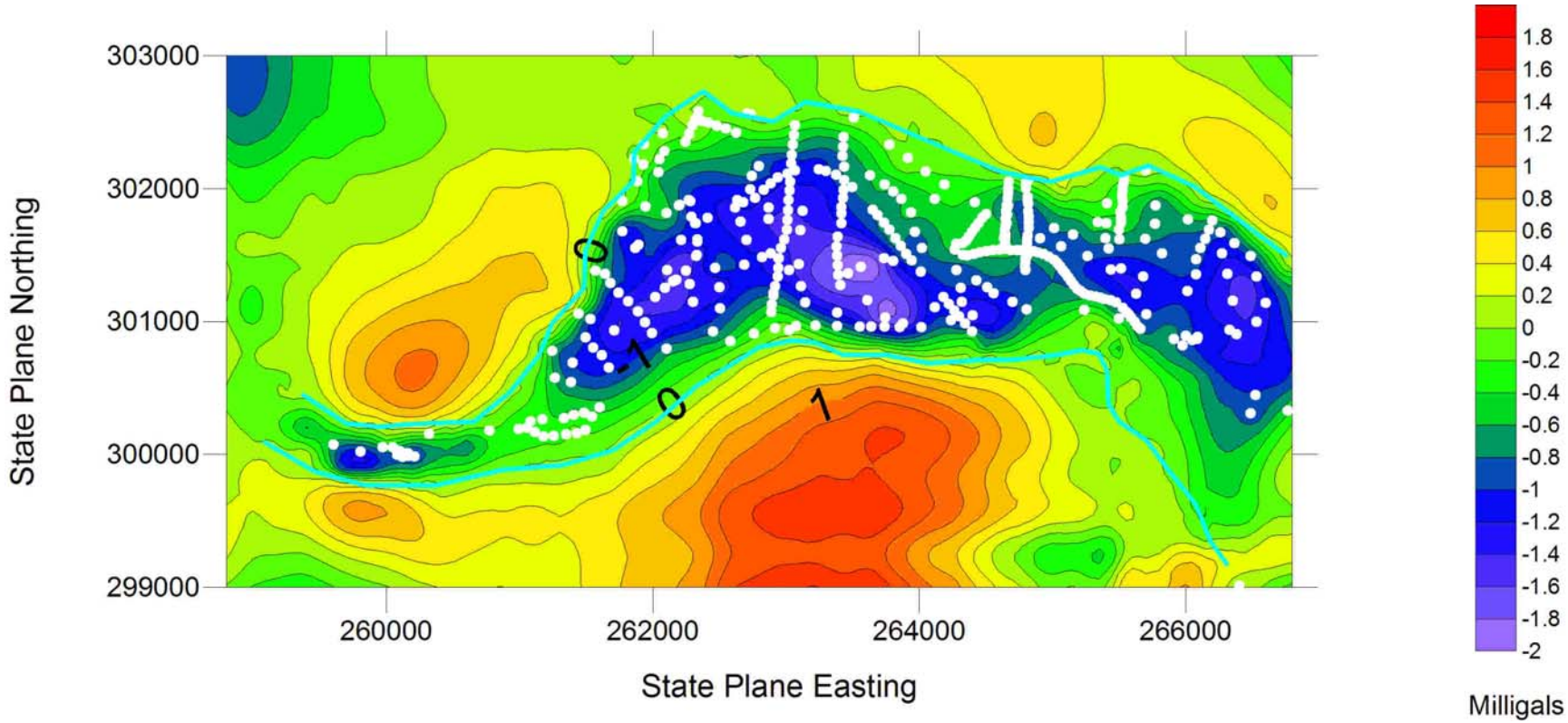

Figure 30: Residual gravity anomaly used by Nyquest (2001) to construct his depth to bedrock model using the gravity inversion program GI3. The outline of the valley is shown as a light blue line and the data used to construct the grid are shown as white dots. This anomaly was also used in the comparison between the two gravity programs GI3 and GRAVMOD3D.

some statistics need to be employed. The depth to bedrock is known at various locations throughout the survey area. By comparing the estimated depth to bedrock from the computer programs to the known depth, one can calculate how well the estimate fits the known data. Three sets of statistics were used to compare the known depths to the calculated depths: the average residual, the fit of a data to a 1:1 line and the standard error of the estimates. The average residual was found by subtracting the calculated depth from the known depth at each location and then averaging those values throughout the basin. This provides an estimate of how well the calculated depths match known depths, but does not take into account the distribution of the data. High negative and high positive residuals could average out to a near zero average residual. The fit of the observations to a 1:1 line was then calculated by fitting a trendline to a plot of the known depths versus calculated depths. If the calculated depths matched the known depths exactly, the trendline would have a slope equal to 1. Comparing the difference in slope of the trendline from 1 gives an estimate of how well the data fits. This method also does not take into account the data distribution. The plot of known depths versus calculated depths could have a large spread but still have a trend line with a slope close to 1. The final statistic calculated is the standard error of the estimates. The standard error of the estimates is the standard deviation of the difference between the calculated depth and the known depth. This method takes into account the distribution of the data, the less scatter the data has, the lower the stander error of the estimates will be. All of the statistics were calculated using Microsoft Excel's built in statistical functions.

GI3 Methods

Nyquest (2001) used the gravity inversion program GI3 [*Cordell and Henderson*, 1968] to invert the gravity data and estimate depths to bedrock. GI3 calculates the gravitational effect of an array of vertical prisms, of assumed density contrast, to estimate the gravitational signal of a basin. The initial guess at the thickness of each prism is found by the infinite slab formula, which is a general equation used to calculate the gravitational effect of an infinite horizontal sheet. The equation has the form of:

$$\Delta g = 2\pi G\rho h$$

Where:

Δg is the gravity effect

G is the gravitational constant

ρ is the density of the slab

h is its thickness

Using the infinite slab formula, the gravity at each grid point is used to solve for the thickness using the density contrast provided. Using the thickness found, the overall gravitational attraction of the basin is found by summing the gravitational affect of each prism over the basin. The gravity effect of each prism is found using the formula for a vertical right-cylinder-source when the grid point coincides with the observation point and the vertical-line-source for all other points. The calculated gravity is then compared to the actual measured gravity and the thickness of each prism is adjusted based on the difference between the two. This process continues iteratively until the error criteria are met or the maximum number of iterations is performed. GI3 [*Cordell and Henderson*, 1968] does assume a constant density throughout the valley fill. The program also offers

the option to input an initial guess at the thickness of the sediment and the surface topography of the basin. The program uses a fixed point iteration to iteratively find the thickness of the basin. The formula for the fixed point iteration is:

$$z_{k+1}(m,n) = z_k(m,n)\left(\frac{g_{obs}(m,n)}{g_{calc}(m,n)}\right)$$

Where:

$z_{k+1}(m,n)$ = new thickness at point $(m.n)$

$z_k(m,n)$ = old thickness at point $(m.n)$

$g_{obs}(m,n)$ = observed gravity at point $(m.n)$

$g_{calc}(m,n)$ = calculated gravity at point $(m.n)$

To determine the best use of GI3, I performed several experiments. The program was run 20 different times with varying densities: 10 times with no initial guess or surface topography and 10 times with an initial guess and surface topography. The density contrasts used were: -400 kg/m^3, -500 kg/m^3, -600 kg/m^3, -650 kg/m^3, -700 kg/m^3, -725 kg/m^3, -750 kg/m^3, -800 kg/m^3, -900 kg/m^3 and 1000 kg/m^3. The input to each run of the program consisted of a grid of the residual gravity anomaly and, when necessary, grids of the surface topography and the initial thickness guess. Each grid had a grid spacing of 50 meters. The initial guess was constructed from points of known bedrock depths throughout the valley based on drill cores, wells and seismic data. The output of each run of the program was a grid of points in the USGS grid format.

GRAVMOD3D Methods

I developed a second program to invert the gravity data based on code from Chakravarthi and Sunderarajan (2004). GRAVMOD3D works in a similar fashion to GI3 in that it calculates a theoretical gravitational attraction of a basin by summing the effect from a series of prisms and iteratively corrects the thickness of the prisms by comparing the calculated gravity to the actual gravity. This program uses Newton's forward difference formula to adjust the thickness of the model after each iteration. The formula for Newton's forward difference is:

$$z_{k+1}(m.n) = z_k(m,n) + \frac{g_{obs}(m,n) - g_{calc}(m,n)}{2\pi G \Delta\rho(z)}$$

Where:

$z_{k+1}(m.n)$ = new thickness at point (m,n)

$z_k(m,n)$ = old thickness at point (m,n)

$g_{obs}(m,n)$ = observed gravity of the basin at point (m,n)

$g_{calc}(m,n)$ = calculated gravity of the basin at point (m,n)

G = gravitational constant

$\Delta\rho(z)$ = density contrast at depth z

However, unlike GI3, GRAVMOD3D allows the density contrast to change with depth. The program allows the density contrast to increase or decrease with depth along a user defined parabolic curve. The parabolic curve is defined by the formula:

$$\Delta\rho(z) = \frac{\Delta\rho_0^3}{(\Delta\rho_0 - \alpha z)^2}$$

Where:

$\Delta\rho(z)$ = density at depth z

$\Delta\rho_0$ = density contrast at the surface

z = depth in kilometers

α = parabolic function constant alpha

The constant alpha allows the user to change the shape of the curve to match geologic conditions. This program uses an analytical expression to calculate the gravity of a three dimensional rectangle that was developed by Chakravarthi et al. (2002) which takes into account the parabolic density function [*Chakravarthi, et al.*, 2001; *Chakravarthi and Sundararajan*, 2004, 2005].

I also modified the program to accept an initial guess at thickness. The residual anomaly has to be input as an evenly-spaced grid of data points. The input file contains the grid of points in rows and columns. The options contained in the input file are the density contrast at the surface, the constant for the parabolic density function (alpha value), grid dimensions and spacing, the maximum iterations to perform and the maximum depth allowed. The maximum depth allowed is used to keep the iterative process from calculating geologically unreasonable models. By constraining the maximum depth the model is forced to conform to known or inferred maximum depths. This keeps the model from using one or two anomalously deep cells to account for the majority of the anomaly.

In order to determine which parameters resulted in the best fit to known depths, this program was run 50 times with varying density contrasts and alpha values: 40 times with no initial thickness guess and 10 times with an initial thickness guess. The 40 times the program was run with no initial guess I used the same density contrasts as were used in GI3. For each of the density contrasts the program was run with 4 different alpha values: 0.001, 0.01, 0.1, and 1.0. The 10 times the program was run with an initial guess the same density contrasts were used with an alpha value of 0.001. The input grid to the program was a grid of the residual gravity with 250 meter grid spacing; thus, one expects greater granularity in the result than with the GI3 spacing of 50 meters. This spacing was chosen based on the detail retained and the computational time required to run the program. The program was run 3 additional times with density contrasts of -725 kg/m^3, -500 kg/m^3 and -400 kg/m^3 with an alpha value of 0.001 and an input grid spacing of 50 meters to confirm the results found with the coarser grid spacing.

GI3 Results

Tables 5 and 6 show the results from the computer program GI3. GI3, when implemented with no initial guess, minimized the error between known depths and calculated depths at a density contrast of -600 kg/m^3. When known depths are plotted versus calculated depths the departure of a linear trend line from a 1:1 line is 0.043. The mean residual is -2.4 meters and the standard error of the estimates is 9.3 meters. When an initial guess of the thickness was provided the density contrast that minimized the error was found to be -750 kg/m^3. The error associated with this value is 0.007 and is found by again plotting known verse calculated depths and determining the departure of

	No Initial Model					
	Density (kg/m^3)	Average Error (meters)	Standard Deviation of Error (meters)	Slope of Regression Line	Departure of Slope from 1:1 Line	Standard Error of the Estimates
	-400	-17.1	16.9	1.60	0.6	24.0
	-500	-8.2	11.3	1.20	0.2	13.9
Best Fit	-600	-2.4	9.1	0.97	0.03	9.4
	-650	-0.3	8.6	0.87	0.13	8.6
	-700	1.5	8.4	0.81	0.19	8.5
	-725	2.3	8.4	0.77	0.23	8.6
	-750	3.1	8.4	0.74	0.26	8.9
	-800	3.8	7.7	0.75	0.25	8.6
	-900	6.2	8.2	0.65	0.35	10.2
	-1000	8.1	8.9	0.57	0.43	12.0

Table 5. Summary of the results from the gravity inversion program GI3 running with no initial model. The best fit to the known data is found with a density contrast of -600 kg/m^3.

	With Initial Model					
	Density (kg/m^3)	Average Error (meters)	Standard Deviation of Error (meters)	Slope of Regression Line	Departure of Slope from 1:1 Line	Standard Error of the Estimates
	-400	-19.1	20.7	1.80	0.8	28.1
	-500	-9.3	13.0	1.40	0.4	16.0
	-600	-6.1	13.4	1.30	0.3	14.7
	-650	-3.4	11.3	1.20	0.2	11.8
	-700	-1.2	9.9	1.10	0.1	9.9
Best Fit	-725	-0.2	9.3	1.00	0	9.3
	-750	0.7	8.9	0.99	0.01	8.9
	-800	2.3	8.3	0.91	0.09	8.5
	-900	5.0	7.8	0.79	0.21	9.2
	-1000	7.1	7.9	0.70	0.3	10.6

Table 6. Summary of the results from the gravity inversion program GI3 running with an initial model. The best fit to the known data is found with a density contrast of -725 kg/m^3.

the trendline from a 1:1 line. The mean residual is 0.6 meters and the standard error of the estimates is 8.9 meters. Figure 31 shows the departure from a 1:1 line and the standard error of the estimates for each run of GI3 with and without an initial guess. Figure 32 is a map of the bedrock generated from GI3 using a density contrast of -750 kg/m^3 and an initial guess of the bedrock thicknesses. The initial guess forces the program to start closer to the actual solution, which is the global minimum. In contrast, when no initial guess is used the program converges to a local minimum which differs from the actual solution.

GRAVMOD3D results

Tables 7 through 10 show the results from the computer program GRAVMOD3D. Running GRAVMOD3D with an alpha value of 0.001 and 0.01 showed similar results. The error was minimized at a density contrast of -500 kg/m^3. The departure of the trendline from a 1:1 line for both outputs was 0.014. For alpha equal to 0.001 the mean residual was 0.98 meters and the standard error of the estimates was 10.5 meters. For alpha equal to 0.01 the mean residual was -3.9 meters and the standard error of the estimate was 12.6 meters. Running the program with an alpha value of 0.1 also minimized the error at -500 kg/m^3 but improved the error. The departure of a trendline from a 1:1 line for this run of the program was 0.0004. The mean residual was -4.2 meters and the standard error of the estimates was 12.7 meters. Running the program with an alpha value of 1.0 changed the density contrast that minimized the error to -600 kg/m^3 but increased the departure from a 1:1 line to 0.11. The mean residual was -0.7 meters, and the standard error of the estimate was 10.78 meters. There was no significant

	Alpha = 0.001					
	Density (kg/m^3)	Average Error (meters)	Standard Deviation of Error (meters)	Slope of Regression Line	Departure of Slope from 1:1 Line	Standard Error of the Estimates
	-400	-11.5	15.8	1.29	0.3	19.5
Best Fit	-500	-3.9	11.9	0.99	0.0	12.6
	-600	1.0	10.5	0.79	0.2	10.5
	-650	2.9	10.2	0.72	0.3	10.6
	-700	4.5	10.2	0.67	0.3	11.1
	-725	5.3	10.2	0.64	0.4	11.4
	-750	5.8	10.2	0.62	0.4	11.7
	-800	7.0	10.3	0.57	0.4	12.5
	-900	9.1	10.6	0.51	0.5	13.9
	-1000	10.6	11.0	0.45	0.5	15.2

Table 7. Results from the gravity inversion program GRAVMOD3D. The inversion was run with an alpha value of 0.001. The best fit was found with a density contrast of -500 kg/m^3.

	Alpha = 0.01					
	Density (kg/m^3)	Average Error (meters)	Standard Deviation of Error (meters)	Slope of Regression Line	Departure of Slope from 1:1 Line	Standard Error of the Estimates
	-400	-11.6	15.8	1.29	0.3	19.6
Best Fit	-500	-4.0	12.0	0.99	0.0	12.6
	-600	1.0	10.5	0.79	0.2	10.5
	-650	2.9	10.2	0.72	0.3	10.6
	-700	4.5	10.2	0.67	0.3	11.1
	-725	5.3	10.2	0.64	0.4	11.4
	-750	5.8	10.2	0.62	0.4	11.7
	-800	7.0	10.3	0.57	0.4	12.5
	-900	9.1	10.6	0.51	0.5	13.9
	-1000	10.7	10.9	0.45	0.5	15.3

Table 8. Results from the gravity inversion program GRAVMOD3D. The inversion was run with an alpha value of 0.01. The best fit was found with a density contrast of -500 kg/m^3.

	Alpha = 0.1					
	Density (kg/m^3)	Average Error (meters)	Standard Deviation of Error (meters)	Slope of Regression Line	Departure of Slope from 1:1 Line	Standard Error of the Estimates
	-400	-12.2	16.2	1.33	0.3	20.3
Best Fit	-500	-4.2	12.1	1.00	0.0	12.8
	-600	0.8	10.6	0.80	0.2	10.6
	-650	2.7	10.3	0.73	0.3	10.6
	-700	4.4	10.1	0.67	0.3	11.0
	-725	5.2	10.2	0.64	0.4	11.4
	-750	5.8	10.1	0.62	0.4	11.6
	-800	7.1	10.3	0.58	0.4	12.5
	-900	9.0	10.6	0.51	0.5	13.9
	-1000	10.6	10.9	0.46	0.5	15.2

Table 9. Results from the gravity inversion program GRAVMOD3D. The inversion was run with an alpha value of 0.1. The best fit was found with a density contrast of -500 kg/m^3.

	Alpha = 1.0					
	Density (kg/m^3)	Average Error (meters)	Standard Deviation of Error (meters)	Slope of Regression Line	Departure of Slope from 1:1 Line	Standard Error of the Estimates
	-400	-16.6	20.3	1.39	0.4	26.2
	-500	-7.2	13.6	1.18	0.2	15.4
Best Fit	-600	-0.7	10.8	0.89	0.1	10.8
	-650	1.5	10.2	0.80	0.2	10.3
	-700	3.5	10.0	0.72	0.3	10.6
	-725	4.4	10.1	0.68	0.3	10.9
	-750	4.9	10.1	0.66	0.3	11.2
	-800	6.4	10.1	0.62	0.4	11.9
	-900	8.6	10.4	0.53	0.5	13.5
	-1000	10.3	10.8	0.47	0.5	14.9

Table 10. Results from the gravity inversion program GRAVMOD3D. The inversion was run with an alpha value of 1.0. The best fit was found with a density contrast of -600 kg/m^3.

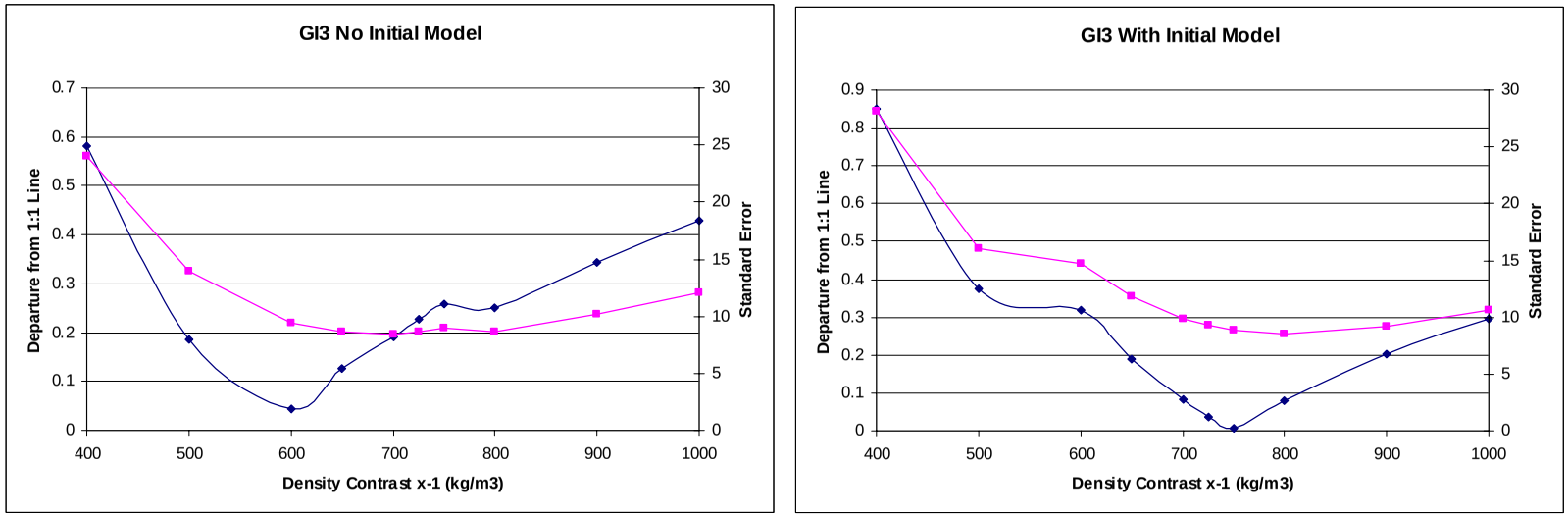

Figure 31: Graphs showing the error associated with the gravity modeling program GI3 run with Nyquest's (2001) data. The blue line represents the departure of the slope of a trendline fit to the plot of the known depths to bedrock versus the calculated depths to bedrock. The magenta line represents the standard error of the estimates. The graph on the left show the result from using GI3 with no initial guess and the graph on the right shows the results from using GI3 with an initial guess.

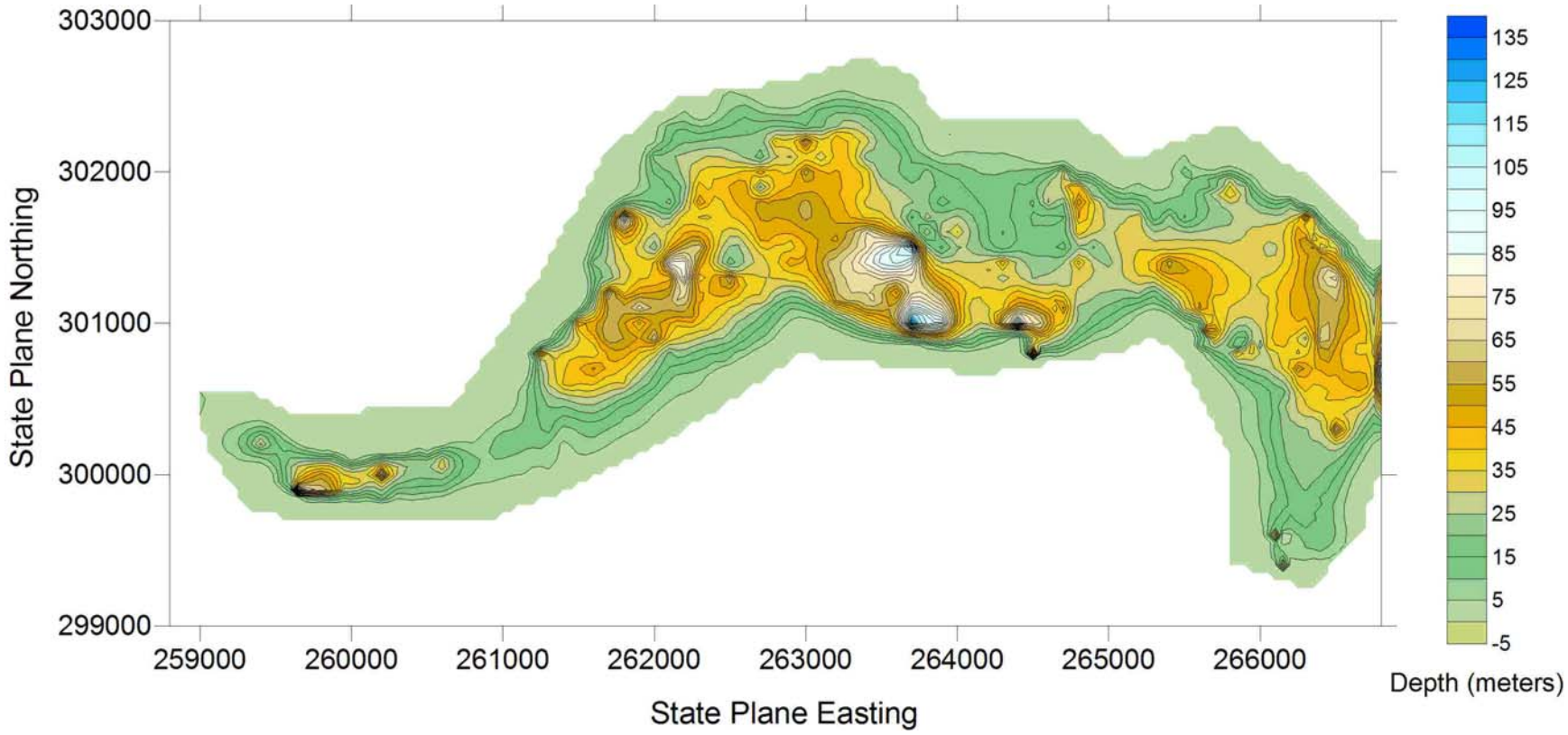

Figure 32: Final model found using the gravity inversion program GI3. This is the model that minimized the difference between the calculated depth and known depths at various locations throughout the valley. The density contrast used was 750 kg/m^3.

change to the results by running GRAVMOD3D with an initial guess of the bedrock depths. Figure 33 shows the departure from a 1:1 line and the standard error for each run of GRAVMOD3D. Figure 34 is a map of the bedrock generated from GRAVMOD3D using a density contrast of -500 kg/m^3 and an alpha value of 0.1.

Comparison of GI3 and GRAVMOD3D

GRAVMOD3D minimizes the error at different density contrasts than GI3, which is most likely a result of the algorithms used in each program. GRAVMOD3D is based on code that was developed to model much larger basins than the Milltown Valley. It can not handle the steeper gradients and small details associated with a small scale basin as well as GI3 can. The difference in how the programs calculate thicknesses from the calculated gravity causes the differences in the final models. Both programs compare the calculated gravity to known gravity and make a correction to the thickness based on how the two compare. GI3 finds the ratio between the observed gravity and the calculated gravity and multiplies the old thickness by this ratio to find the new thickness. GRAVMOD3D finds the difference between the observed gravity and calculated gravity and uses the Bouguer Slab formula to calculate the thickness associated with the difference in gravity and then adds that thickness to the old thickness to find the new thickness. For example if there was a difference between the observed gravity and the calculated gravity of 3 milligals, GI3 would multiply the old thickness by 4 to find the new thickness, where as GRAVMOD3D would add approximately 100 meters to the old thickness to find the new thickness. If the thickness was originally 50 meters the new thickness for GI3 would be 200 meters and for GRAVMOD3D would be 150 meters.

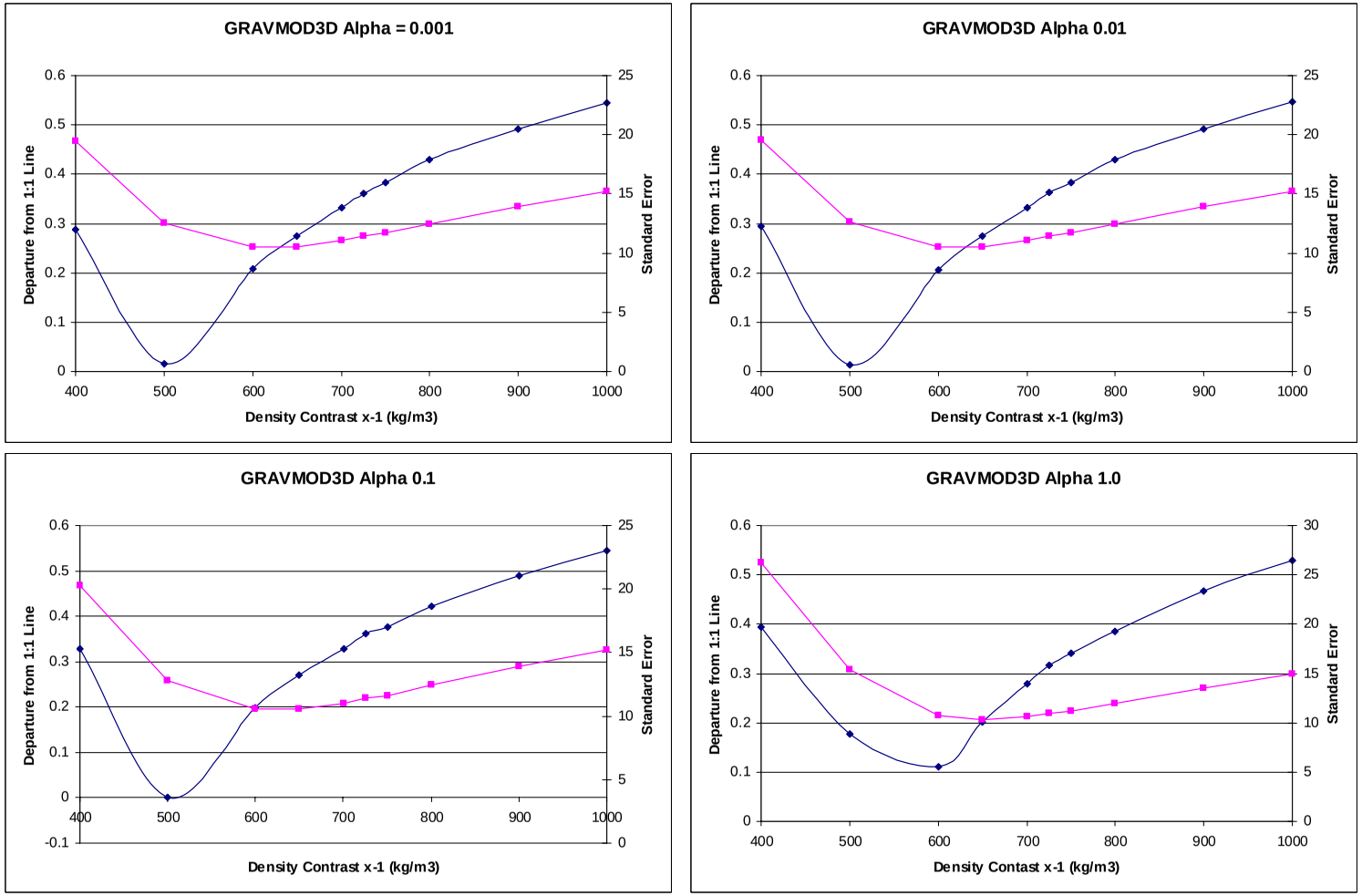

Figure 33: Graphs showing the error for each run of GRAVMOD3D. The blue line represents the departure from the slope of a 1:1 line from a trendline fit to the plot of known depths to bedrock versus calculated depths to bedrock. The magenta line is the standard error associated with each run of the program.

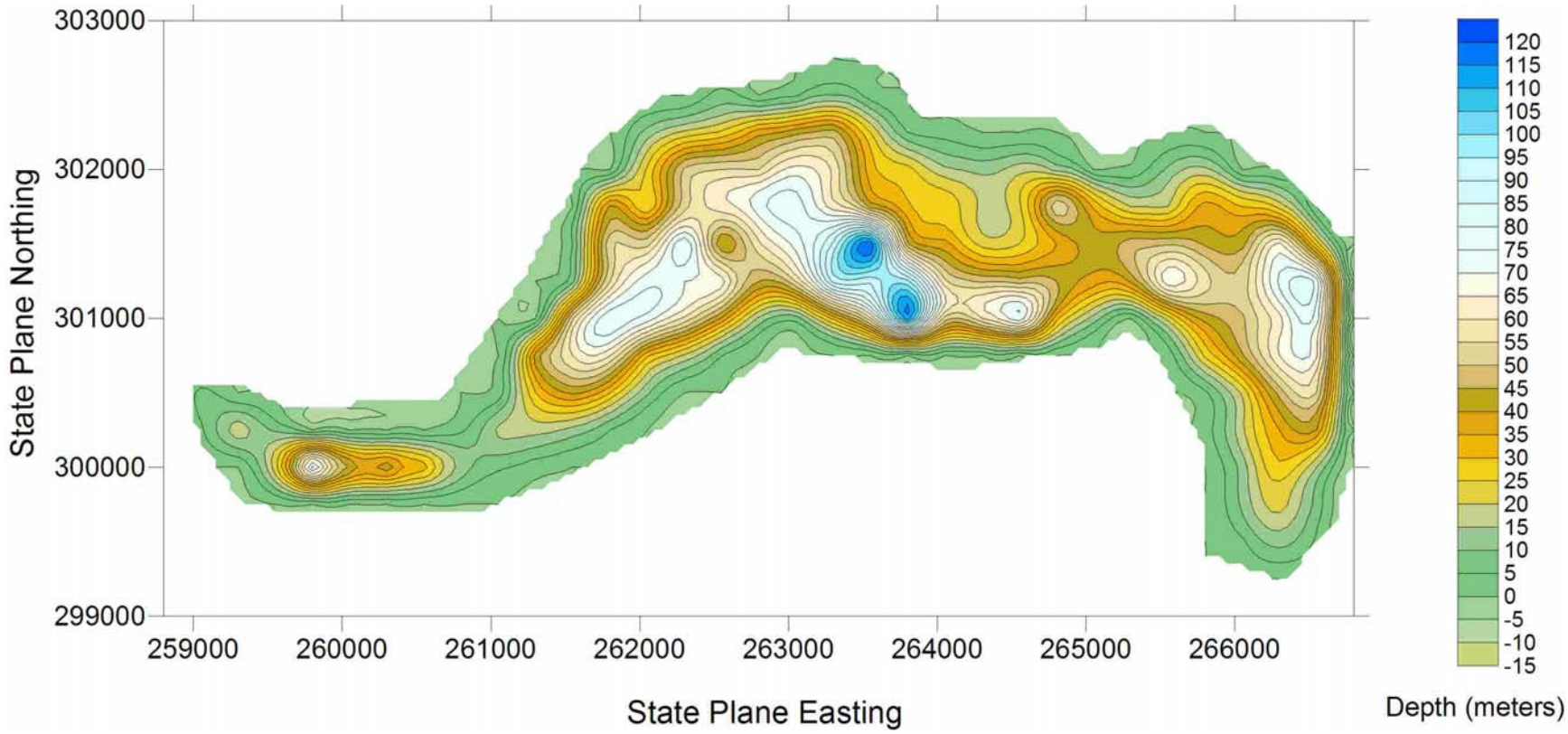

Figure 34: Final depth model created with the gravity inversion program GRAVMOD3D. This is the model that minimizes the difference between the calculated depth and the known depth at various points throughout the valley. This depth model was created using a density contrast of -500 kg/m^3 and a alpha value of 0.1.

This shows how GI3 can assign more thickness to a single cell than GRAVMOD3D and create steeper gradients. Figure 35 shows the final models from both GI3 and GRAVMOD3D side by side. It is apparent that GRAVMOD3D creates a much smoother map with broader features. This is even more apparent when you subtract the final model created by GI3 from the final model created with GRAVMOD3D (Figure 36). The biggest differences between the two occur around the deep "potholes" found throughout the GI3 model. In these areas, the centers of the holes in GI3 have a deeper depth estimate (15 to 40 meters). Around the edges of the holes GRAVMOD3D has a deeper estimate (5 to 30 meters). GRAVMOD3D is creating the same gravitational response with a broad hole which is overall deeper, but has a shallower maximum depth than the holes created by GI3.

GRAVMOD3D more accurately matches the known depths to bedrock when the density contrast is allowed to change very little with depth (alpha value = 0.1 or less). The best fit to known depths using GRAVMOD3D was found with an alpha value of 0.1. At the maximum depth extend found in the study area (≈ 150 meters) an alpha value of 0.1 results in a density contrast change of approximately 30 kg/m^3 from the surface to the deepest point. Increasing the alpha value causes the density contrast to change more rapidly with depth (using alpha = 1.0 causes the density contrast to change by approximately 500 kg/m^3 from the surface to the deepest point). Increasing the alpha value causes GRAVMOD3D to produce depth to bedrock models that do not match known depths as well as it did with smaller alpha values. GI3 produces a model with the best match to known depths and GRAVMOD3D does not improve significantly on GI3's model, especially when the density contrast decreases with depth. Based on these results

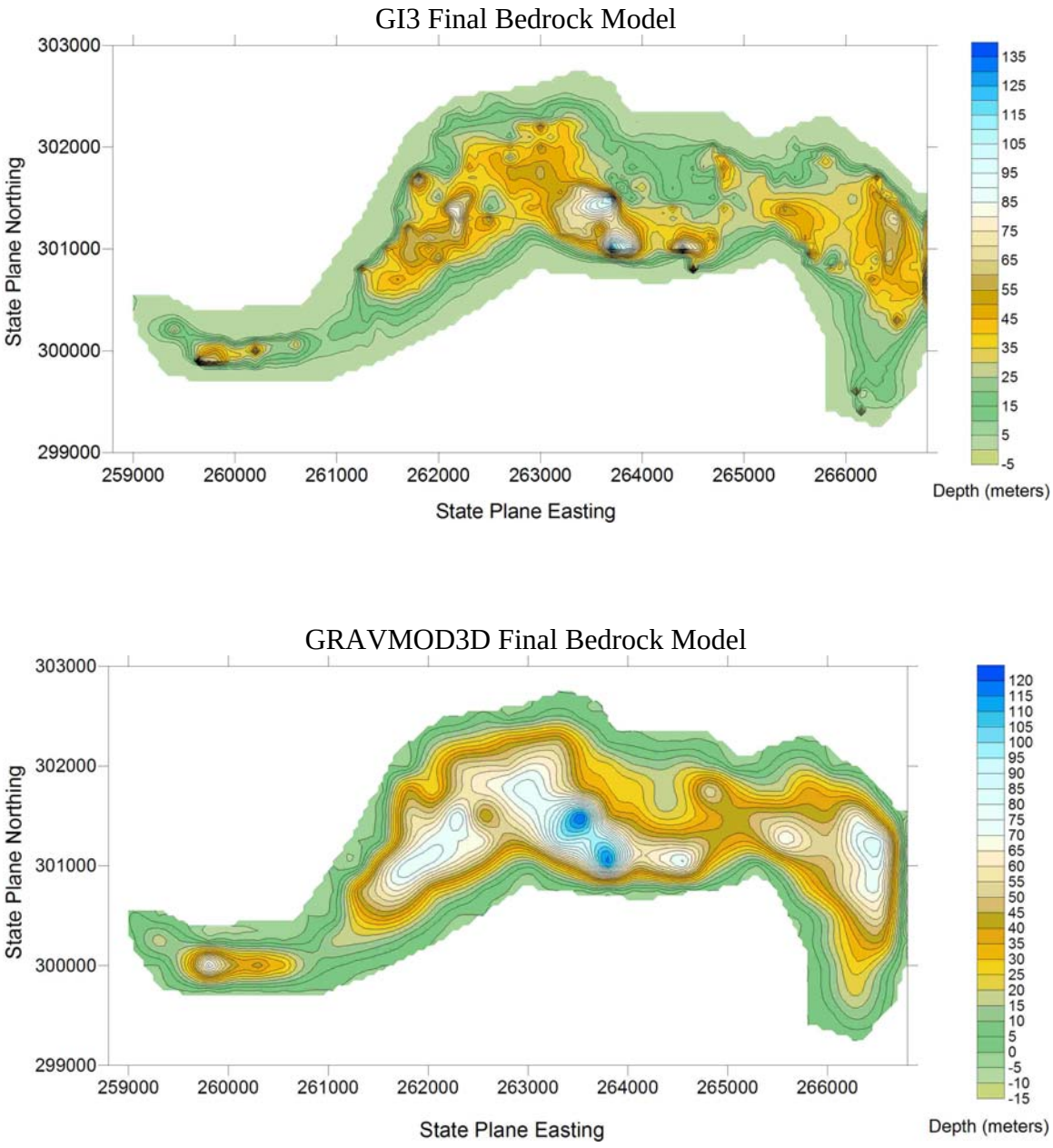

Figure 35. Comparison between the best model found with GI3 and the best model found with GRAVMOD3D. You can see that the program GRAVMOD3D produces a much smoother model, omitting some of the detail seen on the GI3 model.

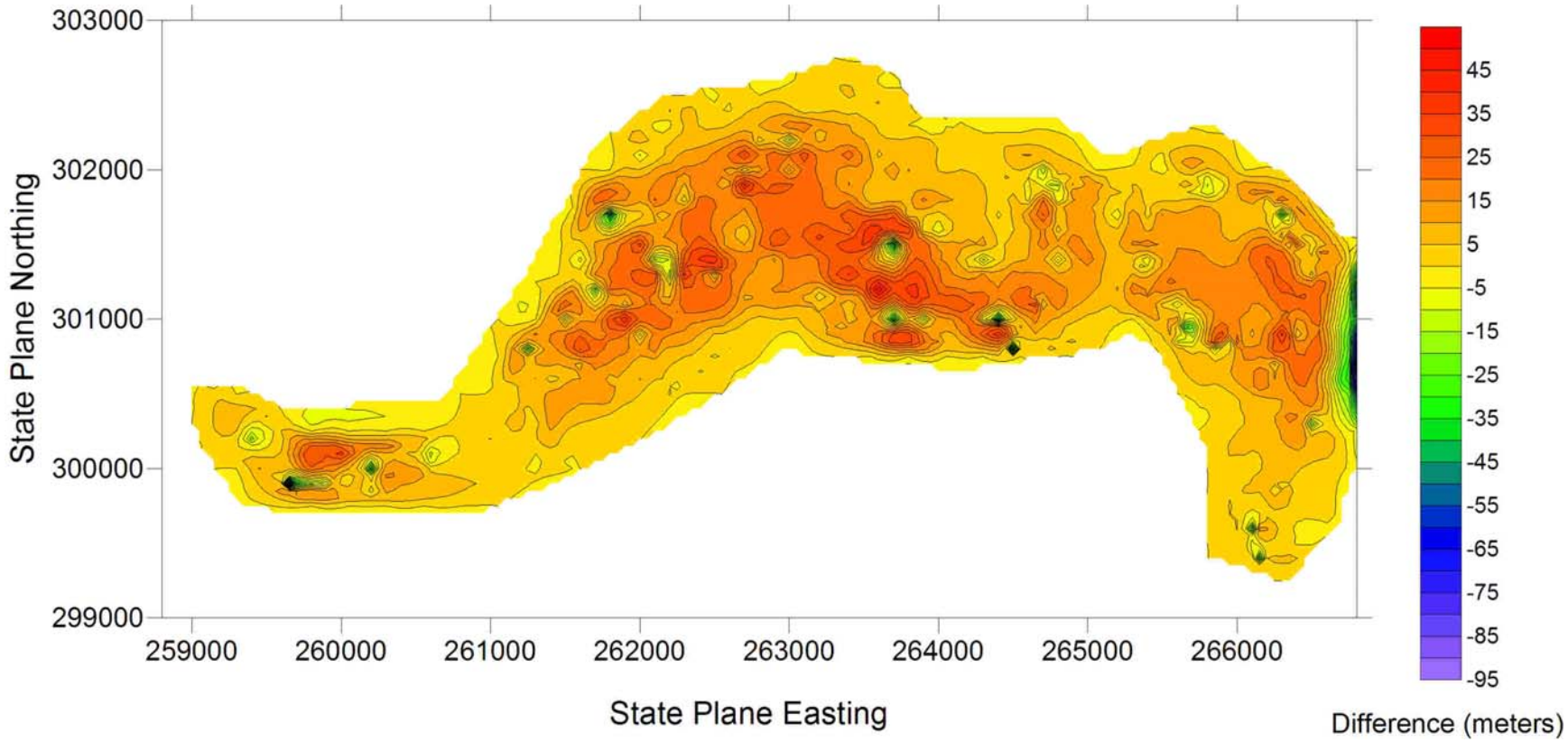

Figure 36: Map showing the difference between the final depth model found using GI3 and the final depth model found using GRAVMOD3D. This was found by subtracting the final model from GI3 from the final model from GRAVMOD3D. It is apparent that GRAVMOD3D creates a much smoother map but is not able to match the steep gradients created by GI3.

I am confident that the density contrast does not vary appreciably with depth. This is not a big surprise for a narrow, fault bounded valley with a depth extent of less than 200 meters. And, from drilling results (Appendix A) we know there are local, steep gradients on the bedrock surface. Therefore when incorporating the new data into the modeling I used GI3.

2006 Addition of New Gravity Data to the Model

During the summer of 2006, Tony Bertholote collected an additional 204 gravity measurements east of the previously collected data (Figure 37). This was done with the intent to extend the bedrock model further to east along the Clark Fork River, to facilitate a new groundwater model. Bertholote followed the same standard procedure as Nyquest (2001) to reduce the gravity measurements to the Complete Bouguer Anomaly. Figure 38 shows the Complete Bouguer Anomaly including both the new and old data. This new data and the previous data were combined into a larger data set, and following the same methods outlined above, were inverted to find a depth to bedrock model. The new depth to bedrock model includes all of the previous gravity data along with the new data, extending the model up the Clark Fork and Blackfoot rivers.

Methods and Results

Since the new data were collected outside the extent of Nyquest's (2001) area, the regional field used to compute Nyquest's (2001) residual gravity anomaly could not be used, and a new regional gravity field had to be developed. The development of the regional gravity field proved to be very difficult for this particular area due to a lack of regional gravity data points near the valley and the shape of the valley itself. In order to

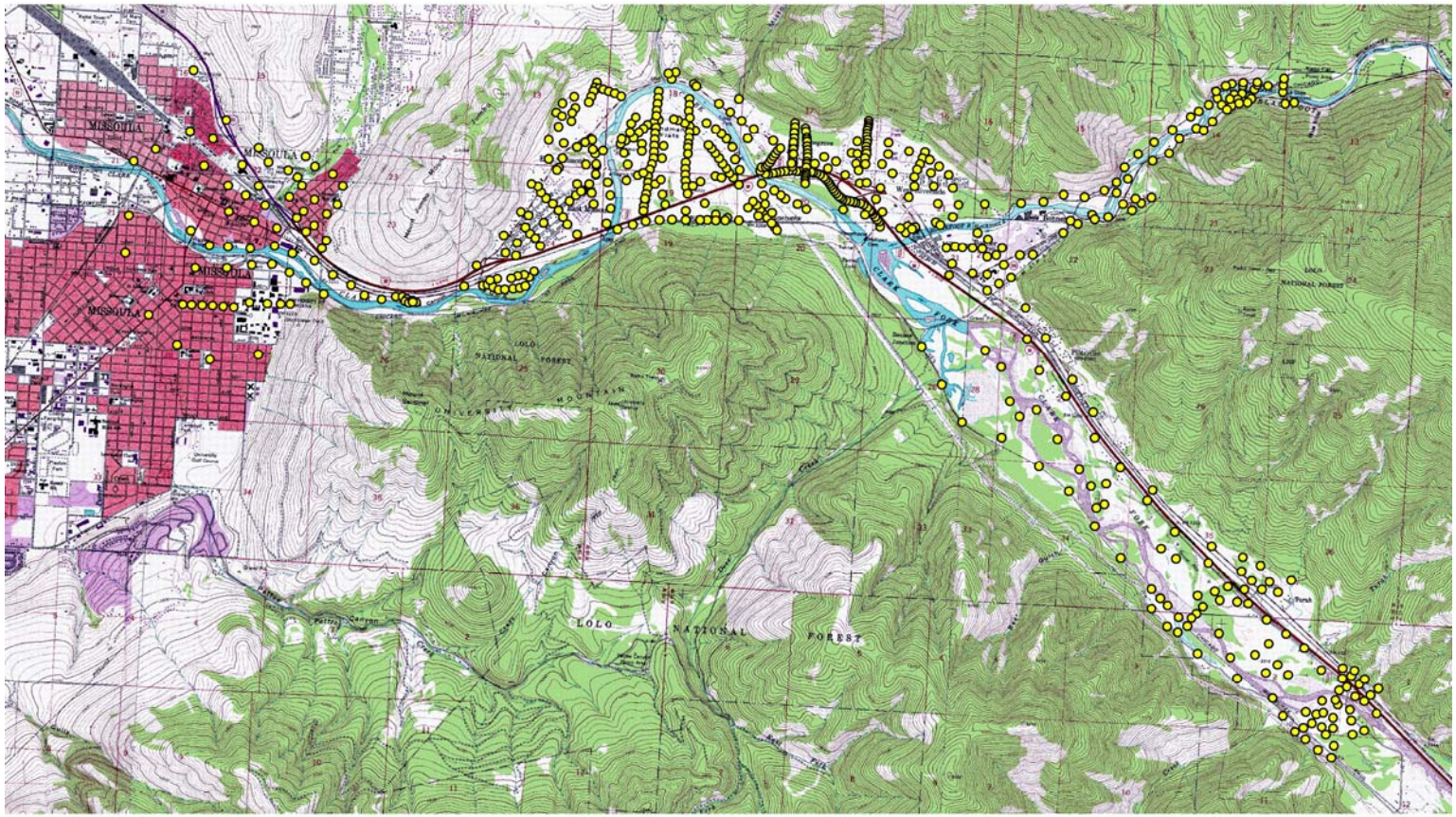

Figure 37. The locations of all of the gravity observations including both the data collected in 2001 and the data collected in 2006. The new data extends the gravity observations up the Clark Fork River and up the Blackfoot river.

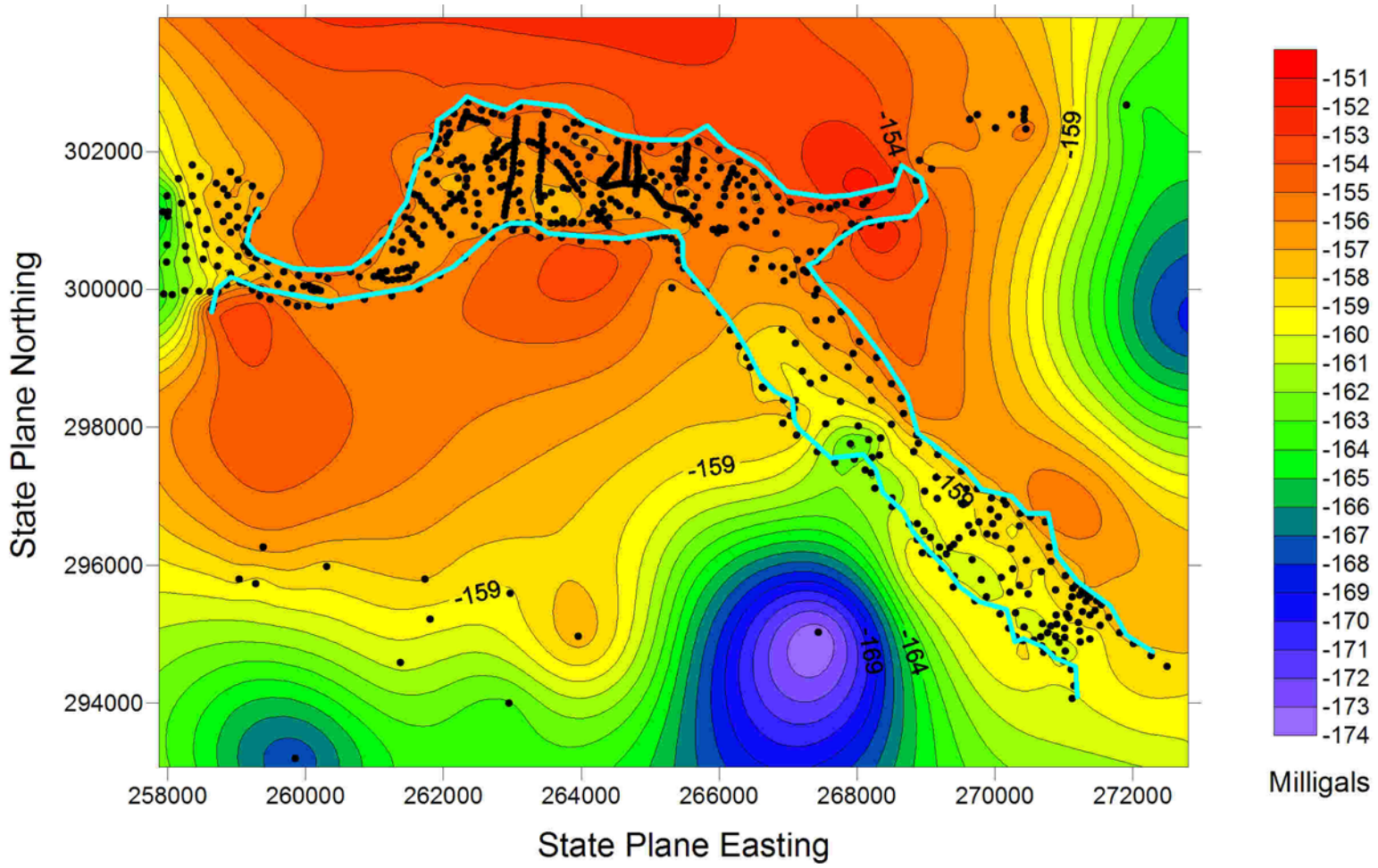

Figure 38: The complete Bouguer anomaly incorporating all of the data, including the data collected in 2001 by Dave Nyquest and the data collected in 2006 by Tony Bertholote. The light blue line represents the edge of the valley and the data used to construct the grid are shown as black dots.

constrain the gravity at the edge of the valley where no gravity measurements exist, synthetic gravity points are created by digitizing points at the edge of the valley along the contact of the bedrock with the valley fill. These points can be used constrain the gravity anomaly because the anomaly must be zero at the edge of the valley. The gravity anomaly is due to the material filling the valley being less dense than the bedrock underneath. At the edge of the valley were the bedrock outcrops there is no less dense material overlying the bedrock so we can assume the gravity anomaly along the edge of the valley must be zero.

To find the gravity value at each digitized point the entire set of real gravity points, including the regional and valley points are gridded. The gravity value at each digitized point is assumed to be the value of the gridded gravity data at the location of the digitized point. The digitized points are then added into the regional gravity data file and force the residual anomaly to go to zero at the edge of the valley. Using this method the regional gravity field was not able to produce a steep enough gradient in the residual gravity anomaly at the edge of the valley and resulted in a residual anomaly that was less than expected. Using this method, the gravity value at the digitized point is based on the gridded surface of all of the known gravity. Assuming that at the valley edge there is a relatively steep gravity gradient, I chose to add one milligal to the gravity value at each edge point. This forces the regional gravity to produce a steep gradient at the edge of the basin in the residual gravity anomaly.

Using the regional gravity data and the digitized valley edge points outlined above a regional gravity field was produced. Figure 39 shows the regional gravity and the points used to create it and Figure 40 show the regional gravity masked to the size of the

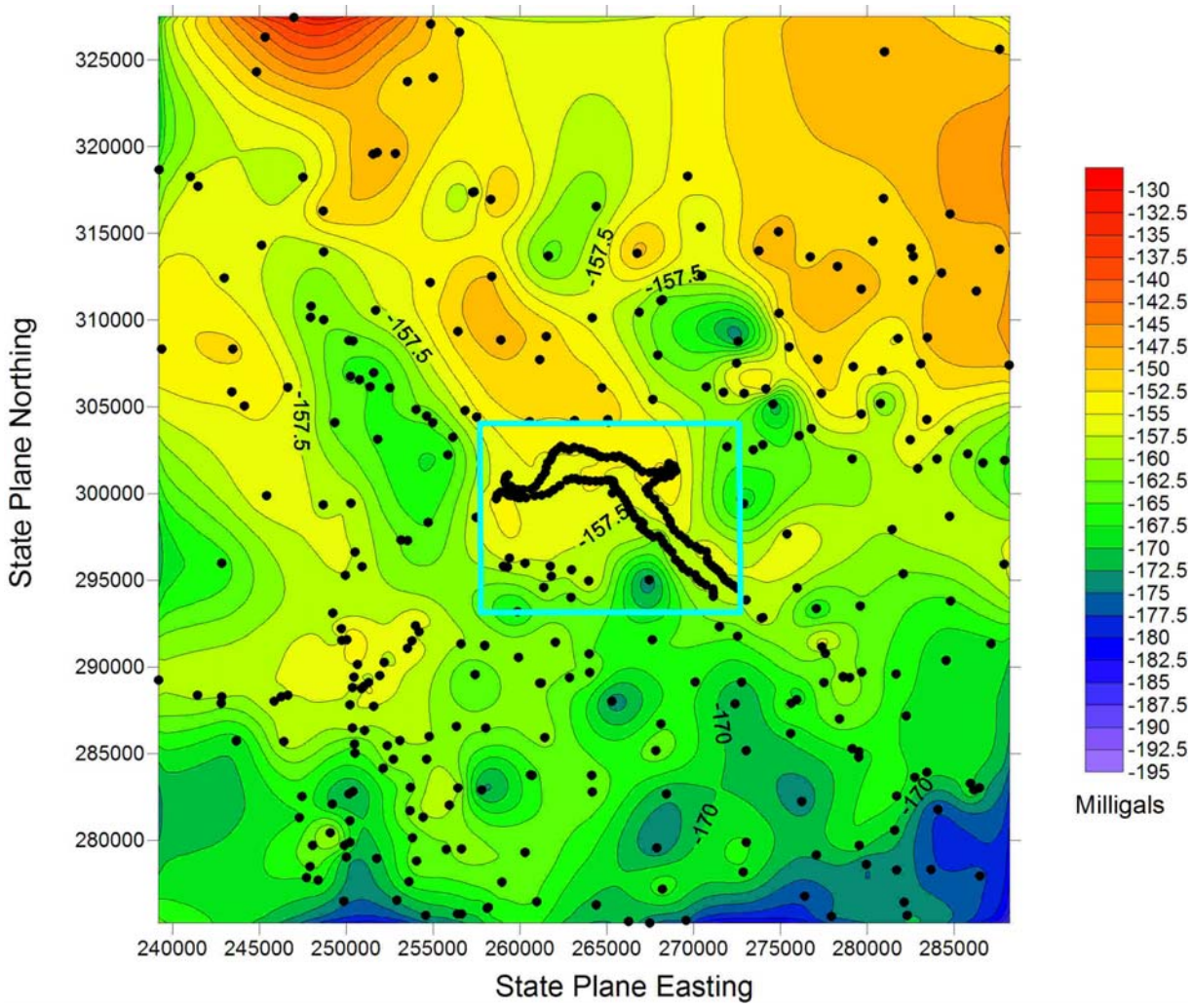

Figure 39: The total regional gravity used to create the residual gravity anomaly. The light blue rectangle represents the area seen in the other figures. The black dots represent all of the data used to construct the regional gravity grid.

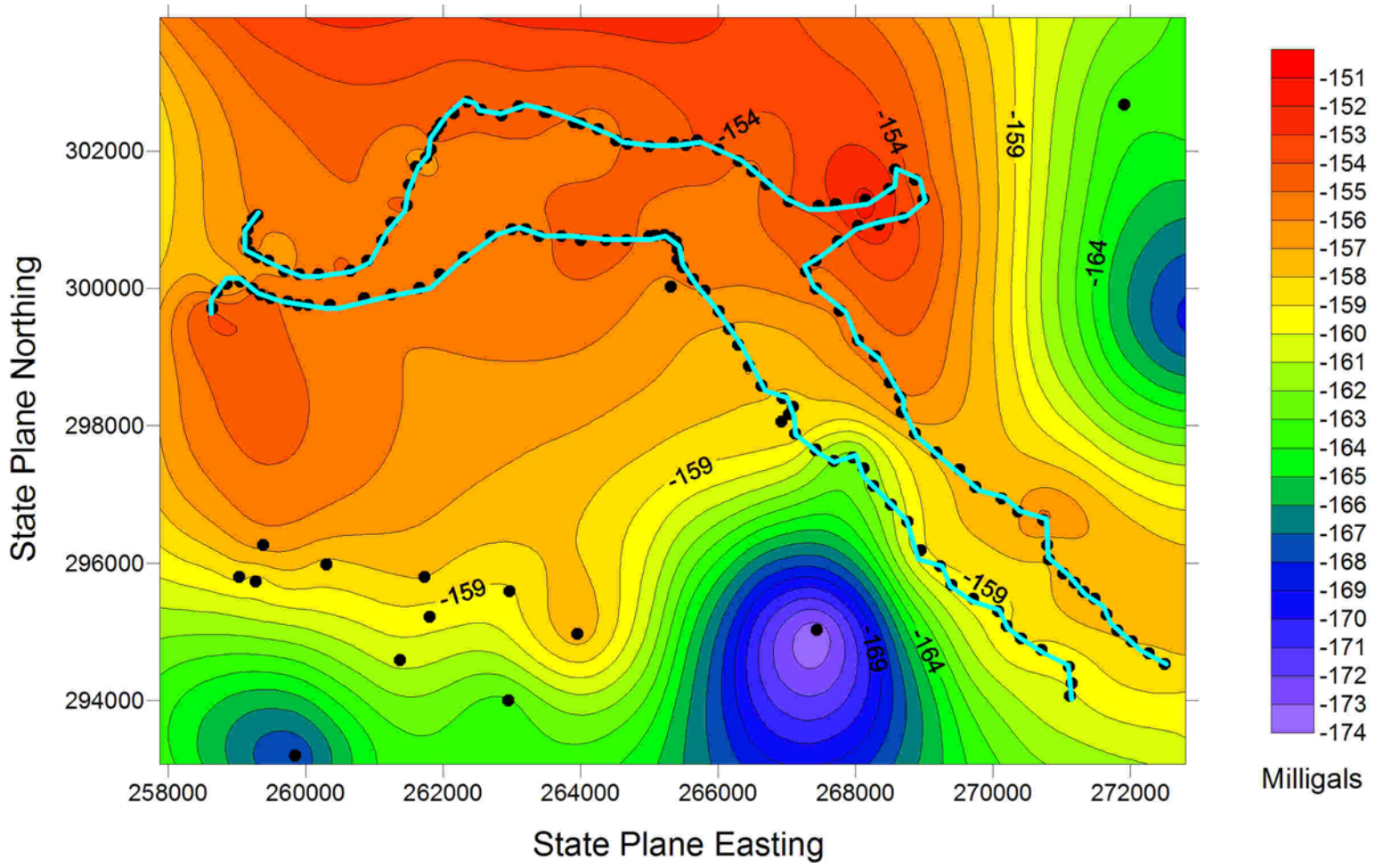

Figure 40: The regional gravity field used to find the residual anomaly. The regional field is an estimate of the broad wave length gravity response in the area. The regional field was constructed using distal points and constrained at the valley edge. The light blue line represents the edge of the valley and the points used to construct the grid are shown as black dots. This map only represents a portion of the total regional grid created. See figure 33 to see the total regional gravity used.

valley. Separating the regional gravity from the total gravity produced a residual gravity anomaly that was similar to the previous work (Figure 41) by Nyquest (2001) where they overlap. The residual anomaly was inverted using GI3 following the same steps given in the previous section. The end result was a best fit to known depths to bedrock using a density contrast of -500 kg/m^3. The departure of the slope of a trend line fitted to the plot of the 173 known depths to bedrock versus the calculated depths to bedrock is 0.11. The mean residual is -1.9 meters and the standard error of the estimates is 15 meters. Figure 42 shows the departure of the trend line from a 1:1 line and the standard error for each run of GI3 with the complete data set. The details of the gravity data processing can be seen in Appendix D including the specific gridding parameters used to develop the grids.

Conclusion

Nyquest (2001), using the smaller data set, found the modeled depths matched the known depths best at a density contrast of -750 kg/m^3, which does not match my results based on the larger data set. GI3 was the only computer model that minimized the error at -750 kg/m^3 using Nyquest's data along with an initial guess at the thickness. All other computer models generated using both GI3 and GRAVMOD3D minimize the error at -500 kg/m^3 or -600 kg/m^3. In order to try and replicate the results found by Nyquest (2001), an initial guess identical to the initial guess used by Nyquest (2001) was created to use in GI3. In the areas outside of Nyquest's (2001) study area where no initial guess yet existed, a simple function was used to estimate the depth to bedrock based on the gravity. By dividing the known depths by their associated gravity response, a constant value of -40 m/mgal was found. Therefore, an initial guess could be calculated by multiplying the gravity at the locations where no initial guess existed by -40 m/mgal.

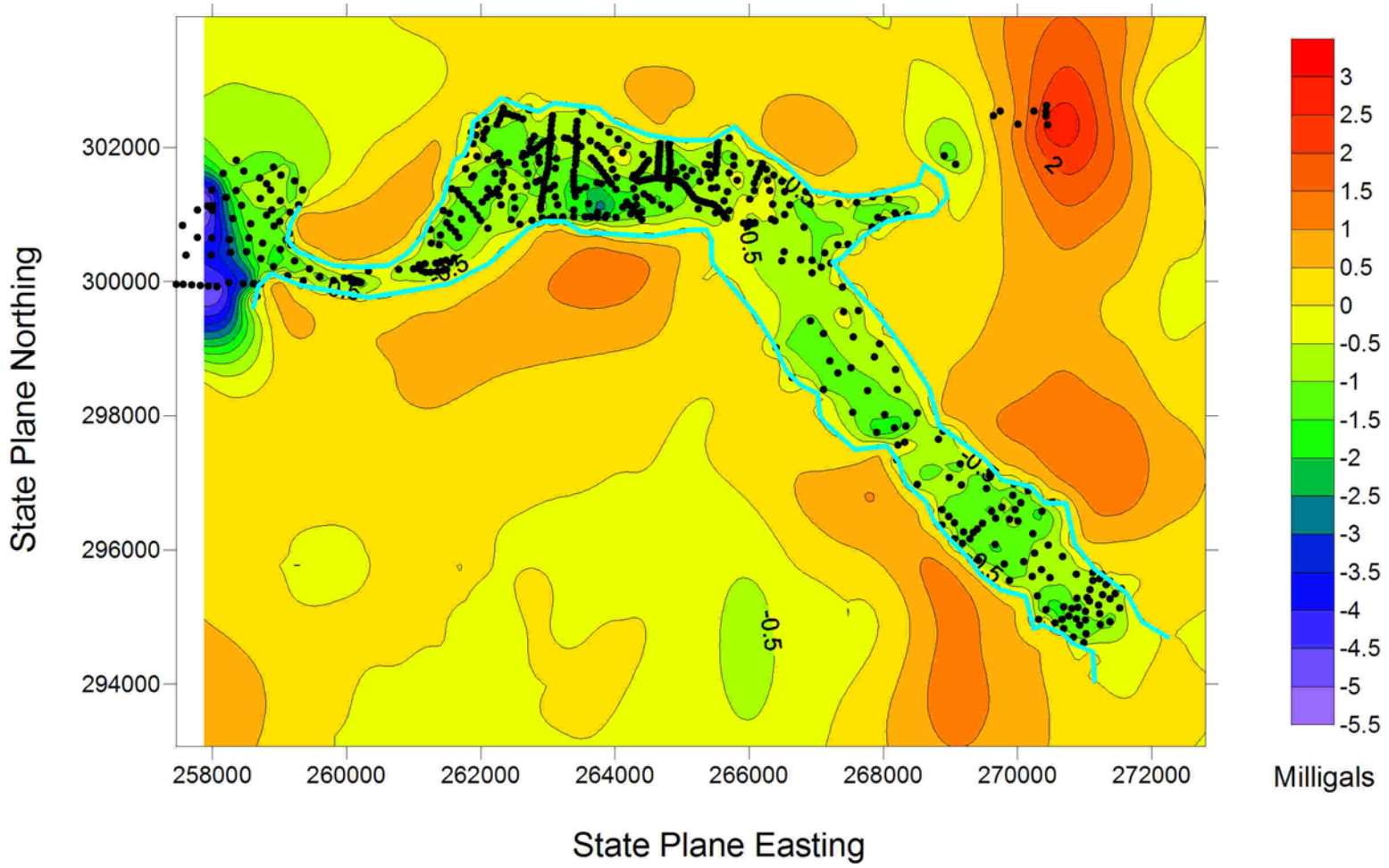

Figure 41: The residual anomaly found by subtracting the regional response from the total CBA. The residual anomaly has a value of zero along the valley edge and is negative inside the valley. The light blue line represent the edge of the valley and the black dots represent the data used to construct the grid.

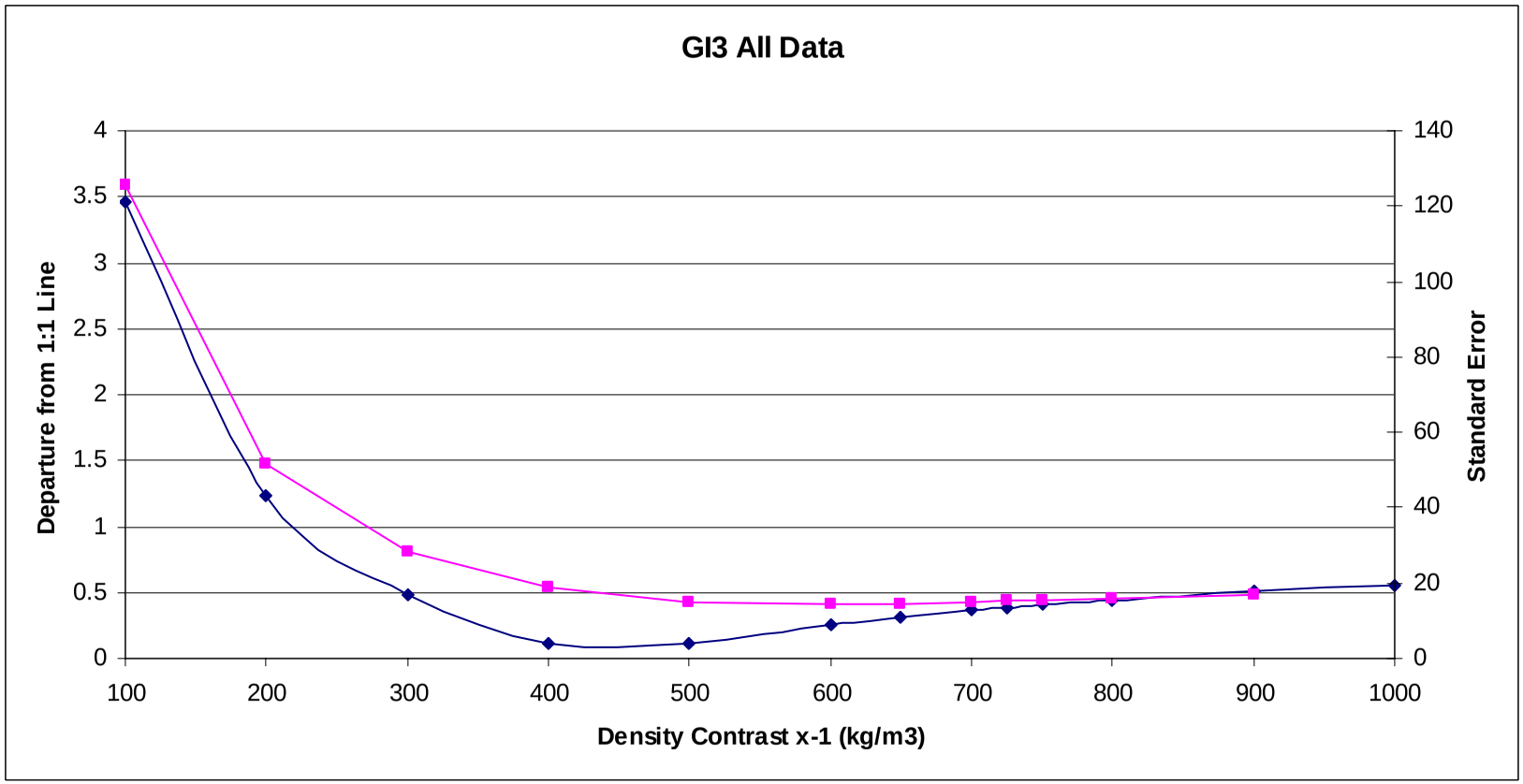

Figure 42: Plot of the departure of the slope of a trendline (in blue) fitted to the plot of the known depths to bedrock versus the calculated depths to bedrock from a 1:1 line and the standard error (in magenta) of each run using GI3 with the complete data set.

Using GI3 with the complete data set and the same initial guess used as Nyquest (2001) for his area also produced a model that minimized the errors at -500 kg/m^3.

Based on the evidence generated by the different computer models and on the data collected by Evans (1997), who found the range of density contrasts in the area to be between -250 and -740 kg/m^3, I believe that the density contrast of -500 kg/m^3 is the best approximation for the Milltown valley area. With the incorporation of the new gravity data the survey area covers a larger area, where the make up and compaction of the alluvium filling the valley may be different. With the larger area it is not unreasonable to assume the average density contrast across the survey area may be different than the average density contrast for the smaller area. A density contrast of -500 kg/m^3 is the minimum possible density contrast that preserves the short wavelength features seen in the residual anomaly and reasonably matches the known depth to bedrock. Decreasing the density contrast between the valley fill and the bedrock causes the depth to bedrock to be too deep and loses the short wavelength features. Increasing the density contrast causes the modeled depth to bedrock to be too shallow. For example, using a density contrast of -100 kg/m^3 produces a model that has a mean residual of -100 meters, meaning the depths calculated are on average 100 meters too deep. Using a density contrast of -1000 kg/m^3 produces a model with a mean residual of 11 meters, meaning on average the depths are 11 meters to shallow. Figure 43 shows examples of how the density contrast affects the estimates of bedrock depth.

Table 11 shows the results from using GI3 with the complete data set and Figure 44 shows the final depth to bedrock model generated from all the current gravity data and is constrained by all available depth to bedrock control data. The error in the depth

	Density (kg/m^3)	Average Error (meters)	Standard Deviation of Error (meters)	Slope of Regression Line	Departure of Slope from 1:1 Line	Standard Error of the Estimates
	-400	-8.5	16.7	1.12	0.1	18.7
Best Fit	-500	-1.9	15.0	0.89	0.1	15.0
	-600	2.4	14.2	0.74	0.3	14.4
	-650	4.1	14.1	0.69	0.3	14.6
	-700	5.5	14.0	0.64	0.4	15.0
	-725	6.2	14.0	0.62	0.4	15.2
	-750	6.8	13.9	0.59	0.4	15.5
	-800	7.9	13.9	0.56	0.4	16.0
	-900	9.7	14.0	0.50	0.5	17.0
	-1000	11.2	14.1	0.45	0.6	17.9

Table 11. Results from the gravity inversion program GI3 using all of the current data. The best fit to the known depths was found using a density contrast of -500 kg/m^3.

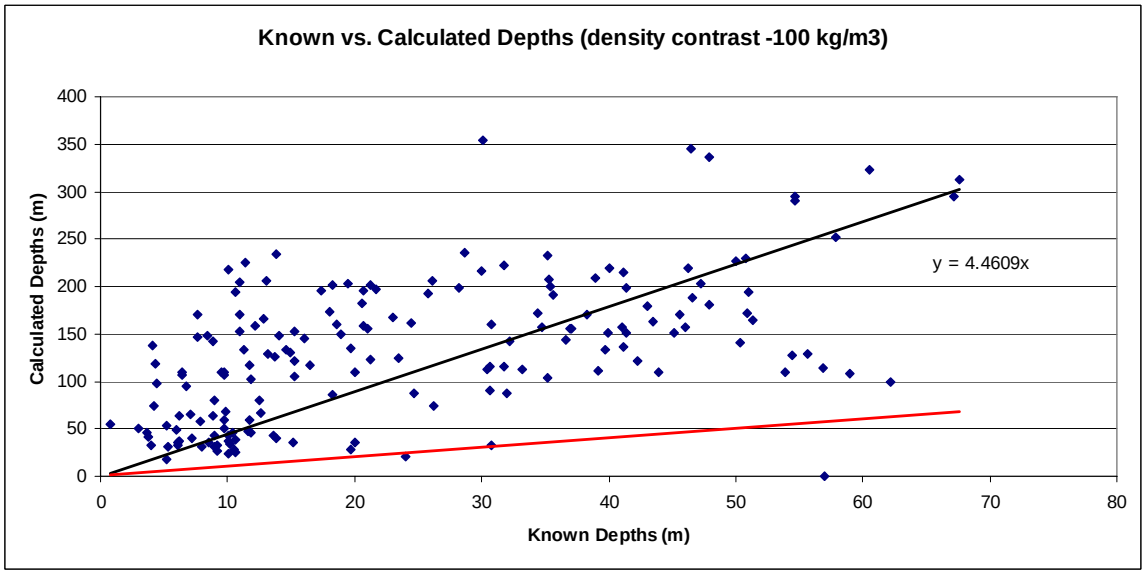

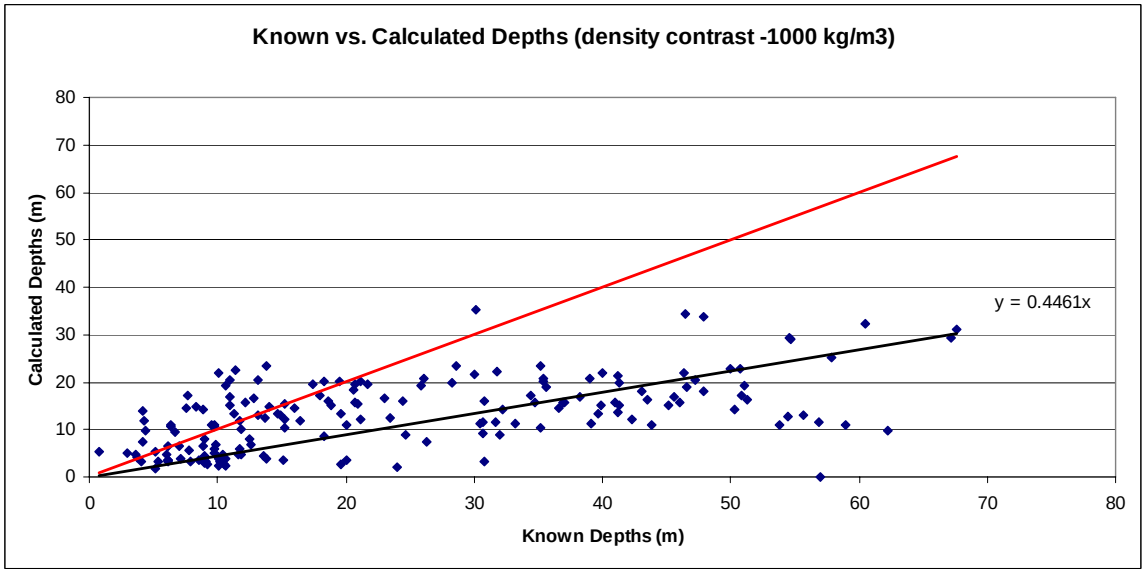

Figure 43: The two charts show the calculated depths verses the actual depths for two different density contrasts. The black line is the trend line fit to the data. The red line is a 1:1 line which represents a perfect fit between known depths and calculated depths. The top graph's calculated depths were found using a small density contrast (-0.1 g/cc) and the bottom graph's calculated depths were found using a large density contrast (1 g/cc). Using the small density contrast the depths are over estimated and using the large density contrast the depths are underestimated.

Figure 44: Final depth model for the entire field area. This is the model that minimizes the error between known depths throughout the valley and the calculated depths found using GI3. This model includes surface topography and an initial guess as inputs into GI3. The density contrasted used to construct this model is -500 kg/m^3.

estimates found using gravity methods comes from the errors associated with collecting gravity data, undetected lateral/vertical changes in density contrast, and possible insufficient observations in areas of steep bedrock gradient. Nyquest (2001) stated a total error associated with his measurements to be 0.15 mgal. Assuming all data used to construct the final model is as accurate as the data collected by Nyquest (2001), then the final model has a standard error of ±15 meters.

As an additional check of the final bedrock model I choose to use the depths calculated by the inversion in a forward model. Forward modeling calculates the gravitational response expected from a particular basin geometry, as opposed to inverse modeling which calculates a basin geometry from a measured gravitational response. Using the thickness model generated by GI3 as an input into GI3's forward modeling module, the expected gravitational response can be calculated (Figure 45). Directly comparing the measured gravitational response to the gravitational response found by forward modeling (Figure 46) shows that the two differ very little across the survey area. For most of the valley the difference between the two is very close to zero and the maximum difference is less than 0.001 mgals.

The residual error for the final map (Figure 44) is found by comparing known depths to bedrock at various locations throughout the study area to the calculated depth at the same location. If the density contrast really is constant throughout the survey area then the value of the residuals should be completely random, i.e. an even distribution of positives and negatives with no dependence on location. However, the map showing the distribution of the residuals (Figure 47) does not confirm this. The map shows a strong dependence on location as to whether the residual is positive or negative. In Hellgate

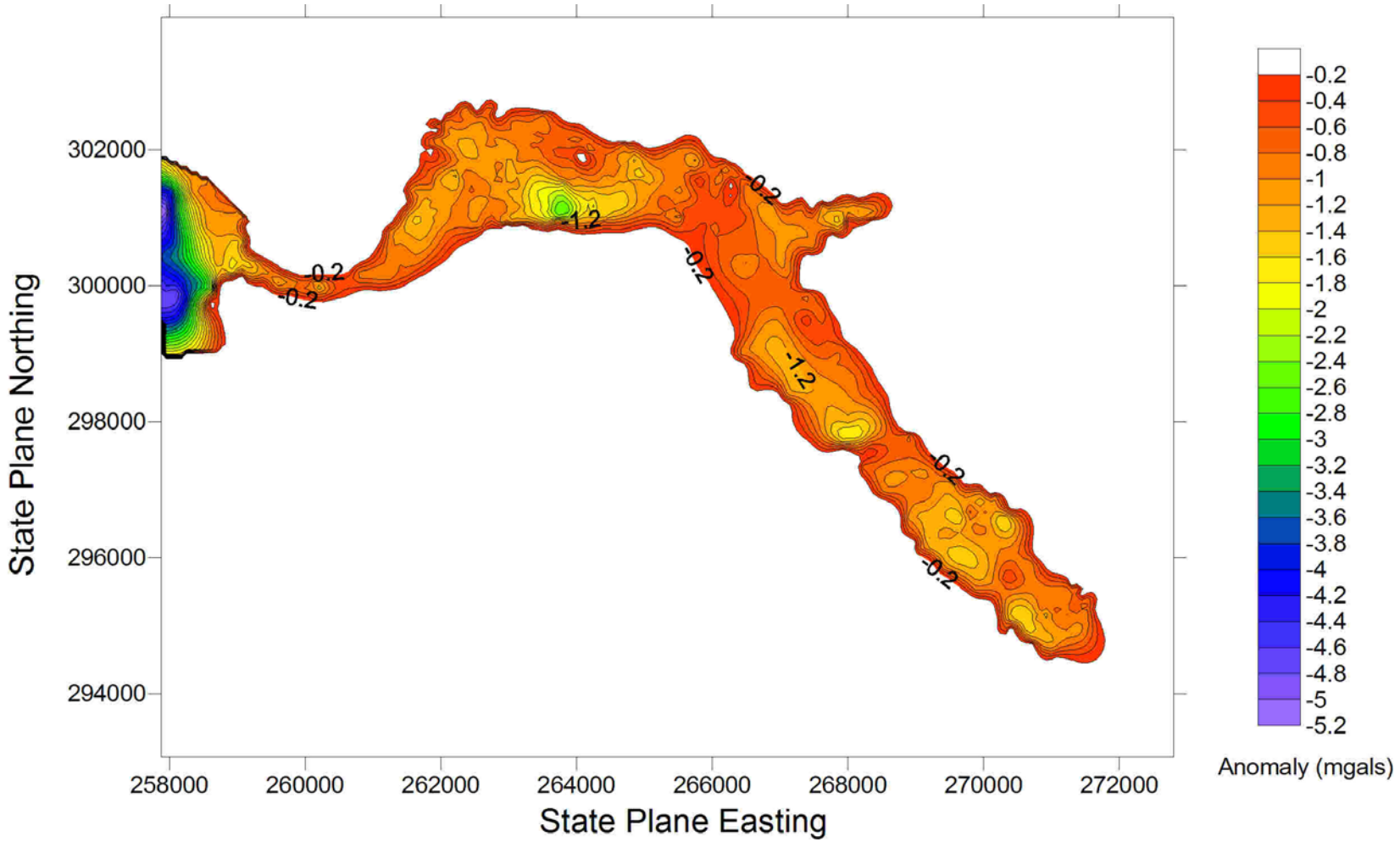

Figure 45: Gravity anomaly created by forward modeling the calculated depths to bedrock. This is the expected gravity anomaly with the bedrock configuration seen in Figure 44.

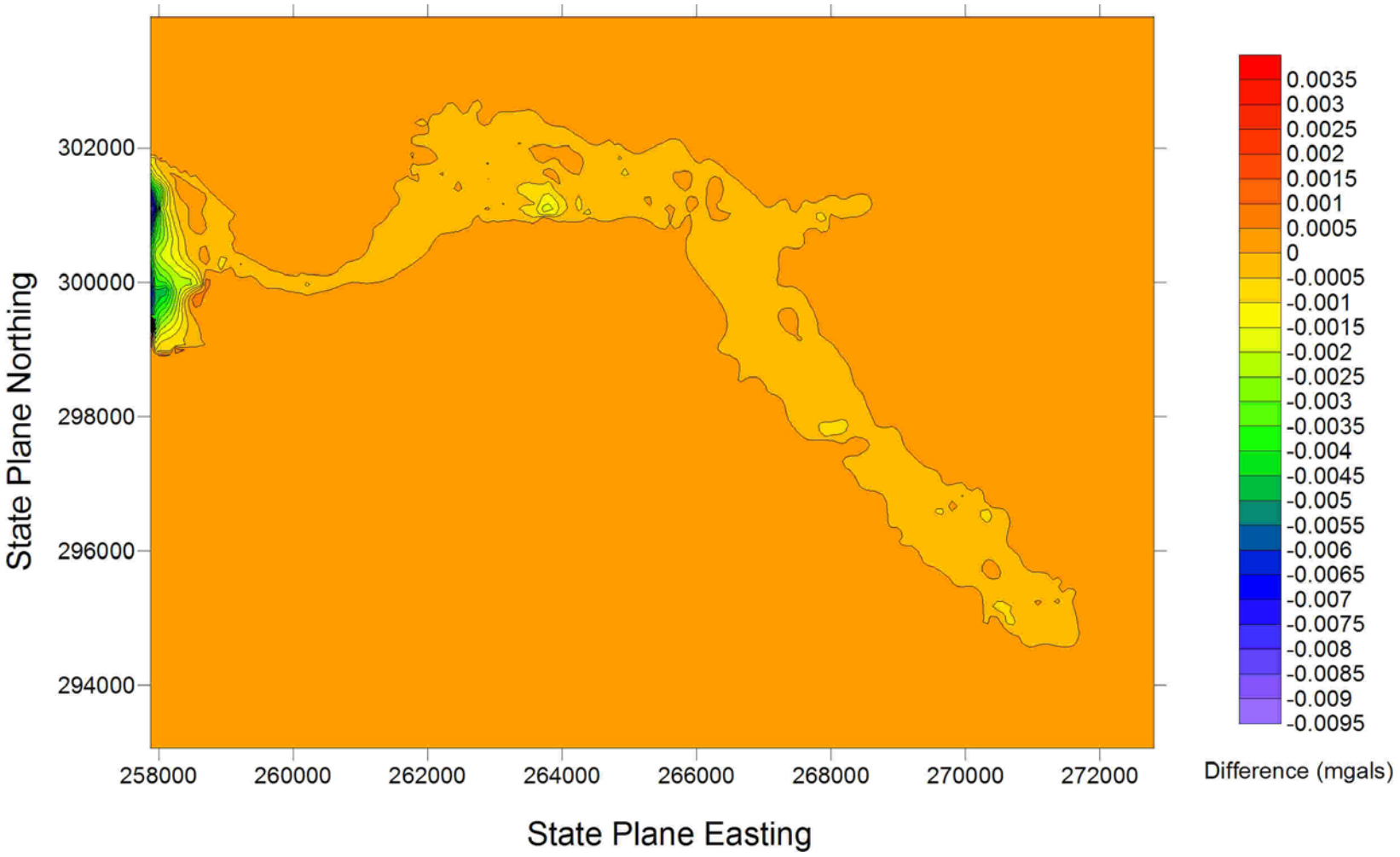

Figure 46: Difference between the measured gravity anomaly and the gravity anomaly calculated by forward modeling the bedrock configuration seen in Figure 44.

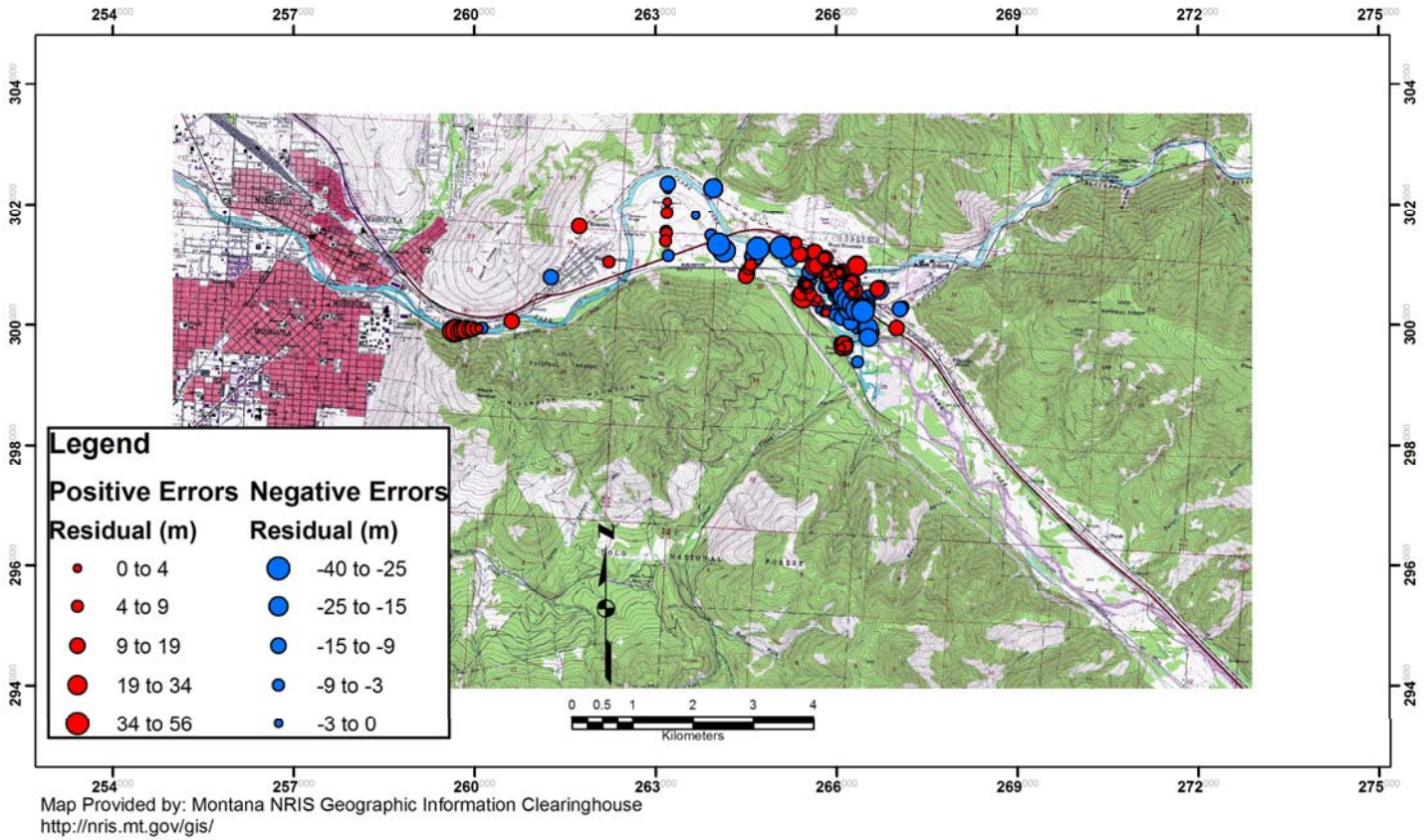

Figure 47: Distribution of the errors in the study area. The residuals were found by subtracting the calculated depth to bedrock from the actual depth to bedrock. Negative values for the residual represent the model over estimating the depth and positive residuals represent the model underestimating the depth.

Canyon the residuals are all positive, which means the model is underestimating the actual depth. Just to the east of the Milltown Dam the residuals are all negative, which means the model is overestimating the depths. In both areas the local geology is affecting the modeled results. In Hellgate Canyon, fault zones nearby causes the bedrock to be less dense than the surrounding rock [J. Sears, personal communication, May 2007], which decreases the density contrast between the valley fill and the bedrock. This causes my selection of a density contrast to be too great for the area and underestimates the depth. A similar problem is found in the area east of Milltown Dam. An igneous sill, which is denser than the surrounding bedrock, has been mapped in that location [J. Sears, personal communication, May 2007]. The igneous sill is a local high density area in the bedrock, such sills have densities as high as 3200 kg/m^3 [Sheriff, personal communication, May 2007]. Above this high density bedrock, there will be a corresponding high in the complete (and residual) Bouguer anomalies. Modeling (or inverting) the gravity using a constant density contrast for the valley fill will result in an artificial bedrock high in the area over the higher density sill, because less low density fill is required to explain the locally higher gravity. Consequently, one must keep in mind that the estimate presented in Figure 44 assumes constant density bedrock across the whole area. For example, a 50 meter thick sill of density contrast + 200 kg/m^3 across half the Milltown Valley would add approximately 0.5 mgals to the anomaly resulting in an artificial high on the order of 25 meters. Undoubtedly, there are local variations in the bedrock density, and the region of Figure 47 with concentrated negative residual overlies the projection of the sill into the subsurface.

Comparing Nyquest's (2001) map to the map I constructed shows several differences. Subtracting Nyquest's (2001) map from the map I constructed (Figure 48) highlights these differences. On average my map is deeper than Nyquest's (2001) map, but there are areas where mine is shallower despite both maps being generated from similar gravity anomalies. The largest differences occur in areas where the gravity measurements are sparse or in areas that were boundaries in Nyquest's (2001) map and are not in mine. I was unable to recover Nyquest's exact methods for developing his residual gravity anomaly; i.e. what data he used and what data he threw out, his gridding parameters, etc; which could account for the differences between his final map and my final map. My final map (Figure 44) incorporates a larger gravity data set and covers more area, and represents the current best estimate for depth to bedrock in the greater Milltown area. All of the gravity data available to me along with my seismic data and previous depth to bedrock information (Appendix A) were used to construct this estimate.

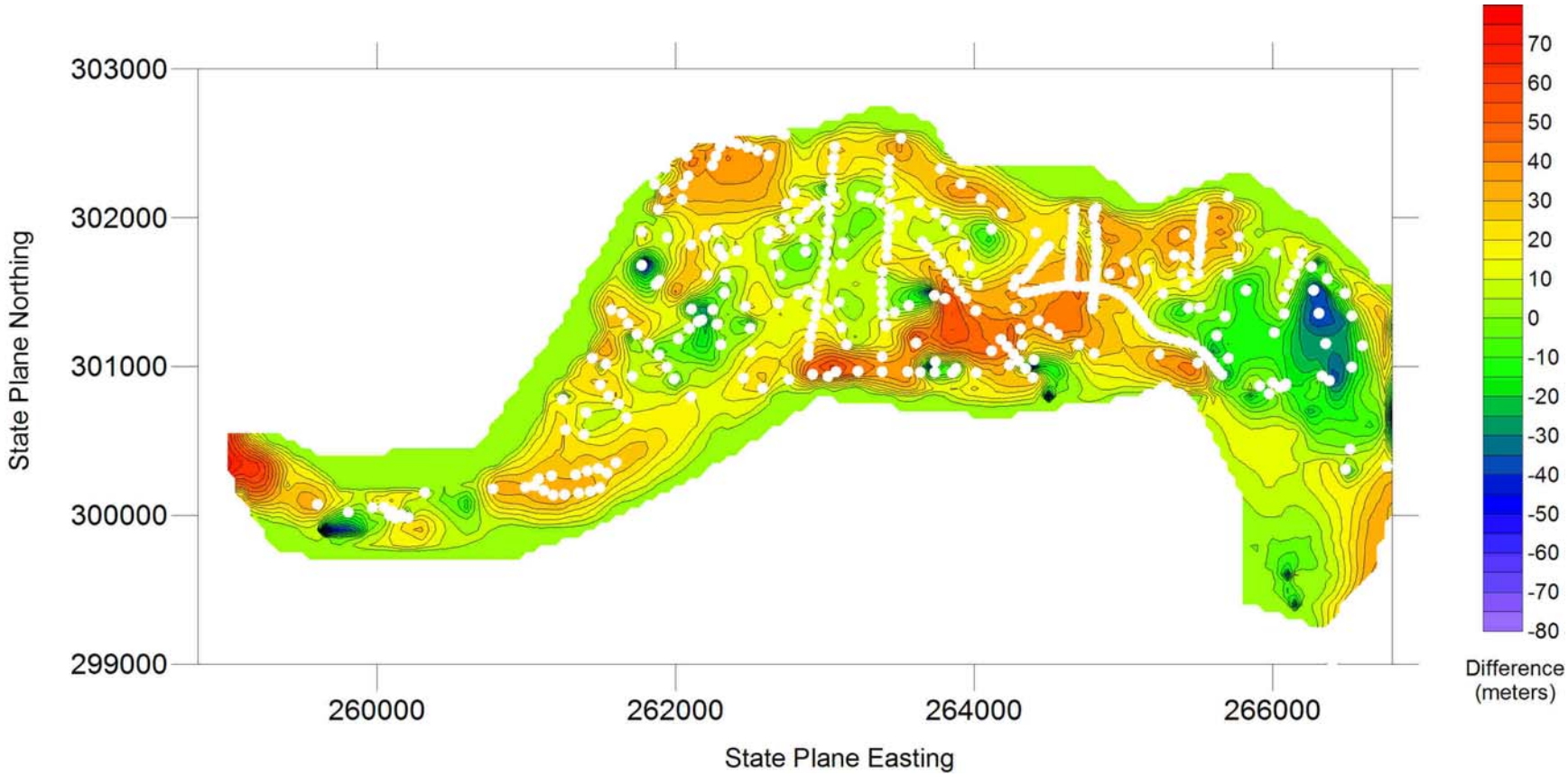

Figure 48: Difference map between the previous map and the new map I created where the two coincide. The map I created was subtracted from the previous map. Positive values represent where the new map is deeper and negative values represent where the new map is shallower. The white dots show the location of the gravity measurements.

COMPARISON OF SEISMIC REFLECTION AND GRAVITY METHODS

The combination of previous seismic results, gravity observations and wells to bedrock, when combined with new reflection seismology and an extended gravity interpretation provides a more extensive map of bedrock topography. The combined data provide a better constrained solution for the bedrock topography in the greater East Missoula Area.

Comparing the seismic data to the gravity data shows a reasonable correlation between the two. The depth estimates from the seismic data match the depth estimates from the gravity at similar locations. Both of the estimates are also similar to known depths to bedrock from well log and drill core data. All three methods, seismic, gravity and well log and drill core data, have inherent errors associated with them. The seismic data depends heavily on the velocity of the layers and on the interpreter's ability to pick reflections. The gravity data depends heavily on the density contrasts and the regional-residual separation. The well logs and drill core data have many ambiguities in them which are a direct result of the process (i.e. did the drill go into a large boulder of bedrock or did it actually hit the bedrock? Did the driller get paid by the foot?). For each depth estimate there is a standard error of at least ± 5 meters.

The velocity analysis of the seismic data at each location does provide some insight into how the density of the valley fill varies in the valley. In a broad sense, the velocity of a material increases with an increase in density of the material. If the density of the valley fill increased in the vertical direction I would expect to see gradual increase in the velocity. If this were the case, the first arrivals in the seismic section would lie along a curved line. In the seismic data collected the first arrivals lie along a straight line

that fits those arrivals with a R^2 value of 0.98 or greater. This supports the conclusion found in the gravity section above that the density of the valley fill does not increase significantly with depth. Looking at the lateral variations in the velocity of the valley fill suggests that the density of the valley fill may change latterly in the valley. The velocity of the valley fill was the greatest in Hellgate Canyon, suggesting that the density of the valley fill was higher. This could account for the gravity model underestimating the depths in this area. If the density of the valley fill were higher, there would be less density contrast in that area between the valley fill and the bedrock. The model would be using too high of a density contrast in that area, which would result in an underestimation of the depth. The opposite is true along Deer Creek Road. This area has the slowest velocity of the valley fill, which suggests that the density of the valley fill in this area is less dense. Here the model overestimates the depth because it is using too low of a density contrast. The velocity found from seismic methods could be a good indicator of how the density of the valley fill varies in a lateral direction.

CONCLUSION

Seismic reflection methods can be used to improve the bedrock map in the study area, although it only works well in areas that are shallower than 40 meters. The best use of seismic in this area would be to provide more data for comparison between the depths found using gravity inversion and depths from other methods (seismic, drill cores and wells) or to further resolve the depth to bedrock in areas where the gravity gradient is high. Another use of seismic methods would be to determine lateral variations in the density of the valley fill through the use of velocity analysis. Performing additional seismic in the area may be difficult though due to land access issues and environmental factors. In order to perform a seismic survey in the study area a source capable of putting a large amount of energy into the ground is needed due to the high attenuation of the alluvium. It would also be expensive to perform a large scale seismic survey in this area (3 to 4 people plus equipment for the seismic versus 1 to 2 people with a gravimeter for a gravity survey).

The seismic reflection data is useful for building a general model of the bedrock, but for modeling the entire basin gravity methods are still the method of choice. Interpreting the gravity data into a depth model is best done with GI3. This computer program has no problem dealing with the small scale of the basin and the high gradients in the anomaly. Also analysis of both the gravity data and seismic data suggest that the density of the valley fill remains constant in the vertical direction, so there is no need to model the gravity data with a program that allows the density contrast to change with depth. Nyquest's (2001) map produced using gravity inversion shows the most detail of the maps that were available at the beginning of this study and was a considerable

improvement to Gestring's (1994) map. Using 598 gravity measurements, ten new seismic reflection lines and data from drill cores, wells completed to bedrock and previous seismic refraction data I constructed a new map. The new map is based heavily on the gravity data and is constrained with the seismic reflection data, drill cores, wells completed to bedrock and the previous seismic refraction data. The seismic reflection data, drill cores, wells completed to bedrock and previous seismic refraction data was used to create an initial bedrock model as a starting point for the gravity inversion and to provide an estimate of how well the gravity inversion fit actual depths.

Using the complete gravity data set the computer modeling converges to the same solution regardless of the initial model. Using the additional seismic data, along with the other known depths to bedrock data to construct an initial model the modeling program converges to the same final model as it did without an initial guess. The collection of seismic data in a situation like this can be used to better constrain the final model by having additional depth data to compare the solution to. This would allow a better understanding of the error associated with the final model and ways to minimize the error further.

The additional gravity data collected, when integrated with the previous data, greatly increased the coverage of the bedrock model. The new data proved difficult to incorporate and model, raising some new problems that had to be overcome. After processing and inverting the combined gravity set, a new bedrock model was created. Additional work that could be done would include the collection of more seismic data to further refine the final model output by GI3. Additional gravity data could also be collected in the study area and in the surrounding areas. The new gravity data set covers

a much bigger area than before but still has portions that need more gravity measurements. Filling in these areas and collecting a series of regional gravity points in the area directly surrounding the valley could greatly improve on the accuracy of the bedrock model.

With the data collected to date, Figure 44 shows the best estimate of the bedrock topography of the Milltown Valley and surrounding area. The map differs from Nyquest's (2001) map in various locations but still provides a geologically reasonable solution. The model incorporates all of the current gravity data and is constrained by depths from drill cores, wells completed to bedrock and seismic refraction and reflection data.

REFRENCES

Associates, H. L. (1987), Volume 1, Milltown Reservoir Data Report Supplemental Investigations Conducted Under the Feasibility Study., Harding Lawson Associates, Denver, Colorado, HLA Job No. 17461,002.10.

Barbosa, V. C. F., et al. (1999), Stable inversion of gravity anomalies of sedimentry basins with nonsmooth basement reliefs and arbitrary density contrasts variations, Geophysics, 64, 754-764.

Bear, G. W., et al. (1995), Linear inversion of gravity data for 3-D density distributions Geophysics, 60, 1354-1364.

Blackhawk Geosciences, I. (1990), Seismic Refraction Survey, Milltown Reservoir Sediments Site, 6-7 pp, Misoula, MT.

Bradford, J. H. (2002), Depth characterization of shallow aquifers with seismic reflection Part 1 - The failure of NMO velocity analysis and quantative error prediction, Geophysics, 67, 89-97.

Camacho, A. G., et al. (2000), Gravity inversion by means of growing bodies, Geophysics, 65, 95-101.

Camp, D., and McKee (1989), Milltown Downstream Screening Study: Data Report.

Chai, Y., and W. J. Hinze (1988), Gravity inversion of an interface above which the density contrast varies exponentially with depth, Geophysics, 56, 837-845.

Chakravarthi, V., et al. (2001), INVER2DBASE - A program to compute basement depths of density interfaces above which the density contrast varies with depth, Computers and Geosciences, 27, 1127-1133.

Chakravarthi, V., and N. Sundararajan (2004), Automatic 3-D gravity modeling of sedimentary basins with density contrast varying parabolically with depth, Computers and Geosciences, 30, 601-607.

Chakravarthi, V., and N. Sundararajan (2005), Gravity modeling of 2 1/2-D sedimentary basins -- a case of variable density contrasts, Computers and Geosciences, 31, 820-827.

Cordell, L., and R. G. Henderson (1968), Iterative three-dimensional solution of gravity anomaly data using a digital computer Geophysics, 33, 596-601.

Evans, C. (1997), A Gravity Interpretation of the Bedrock Structure of the Central Missoula Valley, Montana, University of Montana Missoula, Montana

Garcia-Abdeslem, J. (2003), 2D modeling and inversion of gravity data using density contrast varying with depth and source - basement geometry described by the Fourier series, Geophysics, 68, 1909-1916.

Garcia-Abdeslem, J. (2005), The gravitational attraction of a right rectangular prism with density varying with depth following a cubicv polynomial, Geophysics, 70, j39-j42.

Gestring, S. (1994), Interaction of the Clark Fork River with the,, University of Montana, Missoula, Montana.

Goforth, T., and C. Hayward (1992), Seismic reflection investigations of a bedrock surface buried under alluvium, Geophysics, 57, 1217-1227.

Guspi, F. (1992), Three-dimensional Fourier gravity inversion with arbitrary density contrast, Geophysics, 57, 131-135.

Lankston, R. W. (1988), High resolution refraction data acquistition and interpretation, in Symposium on the Application of geophysics to engineering and environmental problems, edited, Golden, CO.

Li, Y., and D. W. Oldenburg (1998), 3-D inversion of gravity data, Geophysics, 63, 109-119.

Mendonca, C. A. (2004), Inversion of gravity-field inclination to map the basement relief of sedimentray basins, Geophysics, 69, 1240-1251

Nelson, W. H., and J. P. Dobell (1961), Geology of the Bonner Quadrangle, Montana, U.S. Geological Survey Bull. 1111-F, 235

Nyquest, D. (2001), A Depth to bedrock model of the hellgate canyon and bandmann flats area, East Missoula, Montana using constrained inversion of gravity data, Masters thesis, 186 pp, University of Montana, Missoula.

Pullan, S. E., and J. A. Hunter (1991), Delineation of buried bedrock valleys using the optimum offset shallow seismic reflection technique, Investigations in Geophysics 5, 75-87.

Rene, R. M. (1986), Gravity inversion using open, reject, and "shape-of-anomaly" fill criteria, Geophysics, 51, 988-994.

Reynolds, J. M. (1997), An Introduction to Applied and Environmental Geophysics, 796 pp., John Wiley & Sons, Chichester.

Salem, A., et al. (2004), Lineraized least-squares method for interpretation of potential-field data from sources of simple geometry, Geophysics, 69, 783-788

Silva, J. B. C., et al. (2000), Gravity inversion using convexity constraint, Geophysics, 65, 102-112.

Steeples, D. W., and R. D. Miller (1991), Seismic reflection methods applied to engineering, environmental, and groundwater problems, Investigations in Geophysics, 5, 1-30.

Steeples, D. W., and R. D. Miller (1998), Avoiding pitfalls in shallow seismic reflection surveys, Geophysics, 63, 1213-1224.

Thompson, M. D., McGinnis, L. D., Wilkey, P. L., Miller, S. F. (1997), Gas Rich Sediment and Cosatal Wetland Loss in Louisiana, Open Source Report: Argonne National Labratory.

Treitel, S., and L. Lines (2001), Past, present, and future of geophysical inversion - A new millennium analysis, Geophysics, 66, 21-24.

Woessner, W. W. (1988), Missoula Valley Aquifer Study: Hydrogeology of the Eastern Portion of the Missoula Valley Aquifer, Missoula County, Montana, Helena, Montana.

Woessner, W. W. (1993), Clark Fork natural Resource Damage Assessment. Milltown Ground water Injury Report, University of Montana, Missoula, Montana.

Woessner, W. W., et al. (1984), Arsenic Source and Water Supply Remediation Action Study, Milltown Montana.

Woessner, W. W., and W. A. Popoff (1982), Hydrogeologic Survey of Milltown, Montana and Vicinity, Helena, Montana.

Xu, S.-z., et al. (2003), A new method for continuation of 3D potential fields to a horizontal plane, Geophysics, 68, 1917-1921.

APPENDIX A

EMC Depths

ID	State Plane X (m)	State Plane Y (m)	Thickness (m)
904	280243.9069	5194800.449	20.732496
905	280455.7673	5194685.872	21.189696
906	280343.7715	5194797.471	34.448496
907	279626.8576	5195132.562	13.112496
908	279883.2523	5195113.716	32.010096
912	280181.4229	5193880.139	5.187696
914	280156.3836	5195144.626	36.582096
918	280453.0423	5193652.252	8.845296
920	279287.9535	5195374.116	18.294096
099A	280281.51	5194910.634	36.920424
100A	280096.1063	5194861.065	14.938248
101A	280241.0052	5194742.452	18.589752
102A	280407.8131	5194631.236	19.5072
103B	280568.5829	5194590.884	28.639008
104A	280602.7875	5194729.403	25.834848
105A	280375.6536	5194839.848	38.26764
106C	280338.2272	5194997.481	39.940992
107C	280272.744	5194831.094	30.787848
108B	280120.1977	5195134.833	34.7472
109A	280413.8481	5195257.024	43.882056
110A	281092.0159	5194240.775	44.192952
111B	280789.127	5194870.251	46.027848
909B	279982.3915	5195140.167	21.646896
910B	280246.4459	5193906.163	6.711696
911A	280252.8893	5193863.159	6.102096
913A	280212.5887	5193939.935	6.102096
916A	279862.849	5195372.388	30.790896
917A	279702.1218	5195234.877	31.705296
919B	279689.5549	5195474.813	54.412896
921B	279454.0482	5195430.199	23.018496
922B	279354.8845	5195623.168	47.859696
923B	279146.8372	5195538.342	35.362896
B-1	279545.6223	5194938.039	13.77696
B-2	279533.1986	5194923.555	8.5344
B-3	279550.6606	5194943.937	10.48512
B-4D	279538.5814	5194929.794	10.668
B-5	279536.8074	5194960.884	8.9916
B-6	279521.6345	5194943.708	13.59408
B-8	279561.8833	5194957.046	10.2108
B-9	279552.4925	5194977.83	11.82624
BF-C01	279883.4496	5194898.022	5.1816
CD-C03	279613.9457	5194879.959	12.4968
CD-C04	279585.5267	5194936.275	4.0386
DC-C05	280005.8946	5194900.039	8.9916
DC-C07	280116.0646	5194788.172	9.7536

DC-C09	280278.0658	5194670.961	14.6304
DC-C42	280070.1465	5194765.787	10.9728
DC-C52	280208.2422	5194641.801	15.24
DC-C54	280082.2074	5194537.468	10.9728
DC-C61	280288.6515	5194525.257	15.24
DC-C79	280620.4324	5194235.6	12.8016
DC-C80	280672.157	5194158.043	12.192
DD-C01	279910.029	5194472.326	15.24
DH-1	279553.6812	5194935.604	10.39368
DH-10	279588.8338	5194990.797	6.15696
DH-11	279566.2481	5194997.758	6.15696
DH-12A	279542.3883	5194970.756	7.04088
DH-2	279560.4752	5194943.839	5.97408
DH-3	279568.2018	5194953.096	3.74904
DH-4	279574.2308	5194960.399	3.6576
DH-5	279582.4665	5194968.802	2.95656
DH-6	279595.8838	5194970.671	0.79248
DH-7	279595.0334	5194976.956	7.83336
DH-8	279622.121	5195005.4	11.67384
DH-9	279608.024	5194992.071	4.20624
DW-W01	280424.193	5194530.482	12.6492
EB-C01	279571.5284	5194883.104	10.9728
EB-C02	279587.6024	5194883.912	10.0584
EM-C01	280034.3904	5194911.256	19.6596
EM-C02	280195.081	5194759.405	16.4592
EM-C03	280293.2875	5194691.343	18.8976
EM-C04	280378.9363	5194634.193	17.9832
EM-C05	280524.9965	5194535.072	17.3736
EM-C06	280184.6873	5194740.995	11.43
EM-C07	280369.4875	5194616.454	8.382
EM-C08	280078.5254	5194830.515	10.668
EM-C09	280281.0346	5194676.164	13.716
EM-C10	280526.2462	5194503.19	7.62
EM-C11	280005.9221	5194907.202	10.0584
EM-C12	280386.8002	5194647.665	20.0406
EM-C14	280059.2926	5194926.984	20.7264
EM-C15	279966.9382	5195013.456	23.4696
GC-C01	279992.4621	5194948.837	4.4196
GC-C02	279978.89	5194967.372	6.4008
GC-C04	280622.2162	5194067.971	11.8872
GC-C06	280003.7089	5194936.345	8.8392
GC-C07	280027.0447	5194972.429	6.4008
GC-C09	280011.0325	5194960.108	4.2672
HLA-1	279921.6449	5195066.704	30.467808
HLA-2	280048.3868	5195092.066	24.700992
IS-C01	279806.97	5194511.258	4.1148
IS-C03UD	279873.1847	5194465.791	5.334
PZ-ENV-2	280424.7508	5194539.245	10.0584
SP-C02	280574.1912	5194189.81	13.1064

SP-C03	280448.827	5194257.274	14.0208
SP-C04	280330.1165	5194313.729	16.008096
SP-C05	280176.2839	5194393.026	11.271504
SP-C06	280059.4328	5194436.865	9.759696
SP-C07	279908.2123	5194499.788	9.003792
SP-C08	279808.7744	5194568.243	9.7536
SP-C09	279729.6666	5194636.089	7.1628
SP-C10	279658.4166	5194751.556	7.9248
SP-C11	279607.1187	5194861.522	10.594848
SP-C14	280004.1969	5194905.148	9.156192
SP-C15	279988.2955	5194484.859	9.518904
SP-C16	279921.971	5194530.786	9.899904
SP-C17	279816.7967	5194628.481	9.762744
SP-C18	279767.4069	5194687.015	11.591544
SW-C01	279579.5503	5194911.23	10.0584
TP-C01	279499.6401	5194787.785	9.144
TP-C02	279530.6413	5194734.058	11.134344

Seismic Refraction and Well Depths

g1	263165	301272.3	56.96797
g2	263169.1	301396.1	67.60573
g3	263178.5	301517	67.14022
g4	263177.7	301547.1	54.61025
g5	263190.1	301865	50.75121
g6	263197	302049.3	46.3044
g7	263203.2	302249.1	41.16482
g8	263204.6	302322.1	38.98358
g9	263206.6	302347.8	26.12227
g20	264500.6	300812.5	26.26461
g21	264514.2	300844.6	35.17658
g22	264549.4	300926.6	46.57781
g23	264576.4	300989	57.82354
g24	264597.8	301035.3	54.68225
g25	264635.3	301123.2	47.91325
g26	264644.4	301145.3	46.50867
g27	264698.3	301263.3	30.11125
b30	265629.7	300922.4	21.19488
w102	266339.4	300343.4	35.34639
w908	265826.7	300851.7	18.25875
w910	266166.1	299634.7	13.80825
w911	266172.1	299590.9	15.17087
w912	266099.3	299605.6	23.96989
w913	266131.2	299671	20.01137
w923	265132.7	301276.4	31.79973
w922	265332	301357.4	47.2855
w921	265411.1	301167.9	20.6123
w919	265642.8	301206.6	51.31334
w916	265817.2	301104.8	33.22279
w917	265656.8	300971.8	39.67708
w907	265588.7	300870	11.70927

w909	265937.7	300866.2	30.69156
w108	266045.3	300853.1	37.02915
w914	266100.3	300879.1	41.16732
w109	266339.1	300981.5	53.8435
w100	266038.7	300593.4	19.66637
w106	266268.9	300721.2	41.35597
w99	266218.9	300633.7	40.99834
w904	266153.7	300530.8	20.98495
w101	266168.8	300465.4	24.47319
w105	266305.2	300567.5	45.61889
w106	266275.9	300531.4	50.9029
w905	266372.4	300413.4	28.26625
w103	266472.8	300315.3	35.14606
w104	266512.5	300455.5	35.66933
w111	266688.9	300592.9	51.02879
w110	266975.9	299946.7	44.19653
HG1	260616	300058	39.17331
HG2	261264	300786	30.0197
HLA1	265870	300802	30.66921
HLA2	265990	300825	32.17965
HG12	261731	301640	42.31381
HG39	263961	302274	7.58183
MW3	263214	301147	60.50444
MW5	262227	301044	49.97343
G4	259650	299892	62.23071
G4	259702.9	299898	58.97242
G4	259755.8	299904	56.92923
G4	259808.7	299910	55.71002
G4	259861.6	299916	50.29428
G4	259914.5	299922	45.17138
G4	259967.4	299928	43.49226
G4	260020.3	299934	43.06811
G4	260073.2	299940	41.33207
G4	260126.1	299946	40.04174

APPENDIX B

Bonner School Field Seismic Lines

GPS Coordinates of first geophone

Line 1: 281198 mE 5194337 mN
Line2: 281256 mE 5294379 mN

Line Direction

Line1: N35E
Line 2: N50E

Deer Creek Road Seismic Lines

GPS Coordintates of first Geophone

Line 1: 278262 mE 5195258 mN
Line 2: 278173 mE 5195358 mN
Line 3: 278170 mE 5195364 mN
Line 4: 278043 mE 5195509 mN
Line 5: 277781 mE 5195836 mN

Line Directions

All lines were run parallel to Deer Creek Road

Hellgate Canyon Park Seismic Lines

GPS Coordinates of the first Geophone

Line1: 274263 mE 5193964 mN
Line 2: 274262 mE 5193952 mN
Line 3: 274261 mE 5193928 mN

Line Directions
All Lines were run parallel to Highway 200

See data CD for raw field data

APPENDIX C

- Field data was stored in the onboard memory of the Smartseis until it could be transferred to a PC in the lab using a serial cable.

- Data was sorted into site specific folders and backed up in multiple locations

- The file names assigned by the Smartseis had to be changed from the numeric naming convention used by the Smartseis to an alpha-numeric scheme. Names were chosen based on the location and number of the shot at the location

- The individual Smartseis files were combined into a single Seismic Unix file using a demonstration version of Seismic Unix NT.

- Seismic Unix NT was used to calculated the offset and midpoint of each shot and write the values to the Seismic Unix file.

- The files were analyzed visually to determine the optimum offset for each location.

- All remaining steps were completed using seismic unix running on a Linux based computer system.

- The traces corresponding to the optimum offset were extracted using the *suwind* command and placed in a new file.

- The new file was filtered and gained to produce the final sections

    - Filter Settings: *Sufilter* was used to filter the data using the bandpass settings. The filter tapered from 30 Hz up to 45 Hz and down from 120 Hz to 175 Hz.
    - Gain Settings: *Sugain* was used to gain the filter using automatic gain control. The agc window was set to 0.09 seconds.

APPENDIX D

- Starting with the gravity data reduced to the CBA
- The gravity data was separated into two separate files, one containing all of the gravity points and one containing just the gravity points to be used for the regional.
- Using a geo-referenced topo map the edge of the valley was digitized
- The file containing all of the gravity points was gridded in Surfer using the minimum curvature method with a grid spacing of 75 meters and the default options (see below). This created the total CBA grid.
- The value of the total CBA grid was extracted at each point of the digitized valley edge.
- A constant was added to the value of the CBA at each digitized edge point (1 mgal) in order to create the gravity gradient at the edge of the valley
- The digitized edge points with the value of the CBA plus the constant were added to the file containing just the regional gravity points.
- The regional gravity points, including the digitized edge points were gridded in Surfer using the same settings used to created the total CBA grid. This created the regional gravity grid.
- The regional gravity grid was subtracted from total CBA grid to create the residual anomaly grid.
- The residual anomaly grid was trimmed and cleaned up to be used as an input to the gravity inversion programs.

Note: The above outlined steps are an iterative process that may need to be completed several times in order to achieve acceptable results. Editing of the gravity data by adding or removing points may be necessary.

- After inverting the gravity data using an inversion program the output files from the programs are converted to Surfer grids.
- The value of the output grid is extracted at each location of a known depth.
- Statistical analysis is done to compare the known depth to the calculated depth and determine the error in the depth estimate.

Surfer Grid Settings

- Minimum curvature method
  - Max Residual = 0.039
  - Max Iteration = 10,000
  - Relaxation Factor = 1
  - Internal Tension = 0
  - Boundary Tension = 0
  - Anisotropy Ration = 1

APPENDIX E

Seismic Source: Bison Industries Elastic Wave Generator

Approximately 100 Kg hammer
Hydraulic Control

Seismic Data Aquistion: Geometrics Smartseis

Number of Channels: 24.
Sample Interval: 31, 64, 125, 250, 500, 1000 or 2000 μs.
Record Length: up to 16,000 samples per channel.
Acquisition Filters and Noise Reduction Technology: Many field sites are noisy – moving vehicles, overhead power lines, vibrating machinery. The SmartSeis includes real-time digital filters that you can customize to improve your data in adverse urban environments.
• **32 –bit Stacking:** Reduces contributions from random noise by letting you add repeated hammer blows to improve signal strength.
• **Memory Freeze:** Allows selective stacking of weak channels.
• **Power Line Notch:** Reduces 50/60 Hz and harmonics.
• **Low-Cut Filtering:** Reduces the effects of distant traffic and ground roll. Includes filter frequencies of out, 25, 35, 50, 70, 100, 140, 200, 280, 400 Hz.
• **High-Cut Filtering:** Removes wind noise. Includes filter frequencies of out, 250, 500, 1000 Hz.
• **Display Filters can be run non-destructively after raw data is collected, making costly repeated shots unnecessary. Custom filter frequencies are available.**
Display: High-resolution 640x480 LCD, PC compatible. Visible in bright sunlight.
Noise Monitor: Waterfall style moving trace display, also shows channel continuity and geophone performance.
A/D Conversion: 20-bit result, 32-bit stacker.
Gain Control: Automatic, set by continuously measuring two-stage instantaneous floating-point amplifier. True amplitude is preserved and can be used for ground motion studies.
• Fault Location
• Stratigraphic mapping
• Gravel and aggregate mining
• Thickness of overburden
• Mineral and gold exploration
• Landfill delineation and siting
• IBC Vs30 site classification
Data Display: Wiggle-trace, shaded or variable area, trace clipping, automatic gain control, fixed gain and post-acquisition

filtering included.
Energy Sources: Hammer, weight drop or explosives.
Pretrigger: Allows viewing of data before trigger.
Delay: 0 to 9999 ms in 1 ms increments.
Data Storage: Sufficient for several days recording. Includes both floppy and hard drive storage.
In-field Processing:
• Automatic first break picking with manual over-ride.
• On-screen travel time plots.
• Automatic layer assignments with manual over-ride
• Automatic calculation of depths below shots and geophones. Built-in software ray traces model and indicates where data quality might be poor. Prints table of all data, depth calculations and a quality control plot showing questionable data. Report-ready cross section annotated with calculated velocities. Analysis and interpretation software from Rimrock Geophysics. PCbased packages also available. Please contact the factory.
Interfaces: RS-232, video, keyboard and printer.
Data Format: SEG-2 standard.
Mating Connectors: Cannon NK-27-21C, 12 channels each connector.
Plotter: Built-in four-inch (11 cm) wide thermal printer.
Testing: Full instrument testing available using Geometrics external test oscillator system.
Power: Runs on 12V auto-type battery.

GPS Location: Garmin GPSMAP 60C

12 channel parallel GPS receiver

Gravity Meter: Scintrex Model CG3

Sensor Type Fused Quartz using electrostatic nulling
Reading Resolution 5 µgal
Standard Deviation: <10 µgal
Operating Range 8,000 mgal, without resetting
Residual Long-term Drift (static) Less than 0.02 mgal/day
Range of Automatic Tilt Compensation ±200 arc sec.
Tares Typically less than 5µgal for a 20g shock
Automated Corrections Tide, Instrument Tilt, Temperature, Noisy Reading Rejection
Dimensions 240 mm x 310 mm x 320 mm
9.4" x 12.2" x 12.6"
Weight *(including battery)* 11.0 kg (24.2 lbs)
Power Consumption 4.5 watts at 25 C

Operating Temperature -40 C to +45 C (optional ranges available)
Memory 48k RAM, suitable for up to 1200 readings
Real Time Clock Internal provides day, month, year, hours, minutes, seconds **Digital Data Output** RS-232C serial interface